Department of AERONAUTICS and ASTRONAUTICS
STANFORD UNIVERSITY

RONALD BUSCH
IRMGARD FLÜGGE-LOTZ

THE ATTITUDE CONTROL OF A SATELLITE IN AN ELLIPTIC ORBIT

APRIL
1966

This research was sponsored by the
National Aeronautics and Space Administration
Under Research Grant NsG 133-61

SUDAAR
NO. 261

Department of Aeronautics and Astronautics
Stanford University
Stanford, California

THE ATTITUDE CONTROL OF A SATELLITE IN AN ELLIPTIC ORBIT

by

Ronald Busch
and
Irmgard Flügge-Lotz

SUDAAR No. 261
April 1966

This research was sponsored by
the National Aeronautics and Space Administration
under Research Grant NsG 133-61

ACKNOWLEDGMENT

The contribution of the National Aeronautics and Space Administration is gratefully acknowledged; the work was sponsored by NASA under Research Grant NsG 133-61.

ABSTRACT

In this dissertation a simple, efficient attitude-control-system is developed for a satellite in an elliptic orbit. Linear time-varying equations, which include the gravity-gradient torque, are used to describe the attitude motion. These equations are obtained by assuming that the attitude angles, attitude angular-rates, and orbital eccentricity are small. The desired attitude is such that one body-fixed axis is earth-pointing and another is normal to the orbital plane.

The control torques are assumed to be supplied by gas jets, and the performance of the control system is judged by a minimum fuel-consumption criterion. Pontryagin's Maximum Principle is employed to obtain necessary conditions on the optimal control. By using the conditions specified by the Maximum Principle, the system is run in reverse-time. Thus, the appearance of the optimal trajectories in the phase planes for various initial conditions is obtained. From this information a form for the suboptimal control system is chosen, and the system parameters are then optimized. The final system is quite simple, yet its performance is near optimal for limited but realistic ranges of eccentricity and moment-of-inertia values. This development is accomplished by using analog-computer simulations.

To further check the performance of the developed control system, it is used to control the motion described by the full nonlinear attitude equations. These equations are integrated by using a digital computer. For small errors the results check those that are obtained by using the

linear equations. In addition, the system is found to perform quite well when the attitude errors are large.

For a satellite in an elliptic orbit and attitude equations written with respect to an earth-pointing reference frame, the pitch equation contains a time-dependent forcing term. Thus, continual steady-state control is necessary. A satisfactory solution, under most conditions, is obtained by adding a small pitch-reaction-wheel for the steady-state phase of the control. The steady-state fuel consumption is then very small, as is the power required by the wheel.

TABLE OF CONTENTS

TABLE OF CONTENTS (Continued)

LIST OF TABLES

LIST OF ILLUSTRATIONS

LIST OF ILLUSTRATIONS (continued)

I. INTRODUCTION

A. Mission Requirements and Disturbances

The satellite considered in this report is assumed to be on a mission that requires it to be earth-pointing, i.e., a particular side of the satellite must face the earth. While most frequently such satellites are in circular orbits, they may also be required to be in, or may accidentally be put into, elliptic orbits of small eccentricity. Other similar missions could conceivably require the satellite to be earth-pointing for short periods of time for data transmission purposes. In either case, the acquisition phase of the problem is the same; only the steady-state portion differs.

Also, the mission is assumed to have a fairly long life-time, i.e., up to one year. Thus, besides being able to place the satellite in the proper attitude and hold it there, the control system must do this efficiently. Otherwise the required fuel load may be prohibitively large.

In orbit the satellite encounters many disturbances which cause it to deviate from its desired attitude. Thus, besides the original ejection error, the control system must correct for errors induced by the gravity gradient, aerodynamic drag, solar radiation pressure, earth's magnetic field, and collisions with micrometeors. Solar pressure and magnetic effects are small and, consequently, cause slow increases in the attitude errors. The size of the torque due to the aerodynamic drag depends on the altitude of the orbit and the shape and attitude of the

satellite. In most realistic cases it is less than the gravity gradient torque. In an elliptic orbit of eccentricity around 0.1 or larger, the drag force behaves like a pulse at the perigee of the orbit. Collisions with micrometeors, also pulse disturbances, are not too common.

In deriving the equations of the attitude motion that are used in this report, the gravity-gradient torque is included. The other torques that are mentioned above are assumed to be disturbances to the final motion.

B. Control Methods and Performance Criteria

There are many means through which the satellite can be controlled to reach and keep the desired attitude. In general, these methods are classed into two groups, passive control and active control. Passive devices use inherent damping effects, e.g. in beam flexure, and take advantage of gravity and magnetic torques. As the name implies, there is no power input. Active controls include momentum transfer and mass expulsion devices. Some examples of momentum transfer devices are reaction wheels and spheres, gyroscopes, and fluid flywheels. Mass-expulsion control methods include cold-gas jets, hot-gas jets, and ion propulsion. Attitude control by one or more of these methods is discussed by Cannon [9], Haefner [17], and Nichol [18]. Other methods for attitude control include magnetic control (Wheeler [19]) and spin stabilization (Kane and Barba [20]).

In this report cold-gas jets are used for the attitude control of the satellite. Cold-gas jets were chosen because of their simplicity, their ability to produce small torques, and the fact that there are no coupling effects due to the controller.

When considering satellite attitude control, the most significant and most frequently used performance criteria are minimum-time, minimum-energy, and minimum-fuel-consumption. Since in this report the satellite is assumed to be on a mission of long lifetime, the time used to correct attitude errors is not extremely critical. Therefore, the minimum-time criterion does not apply. Minimum-fuel and minimum-energy are somewhat related criteria except that the latter weighs the energy of the state of the system in addition to the control energy. When considering control effort with a cold-gas jet system the fuel criterion is more applicable than the energy criterion because of the characteristics of the jets, i.e., torque is directly proportional to the fuel consumption. The fuel consumption is important because of the long duration of the mission. Thus, the minimum-fuel criterion is used in this report to rate the performance of the control system. The energy of the state is also considered in the final choice of the system, but it is not included in the original development.

C. Previous Research and New Results

A considerable amount of work has been done in the last few years in the area of minimum-fuel control of the attitude of a satellite. Meditch [10] assumed large control torques and, consequently, did not include gravity gradient effects. Craig and Flügge-Lotz [7] and Marbach [8] assumed small control torques and included the gravity gradient effects, but limited the study to satellites in circular orbits. Hyver [21] considers the same problem but assumes that measured values of the states are noisy. All of these reports used linearized attitude equations.

Hales [16] considers the more general problem of an elliptic orbit and large attitude errors. He uses the nonlinear attitude equations and solves the problem using a modified steepest-descent method. The end result, however, is not a feedback control system.

In this report the control torques are assumed to be small and the satellite is assumed to be in an orbit of small eccentricity. The linearized equations that describe the small attitude motion are time-varying. Thus, the assumption of an elliptic orbit introduces parametric excitations and forcing terms which are not present when a circular orbit is assumed. Pontryagin's Maximum Principle is applied to these time-varying equations to determine the characteristics and form of the minimum-fuel optimal control. Based on this information a suboptimal, feedback, attitude-control system is developed that is both simple and efficient. Using the nonlinear attitude equations the suboptimal control system is shown to work equally well when the attitude errors are large. Also, the problem of steady state control is discussed to some extent. In all cases it is assumed that through the use of star trackers, sun sensors, and/or horizon scanners, the state of the attitude motion is known completely and accurately.

II. PRELIMINARY DEVELOPMENTS

This chapter contains the development and discussion of several topics which are essential to the following chapters but in themselves are not new. They are included for the sake of clarity and completeness.

A. Equations of Satellite Attitude Motion

The equations of the attitude motion of an earth satellite have been derived by many persons and in many forms. The following derivation and resulting equations are essentially the same as those of Kane [2] and DeBra [1].

1. Reference Frame and Parameters

The satellite is assumed to be on a mission which requires it to be earth-pointing, i.e., a particular face of the satellite is to be as nearly as possible normal to the local vertical. The local vertical is defined as a line passing through the mass centers of the satellite and the earth. Thus, it is convenient to choose a reference frame which is fixed with respect to the local vertical. Such a reference frame, denoted by R, is defined by the right-handed, mutually-perpendicular set of axes shown in Figure 2.1. The 1-axis is directed away from the earth along the local vertical, and the 3-axis is normal to the orbital plane such that the dot product of the velocity of the center of mass of the satellite and the $\bar{e}_2$ unit vector* is positive. The origin of this set of axes is assumed to coincide with the mass center of the satellite.

---

* $\bar{e}_i$ is a unit vector directed along the i-axis, $i = 1,2,3$.

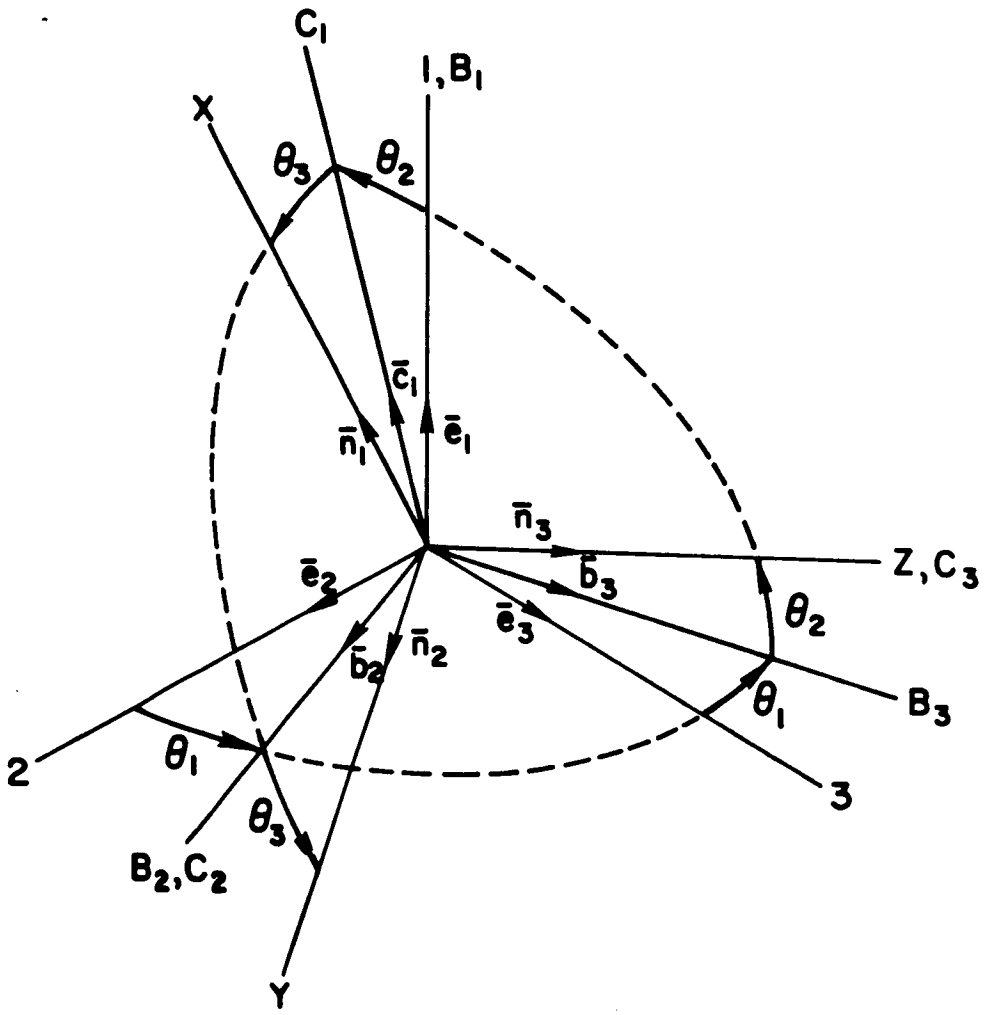

Figure 2.1 Three-Axes Euler Angles.

The attitude of the satellite with respect to R is determined by what may be referred to as "Three-Axes Euler Angles". They are formed by making the following ordered right-handed rotations (see Figure 2.2):

$$\begin{aligned} &\theta_1 \text{ about } 1 \Rightarrow B_1,\ B_2,\ B_3\ (\bar{b}_1 = \bar{e}_1) \\ &\theta_2 \text{ about } B_2 \Rightarrow C_1,\ C_2,\ C_3\ (\bar{c}_2 = \bar{b}_2) \\ &\theta_3 \text{ about } C_3 \Rightarrow X,\ Y,\ Z\ (\bar{n}_3 = \bar{c}_3) \end{aligned} \qquad (2\text{-}1)$$

The XYZ set of axes is fixed in the satellite.

This set of angles uniquely determines the attitude of the satellite with respect to R except when $\theta_2 \equiv \pm 90^\circ$. However, this presents no difficulties since, as will be discussed later, the attitude angles are assumed to remain small. When θ_1, θ_2, and θ_3 are small they may be regarded as the yaw, roll, and pitch angles, respectively.

2. Derivation of Attitude Equations

The motion of a rigid body about its center of mass is described by Euler's Dynamical Equations which are easily derived from the Angular Momentum Principle. Referred to body fixed coordinate axes, X, Y, and Z, which are aligned with the principal axes of the body, the Euler equations have the following form:

$$\begin{aligned} I_1\dot{\omega}_1 + \omega_2\omega_3(I_3-I_2) &= M_1 \\ I_2\dot{\omega}_2 + \omega_1\omega_3(I_1-I_3) &= M_2 \\ I_3\dot{\omega}_3 + \omega_1\omega_2(I_2-I_1) &= M_3 \end{aligned} \qquad (2\text{-}2)$$

where I_1, I_2, and I_3 are the principal moments of inertia of the body; $\omega_i = \bar{\omega}\cdot\bar{n}_i$, $i = 1,2,3$, with $\bar{\omega}$ the angular velocity of the

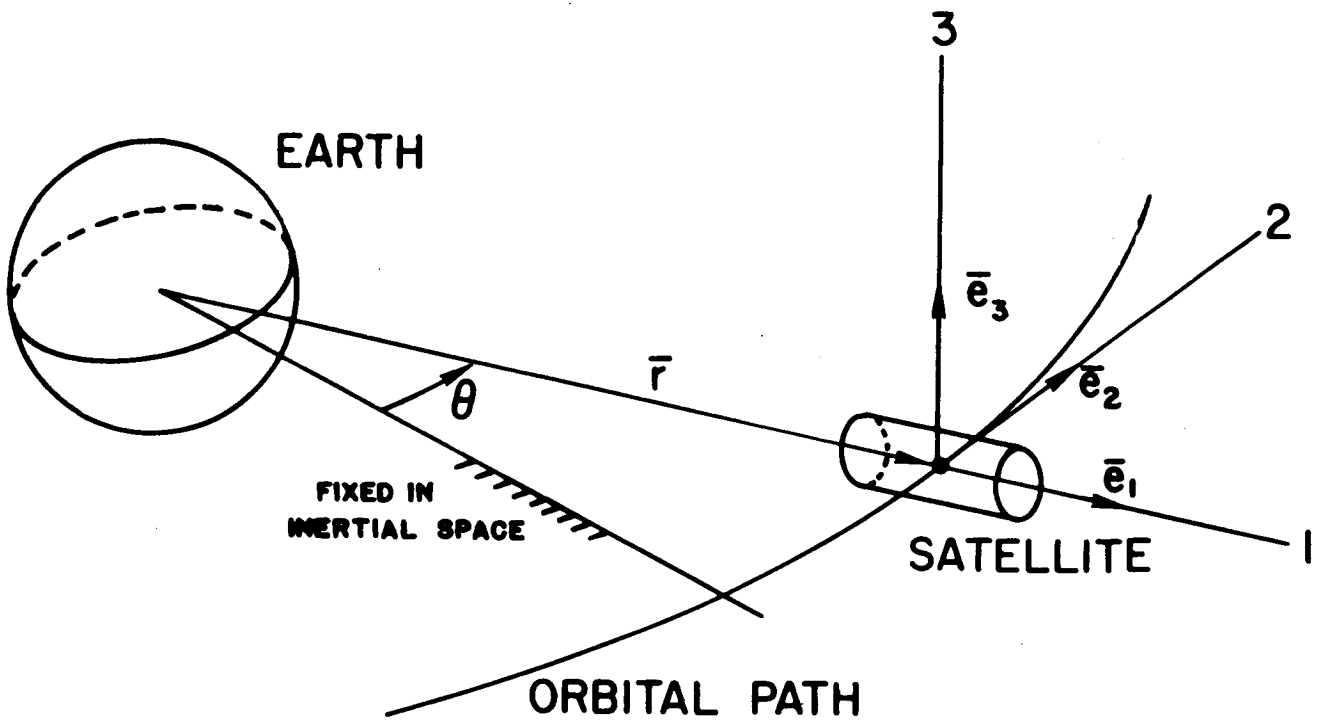

Figure 2.2 Attitude Reference Frame, R .

body in an inertial reference frame and $\bar{n}_i$, $i = 1,2,3$, unit vectors aligned with X, Y , and Z , respectively; and $M_i = M \cdot \bar{n}_i$ with $\bar{M}$ the total external moment acting on the body. The dot $(\cdot)$ denotes differentiation with respect to time.

In applying Euler's Equations (2-2) to an earth satellite the following assumptions are made: the satellite is a rigid body whose principal axes are the body fixed axes, X, Y , and Z , and the center of mass of the earth is fixed in inertial space. The validity of the first assumption depends on the type of equipment carried by the satellite. The second assumption is quite reasonable.

The angular velocity of the satellite in an inertial reference frame is

$$\bar{\omega} = \dot{\theta}\bar{e}_3 + \dot{\theta}_1\bar{e}_1 + \dot{\theta}_2\bar{b}_2 + \dot{\theta}_3\bar{n}_3 \tag{2-3}$$

where $\dot{\theta}$ is the orbital rate of the satellite (see Figure 2.1). The unit vectors in Equation (2-3) are shown in Figure 2.2 and are related to the body fixed unit vectors as follows:

$$\begin{aligned}
\bar{e}_1 &= c_2c_3\bar{n}_1 - c_2s_3\bar{n}_2 + s_2\bar{n}_3 \\
\bar{e}_3 &= (s_1s_3 - c_1s_2c_3)\bar{n}_1 + (s_1c_3 + c_1s_2s_3)\bar{n}_2 + c_1c_2\bar{n}_3 \\
\bar{b}_2 &= s_3\bar{n}_1 + c_3\bar{n}_2
\end{aligned} \tag{2-4}$$

where $c_i = \cos\theta_i$ and $s_i = \sin\theta_i$, $i = 1,2,3$.

The components M_i of the external torques acting on the satellite, excluding the control torques, are assumed to consist only

of those due to the gravity gradient. All others, which are either smaller or behave as pulses, will be considered as disturbances to the final motion. The gravity-gradient torque is simplified by assuming that the earth is a homogeneous sphere* and, thus, possesses an inverse-square-law central-force gravitational field. Thus, referred to the body fixed axes, the gravity-gradient torque about the center of mass of the satellite is [3]

$$\bar{M} = \frac{3\mu}{r^3}\left[a_2a_3(I_3-I_2)\bar{n}_1 + a_3a_1(I_1-I_3)\bar{n}_2 + a_1a_2(I_2-I_1)\bar{n}_3\right] \qquad (2\text{-}5)$$

where $\mu = GM$, with G the universal gravitational constant and M the mass of the earth; r is the distance between the centers of mass of the earth and the satellite; and $a_i = \bar{n}_i \cdot \bar{e}_1$, $i = 1,2,3$.

Substituting relations (2-3), (2-4), and (2-5) into Euler's Equations (2-2) and solving for $\ddot{\theta}_1$, $\ddot{\theta}_2$, and $\ddot{\theta}_3$, yields the following equations for the attitude motion of an earth satellite in an elliptic orbit:

$$\ddot{\theta}_1 = \frac{1}{c_2}\left[\dot{\theta}_1\dot{\theta}_2 s_2 - \dot{\theta}_2\dot{\theta}_3 + \dot{\theta}_2\dot{\theta}c_1c_2 - \dot{\theta}_1\dot{\theta}s_1s_2 - \dot{\theta}_3\dot{\theta}s_1 + \ddot{\theta}c_1s_2 - k_1c_3\left(\frac{3\mu}{r^3}c_2s_2s_3+\omega_2\omega_3\right) - k_2s_3\left(\frac{3\mu}{r^3}c_2s_2c_3-\omega_1\omega_3\right)\right] \qquad (2\text{-}6)$$

$$\ddot{\theta}_2 = \dot{\theta}_1\dot{\theta}_3c_2 - \dot{\theta}_1\dot{\theta}c_1 - \dot{\theta}_3\dot{\theta}c_1s_2 - \ddot{\theta}s_1 - k_1s_3\left(\frac{3\mu}{r^3}c_2s_2s_3+\omega_2\omega_3\right) + k_2c_3\left(\frac{3\mu}{r^3}c_2s_2c_3-\omega_1\omega_3\right) \qquad (2\text{-}7)$$

---

* Actually, it is sufficient to assume that the earth is a sphere whose mass density is a function only of the distance from its mass center.

$$\ddot{\theta}_3 = \dot{\theta}_1\dot{\theta}c_2s_1 - \dot{\theta}_1\dot{\theta}_2c_2 - \ddot{\theta}_1s_2 + \dot{\theta}_2\dot{\theta}s_2c_1 - \ddot{\theta}c_1c_2$$

$$- k_3\left(\frac{3\mu}{r^3}c_2^2s_3c_3+\omega_1\omega_2\right) \qquad (2\text{-}8)$$

where

$$\begin{aligned}\omega_1 &= (\dot{\theta}s_1+\dot{\theta}_2)s_3 - (\dot{\theta}c_1s_2-\dot{\theta}_1c_2)c_3\\ \omega_2 &= (\dot{\theta}s_1+\dot{\theta}_2)c_3 + (\dot{\theta}c_1s_2-\dot{\theta}_1c_2)s_3\\ \omega_3 &= \dot{\theta}c_1c_2 + \dot{\theta}_1s_2 + \dot{\theta}_3\end{aligned} \qquad (2\text{-}9)$$

and k_1, k_2, and k_3 are inertia parameters defined by

$$k_1 = \frac{I_3 - I_2}{I_1} \quad , \quad k_2 = \frac{I_1 - I_3}{I_2} \quad , \quad k_3 = \frac{I_2 - I_1}{I_3} \qquad (2\text{-}10)$$

However, the attitude motion is not completely specified, i.e., the above equations cannot be solved, until expressions for r and $\ddot{\theta}$ are obtained.

Since the largest dimension of the satellite is many orders of magnitude smaller than the distance between the mass centers of the satellite and the earth, the satellite can be considered as a particle moving in the central-force gravitation field of the earth. The motion of the particle is governed by the equations (see Goldstein [13])

$$\ddot{r} - r\dot{\theta}^2 = -\mu/r^2 \qquad (2\text{-}11)$$

$$r^2\dot{\theta} = h \qquad (2\text{-}12)$$

where h is a constant that is proportional to the angular momentum of the particle about the center of mass of the earth. The solution to Equations (2-11) and (2-12) is the equation of an ellipse,

$$\frac{h^2}{\mu r} = 1 + e \cos \theta \tag{2-13}$$

where e is the eccentricity and θ is measured from the perigee (see Figure 2.3).

Combining Equations (2-12) and (2-13) and defining $n = \mu^2/h^3$ yields the following relations:

$$\frac{\mu}{r^3} = n^2(1+e \cos \theta)^3 \tag{2-14}$$

$$\dot{\theta} = n(1+e \cos \theta)^2 \tag{2-15}$$

From Equation (2-15) it is apparent that n represents the average orbital angular velocity of the satellite, i.e., $n = 2\pi/P$, where P is the orbital period. The orbital angular acceleration $\ddot{\theta}$ is found by differentiating Equation (2-15):

$$\ddot{\theta} = -2n^2 e \sin \theta(1+e \cos \theta)^3 \tag{2-16}$$

Substituting Equations (2-14) and (2-15) into Equations (2-6), (2-7), and (2-8) gives three second-order differential equations which, together with Equation (2-16), completely describe the attitude motion of an earth satellite in an elliptic orbit.

3. Stability of Attitude Motion

The four second-order equations, (2-6) to (2-8) and (2-16), that describe the attitude and orbital motion of the satellite are highly non-linear and, thus, quite difficult to analyze. However, many investigations into the stability of these or similar equations have been made, for example, DeBra [1], Kane [2], and Kane and Barba [20]. Their results

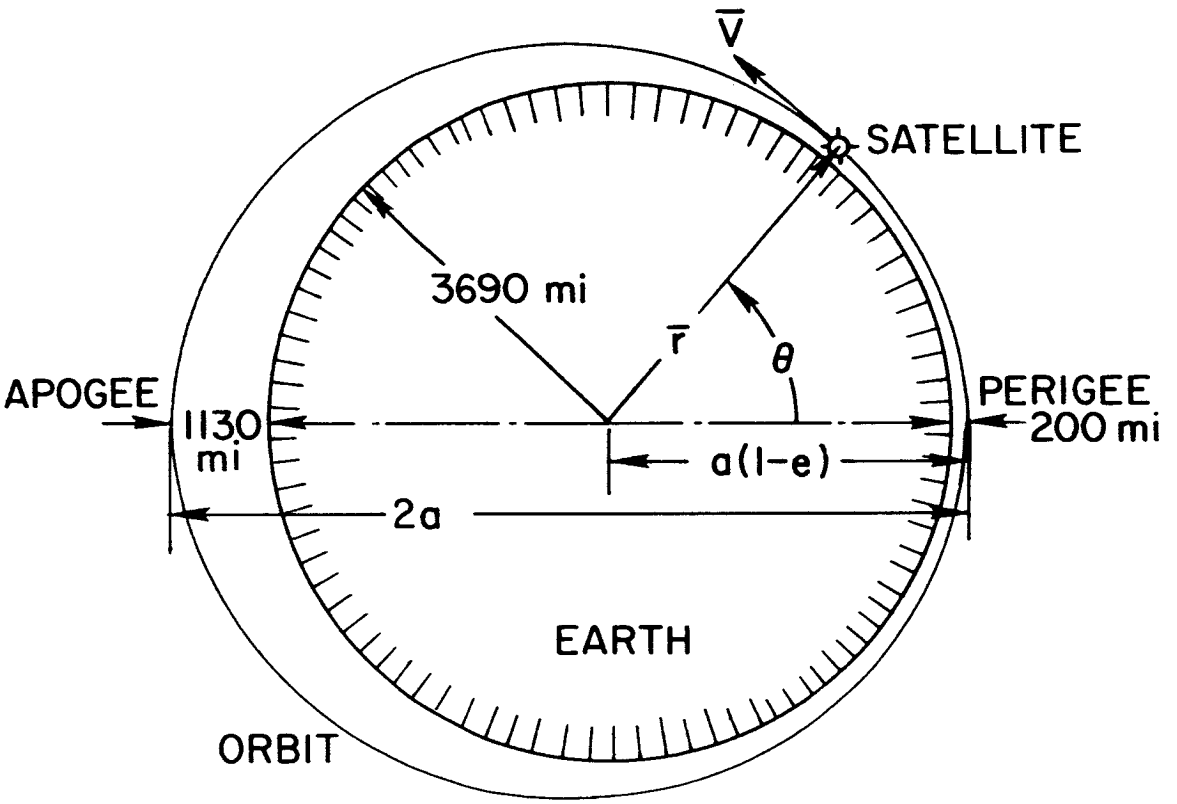

Figure 2.3 Elliptic Orbit, e = 0.1 .

indicate that not too many satellite configurations are stable, particularly in an elliptic orbit.

The purpose of discussing stability here is to attempt to justify linearization of the attitude equations. Obviously, the behavior of an unstable nonlinear system cannot be described by linearized equations. Since the attitude equations will be linearized in the following, ideally it would be necessary to find a satellite configuration whose motion is bounded within a region where linearization is likely to be justifiable, say errors of less than one-half radian.

DeBra [1] gives several stability charts for various satellite shapes and various orbital eccentricities. His stability bound of ninety degrees is too large for purposes here, but inertia properties that result in stability according to these charts should still be chosen. Such a configuration is one that has moment-of-inertia ratios of $I_1/I_3 = 0.1$ and $I_2/I_3 = 0.95$. According to DeBra's charts, it is stable for eccentricities up to 0.1 . However, these values were modified slightly since they turned out to be very close to an unstable region of the instability charts of Kane [2]. Thus, the final nominal moment of inertia values that were picked to be used in the following are $I_1/I_3 = 0.12$ and $I_2/I_3 = 0.97$, which result in moment of inertia parameter values of $k_1 = 0.25$, $k_2 = -0.91$, and $k_3 = 0.85$. This represents a fairly realistic satellite configuration (see Appendix A).

To further examine the behavior and stability of the attitude motion of this configuration, the four second-order orbital and attitude equations were integrated on a Burroughs B5500 digital computer using a

Kutta-Merson finite-difference integrating procedure.* Some of the results are shown in Figures 2.4 and 2.5, which are phase plane (normalized angular velocity $\dot{\theta}_i/n$ versus angular position θ_i) plots of the attitude motion. The length of integration was approximately three orbits. For quite small eccentricities as in Figure 2.4 ($e = 0.01$) the motion was well behaved, although the yaw error did grow to three times its initial value. For larger eccentricities, the roll and pitch motion, while quite different in appearance, still remained bounded at roughly the magnitude of the initial conditions. However, the yaw motion was not so well behaved. For $e = 0.05$ (Figure 2.5) the satellite was just beginning to spin about the yaw axis, and for $e = 0.1$ this spinning occurred much sooner. For smaller initial conditions, the behavior was similar only the error growth in yaw was much slower.

Thus, while this configuration cannot be called stable, except possibly for very small eccentricities, it is fairly well behaved. The only large error growth occurred in yaw. However, since the moment of inertia about this axis is the smallest, this motion is the easiest to control. Therefore, this satellite configuration will be used in the following chapters.

4. Linearization of Attitude Equations

It is a formidable task to develop an optimal or near optimal attitude controller using the full nonlinear equations.** Thus, it is

---

* The procedure was written by John H. Welsch and was obtained from the program library (Program No.95) of the Stanford Computation Center. For a description of the Kutta-Merson method, see Fox [15].

** See Hales [16] for one solution to the problem.

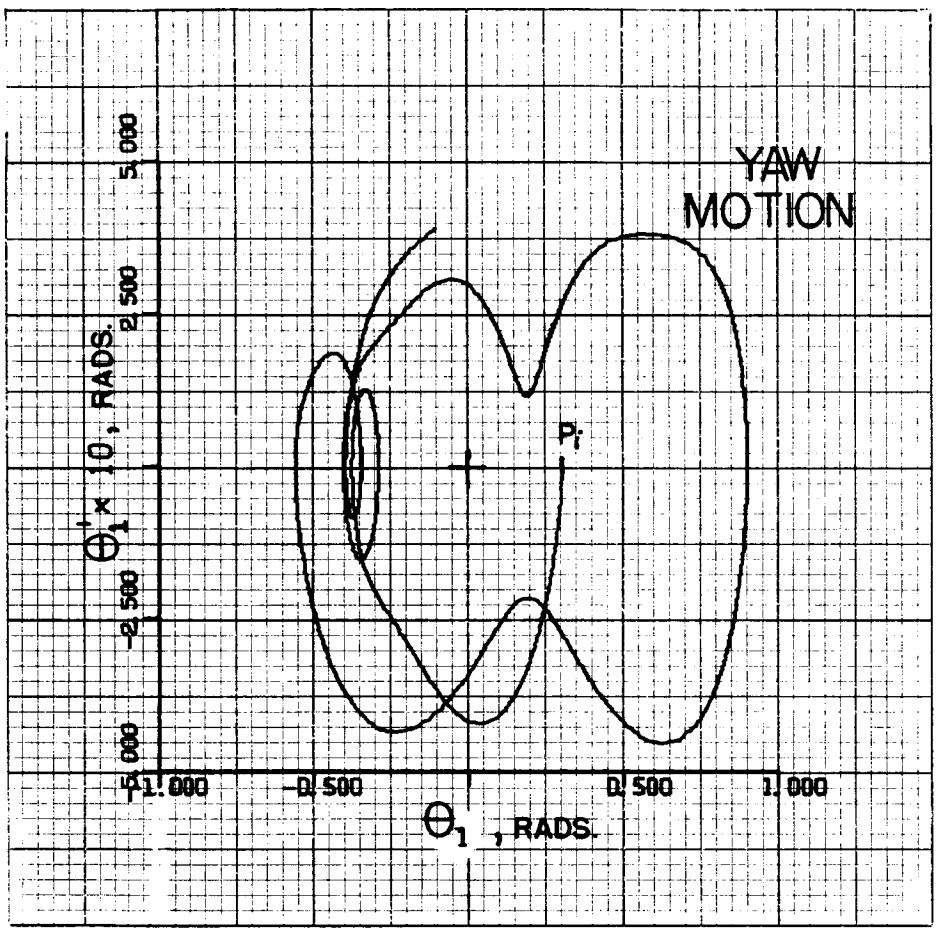

a. Yaw Phase Plane

Figure 2.4 Uncontrolled Attitude Motion, e = 0.01 .
Initial Values: $\theta_o = 0$, $\theta_1 = \theta_2 = \theta_3 = 0.3$ rads.

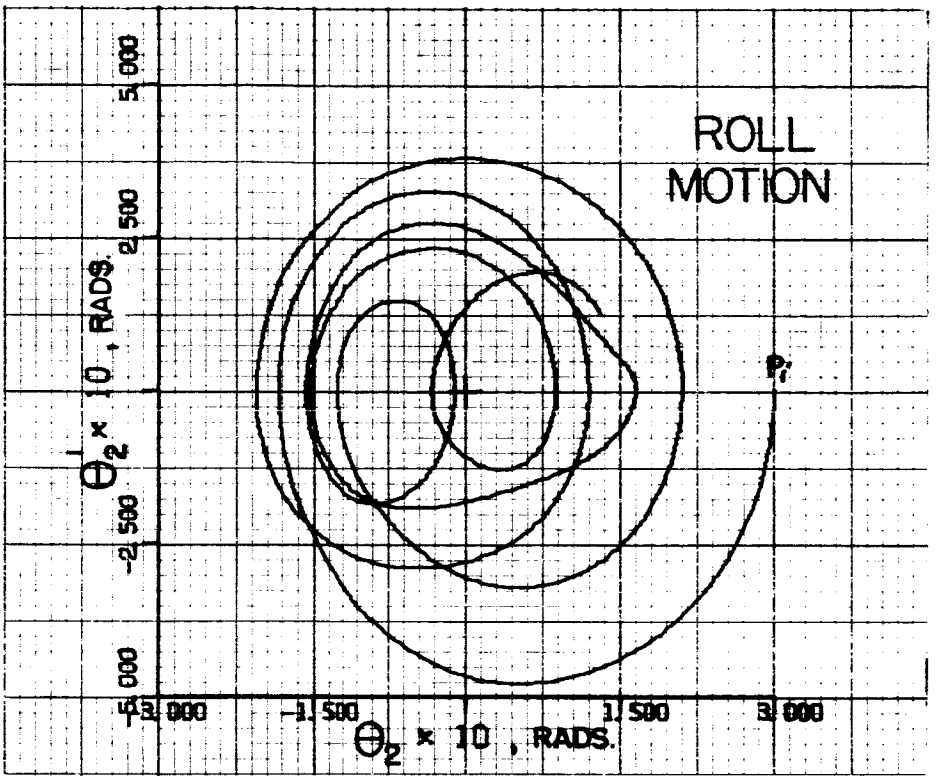

b. Roll Phase Plane

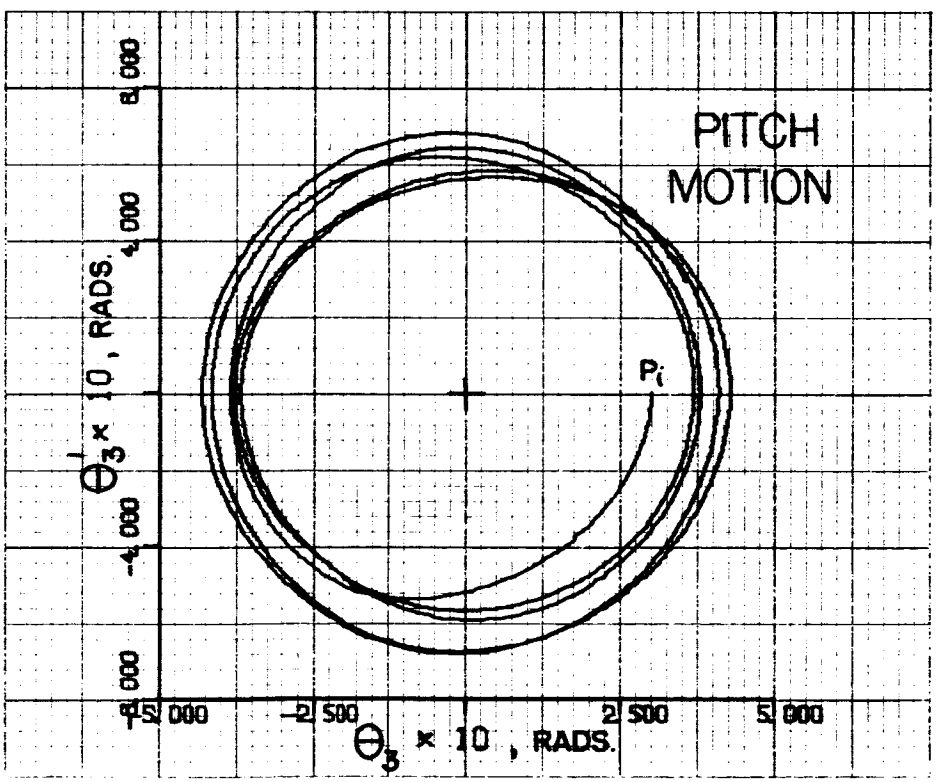

c. Pitch Phase Plane

Figure 2.4 (continued)

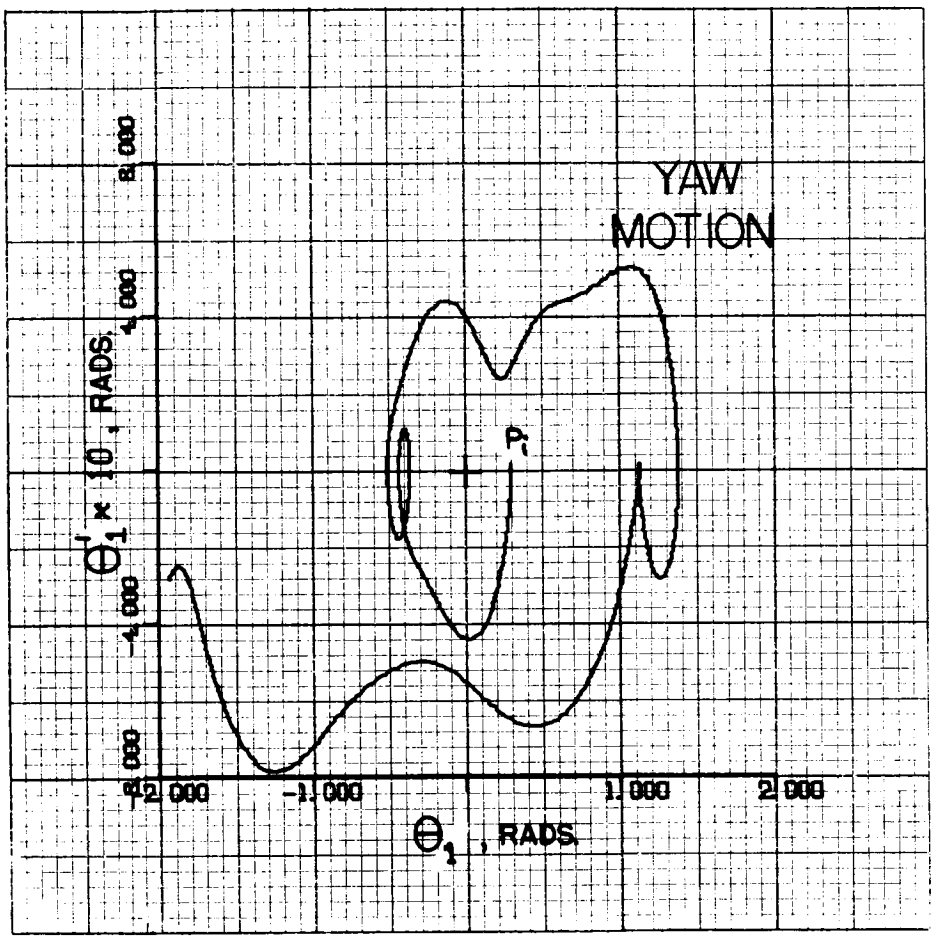

a. Yaw Phase Plane

Figure 2.5 Uncontrolled Attitude Motion, e = 0.05 .
Initial Values: $\theta_o = 0$, $\theta_1 = \theta_2 = \theta_3 = 0.3$ rads.

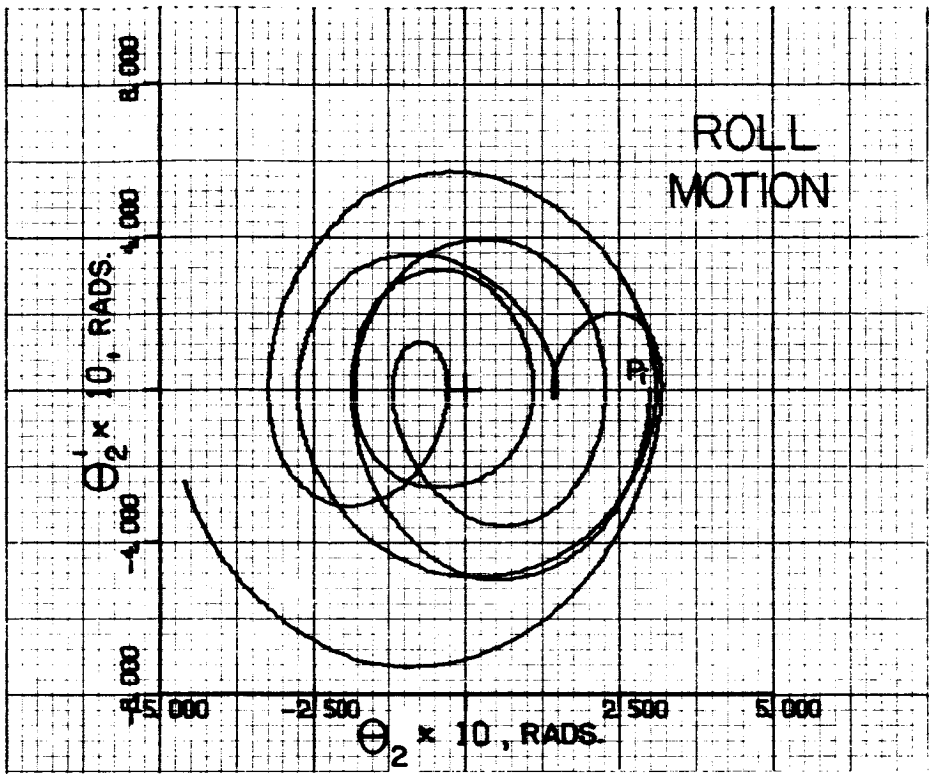

b. Roll Phase Plane

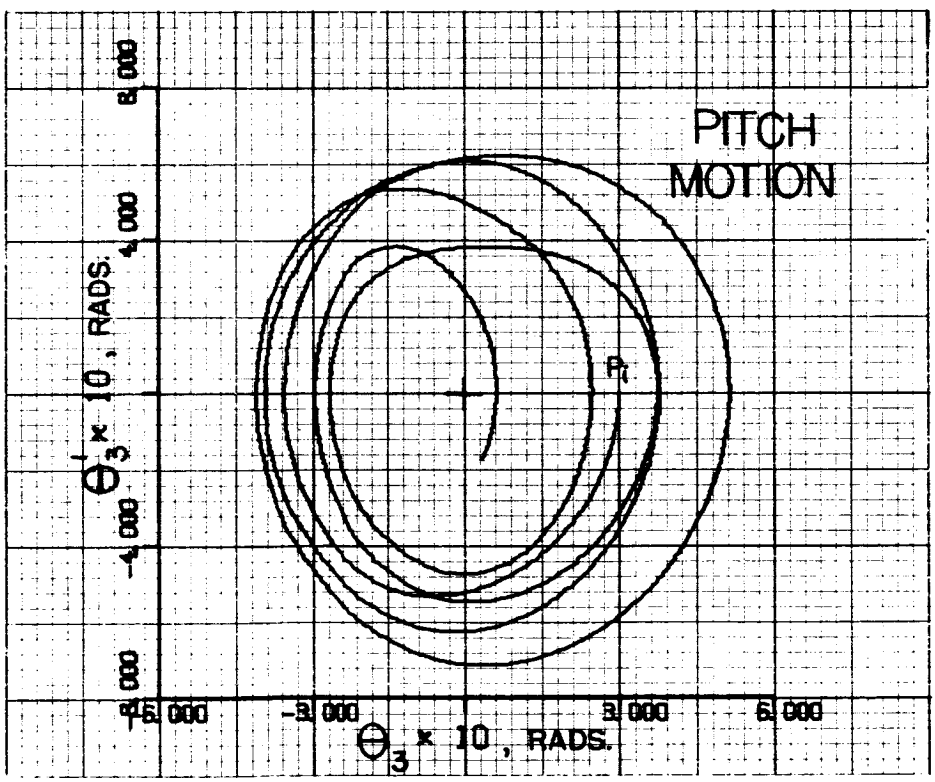

c. Pitch Phase Plane

Figure 2.5 (continued)

desirable to linearize the equations and develop a control system that is optimal or near optimal for small errors. The performance of this system can then be checked using the full nonlinear equations and large errors. This is precisely what has been done in the following chapters.

As discussed in the previous section, the attitude motion for the chosen configuration was not stable in many cases. Thus, since small errors would not always remain small, the linearized equations would not always give an accurate description of the motion. However, if it is assumed that an attitude control system which guarantees asymptotic stability of the attitude motion is added to the satellite, the linearized equations can be used with reasonable accuracy for small errors.

By assuming that all attitude angles θ_i and normalized attitude angular rates $\dot{\theta}_i/n$ are so small that products in these terms can be neglected, the following linearized attitude equations are obtained:

$$\ddot{\theta}_1 = (1-k_1)\dot{\theta}\dot{\theta}_2 - k_1\dot{\theta}^2\theta_1 + \ddot{\theta}\theta_2 \tag{2-17}$$

$$\ddot{\theta}_2 = -(1+k_2)\dot{\theta}\dot{\theta}_1 + k_2\dot{\theta}^2\theta_2 - \ddot{\theta}\theta_1 + \frac{3\mu k_2}{r^3}\theta_2 \tag{2-18}$$

$$\ddot{\theta}_3 = -\frac{3\mu k_3}{r^3}\theta_3 - \ddot{\theta} \tag{2-19}$$

These equations show the pitch motion to be forced by a periodic function and to be decoupled from the yaw and roll motions. Integration of the full nonlinear equations shows that when all errors and error rates are initially zero, the forcing function produces pitch motion as shown in Figure 2.6, and the yaw and roll errors remain zero, i.e., no coupling is present. However, if the yaw and roll errors are not initially zero, the forced oscillations in pitch cause them to grow. The pitch motion, on the other hand, is hardly affected by the growth in the yaw and roll error. Thus, while the linearized equations do not always accurately describe the small attitude motion of the satellite, they serve as a good approximation for the development of the attitude control system.

One further assumption is made in arriving at the form of the attitude equations used in the following two chapters, that of small eccentricity. This assumption is quite reasonable since it is highly unlikely that a mission which requires a large eccentricity would also require the satellite to be earth pointing, except possibly for short periods of time for communication purposes. In most of the following, only orbits of eccentricity around 0.1 or less will be considered. While 0.1 is not a large eccentricity, to an observer on the earth the orbit appears quite elliptic. For instance, if the perigee of the orbit is 200 miles above the earth's surface, then the apogee is 1130 miles above the earth's surface (see Figure 2.3).

Thus, before relations (2-14), (2-15), and (2-16) are substituted into the attitude equations, they are expanded in powers of the eccentricity e. For eccentricities of 0.1 or less, sufficient

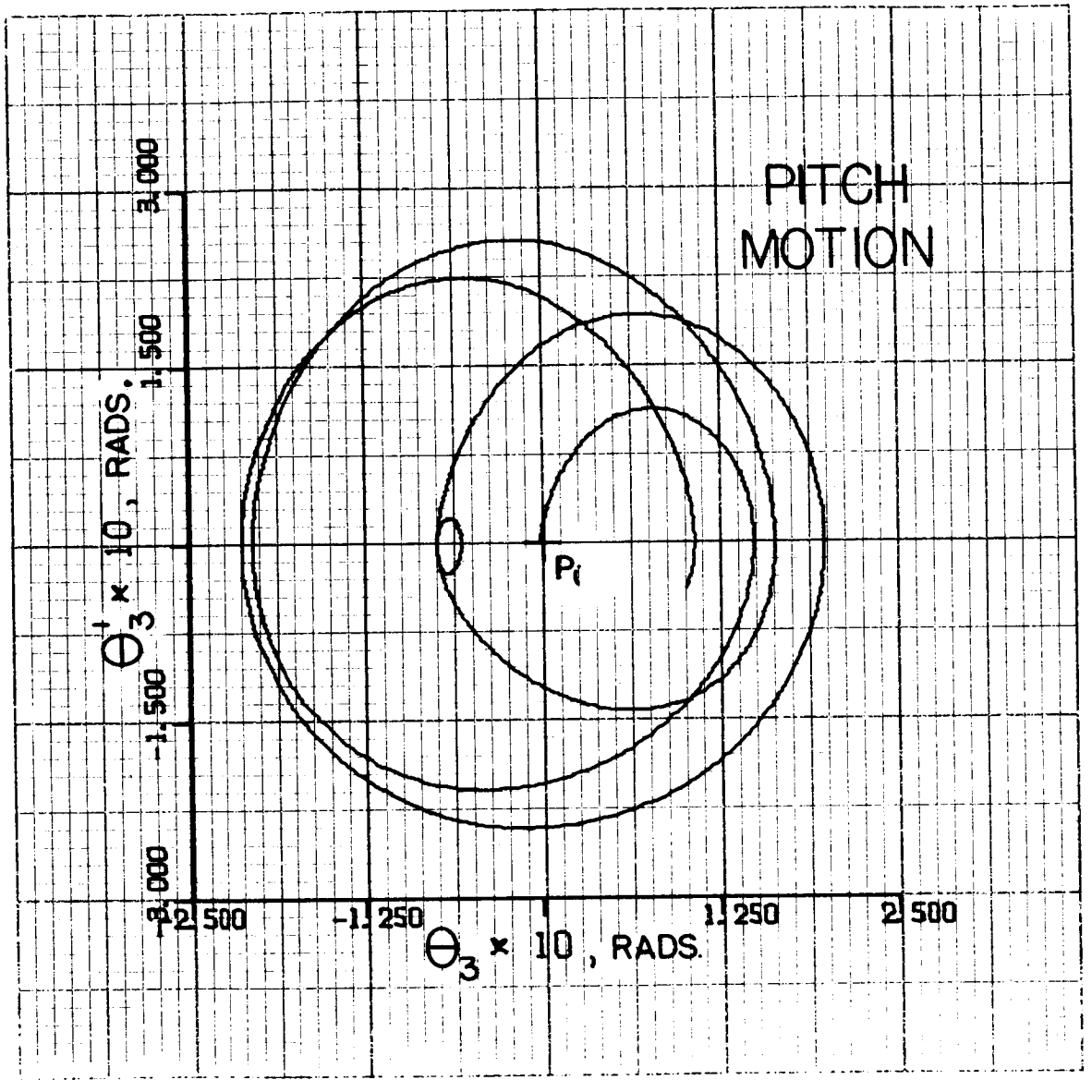

Figure 2.6 Forced Pitch Motion, e = 0.1 .

accuracy is obtained by retaining only first-degree terms.* Therefore,

$$\frac{\mu}{r^3} \approx n^2(1+3e \cos \theta) \tag{2-20}$$

$$\dot{\theta} \approx n(1+2e \cos \theta) \tag{2-21}$$

$$\ddot{\theta} \approx - 2n^2 e \sin \theta \tag{2-22}$$

Also, because of the assumption of small eccentricity, $e \sin \theta$ and $e \cos \theta$ are easily written as explicit functions of time. From Equations (2-12) and (2-13)

$$d\theta = \frac{h}{r^2} dt = n(1+e \cos \theta)^2 dt \tag{2-23}$$

Expanding in powers of e, dropping higher-degree terms, and integrating gives

$$\theta - \theta_o = nt + 2en \sin (\theta-\theta_o) \tag{2-24}$$

where $\theta = \theta_o$ at $t = 0$.

When Equation (2-24) is substituted into $e \sin \theta$ and $e \cos \theta$, only first-degree terms in e are kept. The results are simply

$$e \sin \theta = e \sin (nt+\theta_o) \tag{2-25}$$

and

$$e \cos \theta = e \cos (nt+\theta_o) \tag{2-26}$$

Substituting Equations (2-25) and (2-26) into (2-20) through (2-22) and in turn substituting these into Equations (2-17) through (2-19), produces three second-order time-varying equations that completely

---

* This is shown in Chapter V when the full equations are used.

describe the small attitude motion of an earth satellite in an elliptic orbit of small eccentricity. These equations can be written in a convenient form by introducing the dimensionless parameter τ, where

$$\tau = nt \quad \text{and} \quad ' = \frac{d}{d\tau} , \tag{2-27}$$

and the notation

$$\theta_i = x_{2i-1} , \quad \theta_i' = x_{2i} , \qquad i = 1,2,3 . \tag{2-28}$$

Then, in matrix form the attitude equations are simply

$$\bar{x}' = A(\tau)\bar{x} + \bar{g}(\tau) \tag{2-29}$$

where $\bar{x}$ and $\bar{g}(\tau)$ are the vectors

$$\bar{x}^t = [x_1\ x_2\ x_3\ x_4\ x_5\ x_6] \ * \tag{2-30}$$

and

$$\bar{g}(\tau)^t = [0\ 0\ 0\ 0\ 0\ 2e \sin(\tau+\theta_o)] \tag{2-31}$$

and $A(\tau)$ is the 6×6 time-varying matrix

$$A(\tau) = \begin{bmatrix} 0 & 1 & 0 & 0 & 0 & 0 \\ a_{21} & 0 & a_{23} & a_{24} & 0 & 0 \\ 0 & 0 & 0 & 1 & 0 & 0 \\ a_{41} & a_{42} & a_{43} & 0 & 0 & 0 \\ 0 & 0 & 0 & 0 & 0 & 1 \\ 0 & 0 & 0 & 0 & a_{65} & 0 \end{bmatrix} \tag{2-32}$$

---

* $\bar{y}^t$ denotes the transpose of $\bar{y}$.

where

$$
\begin{aligned}
a_{21} &= -k_1(1+4e\cos(\tau+\theta_o)) \\
a_{23} &= -a_{41} = -2e\sin(\tau+\theta_o) \\
a_{24} &= (1-k_1)(1+2e\cos(\tau+\theta_o)) \\
a_{42} &= -(1+k_2)(1+2e\cos(\tau+\theta_o)) \\
a_{43} &= k_2(4+13e\cos(\tau+\theta_o)) \\
a_{65} &= -3k_3(1+3e\cos(\tau+\theta_o))
\end{aligned}
\tag{2-33}
$$

These final attitude equations, which will be used throughout the next two chapters, contain only the following parameters: θ_o, which depends on the initial orbital position of the satellite; e, which depends on the shape of the orbit; and k_1, k_2, and k_3, which depend on the inertia properties of the satellite.

B. Pontryagin's Maximum Principle

Pontryagin's Maximum Principle is a useful mathematical tool for obtaining necessary conditions for optimal controls. In many cases its application is quite straightforward. However, what is obtained is the control as a function of the adjoint variable. The difficulty is in converting this control to a function of the state variable, i.e., a feedback control.

1. Statement of the Theorem

The optimal control problem consists of the following:

1) A system of differential equations

$$\dot{\bar{x}} = \bar{f}(\bar{x},\bar{u}) \tag{2-34}$$

where $\bar{x}$ is an n-dimensional state vector and $\bar{u}$ is an r-dimensional

control vector, $r \leq n$, which is restricted to an admissible set U. (U is often the set of piecewise continuous functions.)

2) Boundary conditions on the state vector,

$$\bar{x}(t_o) = \bar{x}_o \quad , \quad \bar{x}(t_f) = \bar{x}_f \tag{2-35}$$

3) A cost functional that measures the performance of the control,

$$J = \int_{t_o}^{t_f} \ell(\bar{x},\bar{u})dt \tag{2-36}$$

The optimal control is defined as that control in the set U which produces the desired boundary conditions on the state vector $\bar{x}$ and minimizes the cost functional J with respect to all other controls in U that produce the desired boundary conditions.

Pontryagin's Maximum Principle states [5] that for $\bar{u}$ to be optimal it is necessary that an n-dimensional vector function $\bar{p}$ exist such that the Hamiltonian, defined as

$$H(\bar{x},\bar{p},\bar{u}) = \bar{p}^t \cdot \bar{f}(\bar{x},\bar{u}) - \ell(\bar{x},\bar{u}) \ , \tag{2-37}$$

is a maximum as a function of $\bar{u}$ for all t, $t_o \leq t \leq t_f$. The vector function $\bar{p}$ satisfies the differential equations:

$$\dot{p}_i = - \frac{\partial H}{\partial x_i} \ , \quad i = 1,\ldots,n \ . \tag{2-38}$$

If the system equations, corresponding to Equations (2-34), are nonautonomous, i.e., time appears explicitly, they can easily be made autonomous by introducing a new variable, $x_{n+1} = t$, and adding an additional equation, $\dot{x}_{n+1} = f_{n+1}$, where $f_{n+1} = 1$. The Maximum Principle

holds for this new n+1-dimensional system, for which the Hamiltonian is

$$H_{n+1} = H_n + p_{n+1} \tag{2-39}$$

Thus, as a function of $\bar{u}$ the Hamiltonians for the two systems attain maxima for the same $\bar{u}$. Therefore, in practice the change to an autonomous system is unnecessary.

In using the Maximum Principle it must be remembered that the conditions specified by it are in general only necessary conditions. These conditions guarantee neither that the specified control is optimal (sufficiency), nor that an optimal control exists.

2. Method of Application

Maximizing the Hamiltonian gives the optimal control as an explicit function of the adjoint variable p. However, to obtain a feedback control it is necessary to have the control as a function of the instantaneous state of the system. (Since the attitude equations are time-varying, it is expected that the control will be a time-varying function of the state.) Thus, the solving of the optimal control problem reduces to the solving of 2n-differential equations,(2-34) and (2-38). However, the 2n-boundary conditions, the initial and final state of the system, are all on Equation (2-34). The conditions on the solutions of Equations (2-38) are that they must define a control, $\bar{u}(\bar{p})$, of the form dictated by the Maximum Principle that brings the system from its initial state to the desired end state in the specified amount of time.

The determination of the proper $\bar{p}$ as a function of $\bar{x}$ and t, which would determine the desired feedback control, is not in general an easy problem. One method of approach is "reverse-time"

integration. The 2n-differential equations are integrated backwards in time starting at the desired endpoint $\bar{x}(t_f)$, arbitrarily choosing $\bar{p}(t_f)$, and applying control as determined by

$$\bar{u} = \bar{u}\left(\bar{p}(t^*)\right) \tag{2-40}$$

where $t^* = (t_f - t_o) - t$, i.e., "reverse-time". The initial state of the system, $\bar{x}(t_o)$, (final state in reverse-time) will not be known a priori as it depends on the final state of the adjoint variable, $\bar{p}(t_f)$, the final time, t_f , and the time of solution, $t_f - t_o$. If a sufficient number of these variables are chosen, the resulting initial states will constitute a good coverage of the possible initial states. A careful study of the control behavior and/or the adjoint initial conditions will produce in some cases the optimal control law and in many cases a good suboptimal control law. This reverse-time method will be used in the following two chapters.

C. Optimal Attitude Control of a Satellite

To provide attitude control torques it is assumed that there are three pairs of oppositely-directed cold-gas jets, each pair possessing a maximum torque level. The three pairs of jets are aligned such that the equations of the controlled attitude-motion have the following form:

$$\bar{x}' = A(\tau)\bar{x} + \bar{g}(\tau) + B\bar{u}^* \tag{2-41}$$

where

$$B = \begin{bmatrix} 0 & 0 & 0 \\ 1 & 0 & 0 \\ 0 & 0 & 0 \\ 0 & 1 & 0 \\ 0 & 0 & 0 \\ 0 & 0 & 1 \end{bmatrix}$$

and $\bar{u}^* = (u_1^* \; u_2^* \; u_3^*)$ with the restriction that $|u_i^*| \leq N_i^*$, $i = 1,2,3$.

1. Performance Criterion

As stated in the Introduction, the performance of the control system will be judged on the amount of fuel consumed. This "minimum-fuel" performance criterion is described mathematically by the functional

$$J = \int_{\tau_o}^{\tau_f} \sum_{i=1}^{3} |u_i^*| d\tau \tag{2-42}$$

The $\bar{u}^*$ that minimizes this functional is the desired control.

2. Optimal Control Law

The Hamiltonian for this system is given by

$$\begin{aligned} H &= \bar{p}^t \cdot \dot{\bar{x}} - \ell(\bar{x}, \bar{u}^*) \\ &= \bar{p}^t A\bar{x} + \bar{p}^t \cdot \bar{g} + \bar{p}^t B\bar{u}^* - \sum_{i=1}^{3} |u_i^*| \\ &= H^* + \text{terms not involving } \bar{u}^* \end{aligned} \tag{2-43}$$

Thus, for $\bar{u}^*$ to be optimal it is necessary that H^* be a maximum as a function of $\bar{u}^*$, where

$$\begin{aligned} H^* &= \bar{p}^t B\bar{u}^* - \sum_{i=1}^{3} |u_i^*| \\ &= p_2 u_1^* + p_4 u_2^* + p_6 u_3^* - |u_1^*| - |u_2^*| - |u_3^*| \end{aligned} \tag{2-44}$$

H^* is maximized when $\bar{u}^*$ is the following "coast function" of $\bar{p}$:

$$u_i^* = N_i^* \, \text{CST} \, p_{2i}, \quad i = 1,2,3 \tag{2-45}$$

$$= \begin{cases} N_i^* \, \text{SGN} \, p_{2i} & \text{for } |p_{2i}| > 1 \\ 0 & \text{for } |p_{2i}| < 1 \end{cases} \tag{2-46}$$

where

$$\text{SGN } y = \frac{y}{|y|} \tag{2-47}$$

and the adjoint vector $\bar{p}$ satisfies the equation

$$\bar{p}' = - A^t \bar{p} \tag{2-48}$$

The above relations define the desired optimal control as a discontinuous function of time. The problem that remains is to determine this control as a function of the instantaneous state of the system.

III. PITCH ATTITUDE CONTROL

The linearized pitch equation is decoupled from the linearized yaw and roll equations and, therefore, can be considered separately. The pitch equation is

$$x_5'' = -3k_3\left(1 + 3e\cos(\tau+\theta_o)\right)x_5 + 2e\sin(\tau+\theta_o) + u_3^* \qquad (3\text{-}1)$$

A. Uncontrolled Linearized Pitch Equation

Equation (3-1) without the control u_3 has the form of Mathieu's Equation with a small, periodic forcing-function. The stability of the solutions to such an equation does not guarantee in-the-large stability of the pitch motion, since Equation (3-1) is a linearized version of the pitch equation. However, it is still sensible to choose the parameter k_3 such that the linearized equation is stable.

Since the forcing function is small and periodic, the forced and unforced motions of the uncontrolled pitch equation are fairly similar, except in steady state. In the phase plane, although the motions are at times somewhat far apart, the overall trajectories are basically of the same shape (see Figure 3.1). Thus, one may hope to obtain a good idea of the stability of the linearized motion by considering the stability of the solutions to Mathieu's Equation, which has the form

$$\ddot{x} + (\delta+\epsilon\cos t)x = 0 \qquad (3\text{-}2)$$

The value of the inertia parameter k_3 that was chosen, based on the stability considerations in Chapter II, is 0.85. For this value of k_3 the Mathieu Equation parameters are $\delta = 3k_3 = 2.55$ and $\epsilon = 9k_3e = 7.65e$.

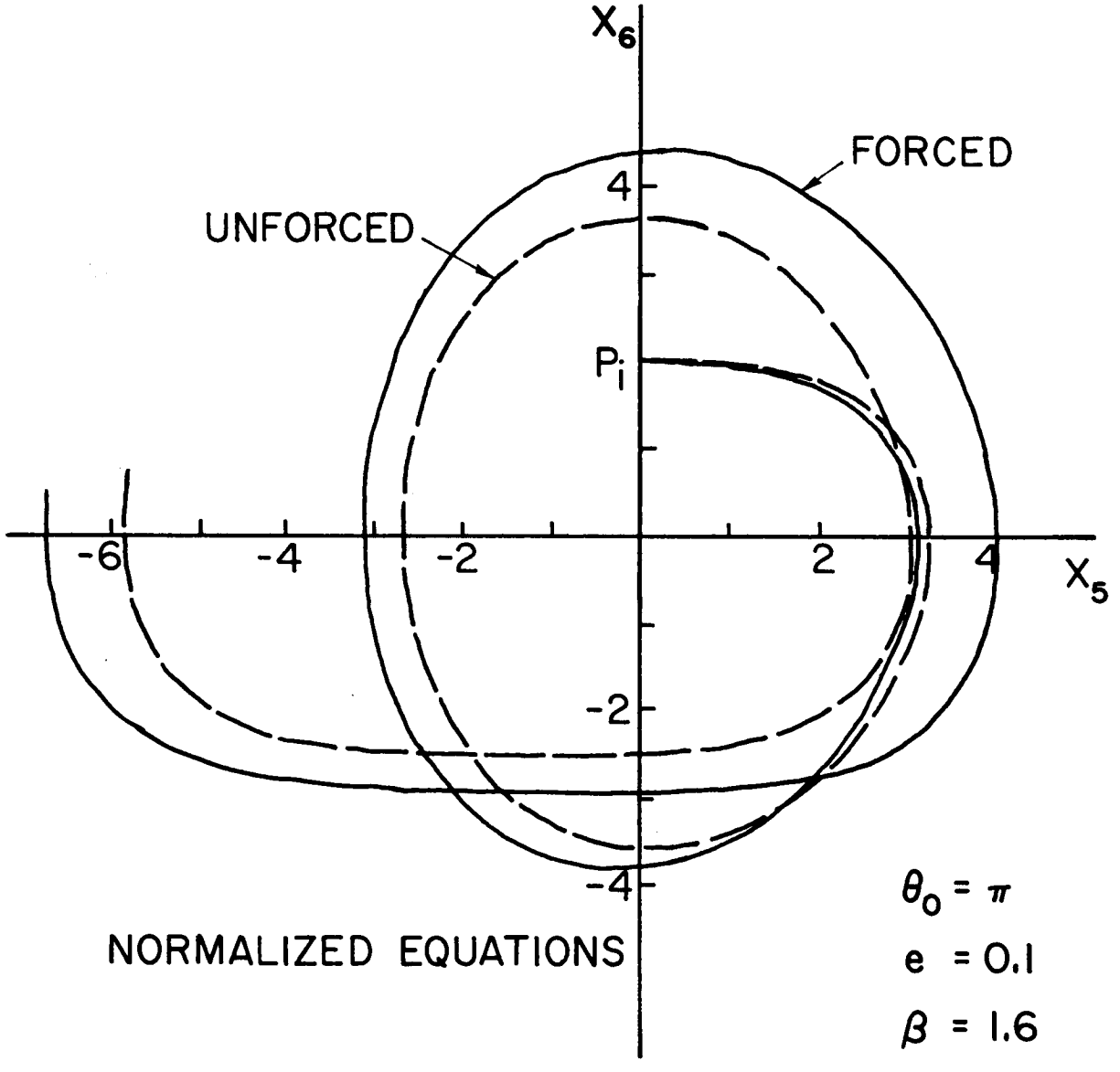

Figure 3.1 Pitch Motion, Forced and Unforced

From the stability chart for Mathieu's Equation [12], the equation is stable for these parameter values for a larger range of eccentricity ($0 \le e \le 0.22$) than is being considered here. Therefore, in the following 0.85 will be used as the nominal value for k_3 .

B. Optimal Pitch Control

Even for small ϵ the phase plane trajectories of the solutions to Mathieu's Equation may deviate considerably in shape from the trajectories of the solutions to the simple pendulum equation ($\epsilon = 0$)* . This is clearly illustrated in Figure 3.2. Thus, the form of the optimal switching lines for Equation (3-1) may be quite different from those for the pendulum equation.

For ease in handling Equation (3-1), a new dimensionless variable $\tilde{\tau}$ will be defined. Let $\tilde{\tau} = n\beta t$ where $\beta^2 = 3k_3$. Then Equation (3-1), written as two first order equations, becomes

$$x_5' = x_6$$
$$x_6' = -\left(1 + 3e \cos\left(\frac{\tilde{\tau}}{\beta} + \theta_o\right)\right) x_5 + \frac{2e}{\beta^2} \sin\left(\frac{\tilde{\tau}}{\beta} + \theta_o\right) + u_3 \qquad (3\text{-}3)$$

where $u_3 = u_3^*/\beta^2$ and $' = d/d\tilde{\tau}$.

With this change in the time scale, the cost functional for u_3 becomes

$$J_3 = \int_{\tilde{\tau}_o}^{\tilde{\tau}_f} |u_3| d\tilde{\tau} \qquad (3\text{-}4)$$

---

* The simple pendulum is equivalent to a $1/(s^2+1)$ plant, i.e., the phase plane trajectories are circles.

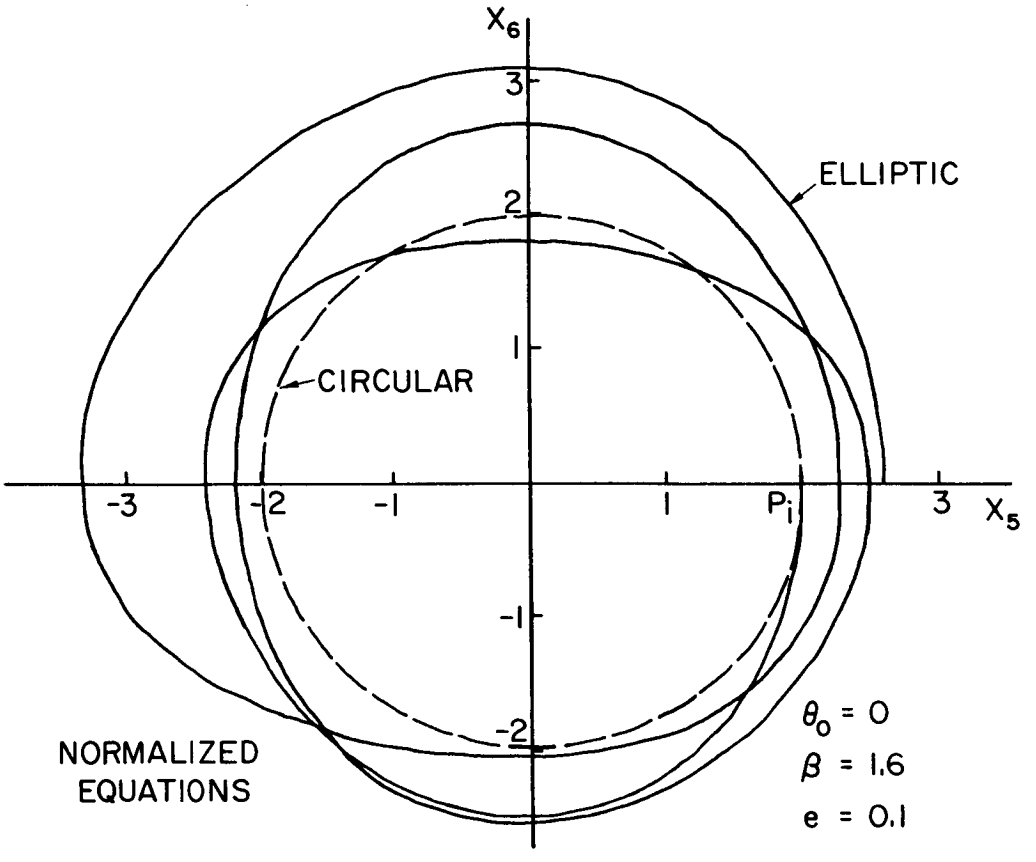

a. e = 0.1

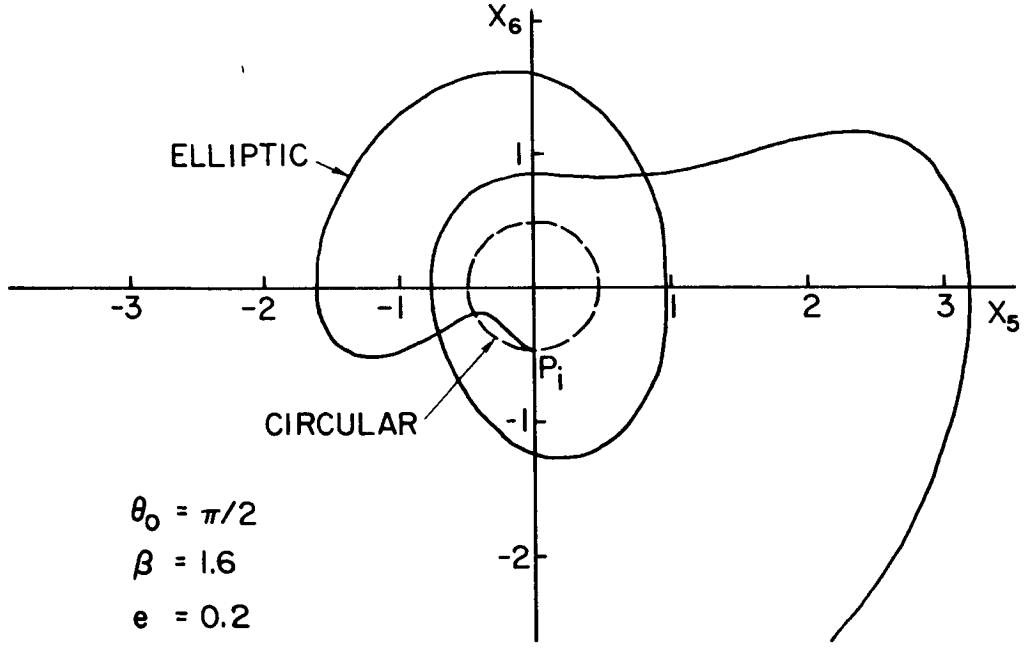

b. e = 0.2

Figure 3.2 Pitch Motion, Elliptic and Circular Orbits.

Thus, as shown in Chapter II, the optimal control with respect to a minimum-fuel performance criterion must satisfy the relation

$$u_3 = N_3 \text{ CST } p_6 \tag{3-5}$$

where $N_3 = N_3^*/\beta^2$ and p_6 satisfies the normalized Mathieu Equation,

$$p_6'' + 1 + 3e \cos(\tilde{\tau}/\beta + \theta_o)\, p_6 = 0 \tag{3-6}$$

Equations (3-5) and (3-6) show that the form of the optimal control as a function of time is not affected by the presence of the forcing function. The only change in the optimal control due to the forcing function is a slight change in the initial conditions on the adjoint equation, with a corresponding shift in the switching times, to guarantee that the origin is reached. Since the forcing function is fairly small and periodic, these variations will not be large. Therefore, the forcing function will be neglected in the remainder of this chapter. Further reasons and justifications are contained in the last section of the chapter. The forcing function will later be included when three-axis and steady-state control are considered (Chapter V).

The optimal control is a coast function of a solution to the normalized Mathieu equation. From Figure 3.3, a phase plane plot of a solution to Equation (3-6), it is apparent that the control need not be of alternate signs separated by dead zones as for the simple pendulum. The dead zones are always present, but it is possible to have a "skipped" control-on interval, i.e., the control-on intervals on each side of a control-off interval are of the same sign. However, this occurs only when the time of solution is sufficiently large, i.e., the initial conditions on the adjoint variables are small.

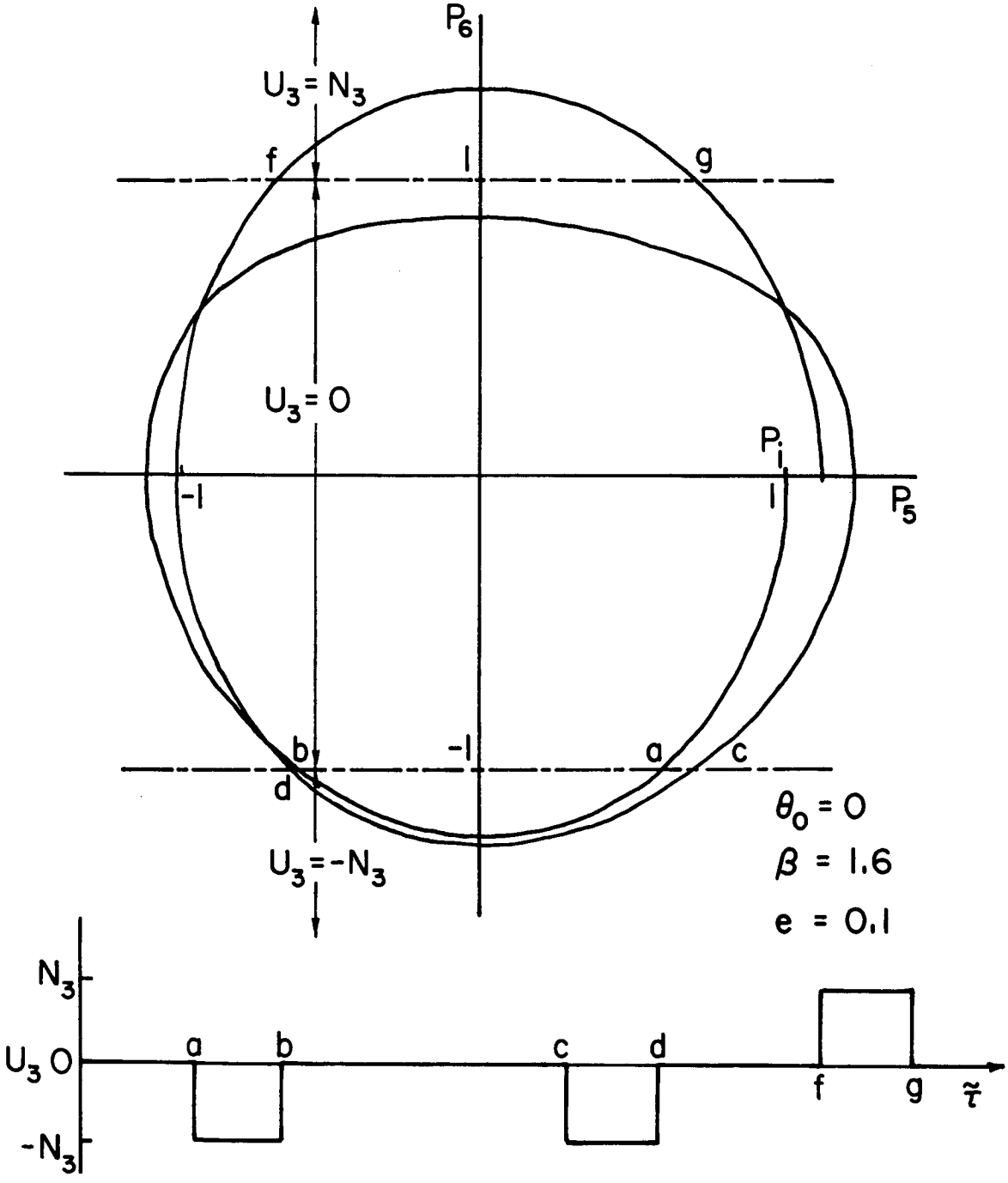

Figure 3.3 Adjoint-Equation Solution and Corresponding Control.

1. Reverse-Time Solutions

A systematic search for the optimal switching surfaces was made on an analog computer by running the system in reverse time,

$$\tau^* = \tilde{T} - \tilde{\tau} , \tag{3-7}$$

where $\tilde{T}$ is the time of solution $\tilde{\tau}_f - \tilde{\tau}_o$. In reverse-time the modified pitch equations and the adjoint equations are

$$\begin{aligned} \frac{dx_5}{d\tau^*} &= - x_6 \\ \frac{dx_6}{d\tau^*} &= \left(1 + 3e \cos\left(\frac{\tau^*}{\beta} - \frac{\tilde{T}}{\beta} - \theta_o\right)\right) x_5 - u_3 \end{aligned} \tag{3-8}$$

$$\begin{aligned} \frac{dp_5}{d\tau^*} &= \left(1 + 3e \cos\left(\frac{\tau^*}{\beta} - \frac{\tilde{T}}{\beta} - \theta_o\right)\right) p_6 \\ \frac{dp_6}{d\tau^*} &= - p_5 \end{aligned} \tag{3-9}$$

A series of runs was made for various values of θ_o, $\tilde{T}/\beta$, $\bar{p}(\tilde{\tau}_f)$, e, and k_3 as given in Table 1. The time of solution $\tilde{T}$ was restricted to less than twice the orbital period of the satellite. One orbital period is equivalent to $\tilde{T}/\beta = 2\pi$.) Also, $\tilde{\tau}_o$ was taken to be zero so that θ_o represents the location of the satellite in its orbit at the time of the disturbance, $\theta_o = 0$ and π corresponding to the perigee and apogee, respectively. Some representative reverse-time phase-plane trajectories, that were drawn by an x - y plotter from the output of the analog computer, are shown in Figures 3.4 - 3.6.*

* The scaling for all of the computer solutions is based on the representative satellite configuration given in Appendix A.

TABLE 3.1

VALUES USED FOR REVERSE-TIME OPTIMAL RUNS

θ_o	$\tilde{T}/\beta$	$\bar{p}(\tilde{\tau}_f)^*$	e	k_3
0	$\pi/2$	$\pm(0,1.5)$	0.05	0.5
$\pi/4$	π	$\pm(.5,1)$	0.075	0.67
$\pi/2$	$3\pi/2$	$\pm(.25,1)$	0.10	0.85
$3\pi/4$	2π	$\pm(1,1)$	0.125	1.0
π	3π		0.15	
$3\pi/2$			0.175	
			0.20	

* The scaling is such that $N_3 = 1.0$.

2. Characteristics of the Optimal Control

The many reverse-time examples that were run on the analog computer, such as Figures 3.4 through 3.6, showed that the optimally controlled trajectories have the following characteristics: almost all "control-on" intervals cross the x_6-axis; when on, $u_3 = - N_3 \text{ SGN } x_6$, except in a few short intervals which occur only with the larger eccentricities in Table 1 (Figure 3.6); and, almost all "control-off" intervals cross the x_5-axis. These are the same general characteristics exhibited by the optimal controller for the simple pendulum [7]. However, in contrast to the simple pendulum equation, no simple form for the switching curves for Equation (3-1) can be recognized. The "control-on" intervals exhibit no uniformity or symmetry, and odd behavior such as the "skipped" control-on interval can occur (Figure 3.5).

The behavior of the optimal controller was studied in more detail by considering the location of the switching points in the phase plane and cost versus error-magnitude curves for various initial and total times. Figures 3.7a and 3.7b are plots of optimal cost J_3 versus initial error magnitude R_o, where

$$R_o^2 = [x_5(\tilde{\tau}_o)]^2 + [x_6(\tilde{\tau}_o)]^2 , \qquad (3\text{-}10)$$

for eccentricities of 0.1 and 0.2, respectively. In Figure 3.7a all points are closely clustered about a straight line. Thus, the initial

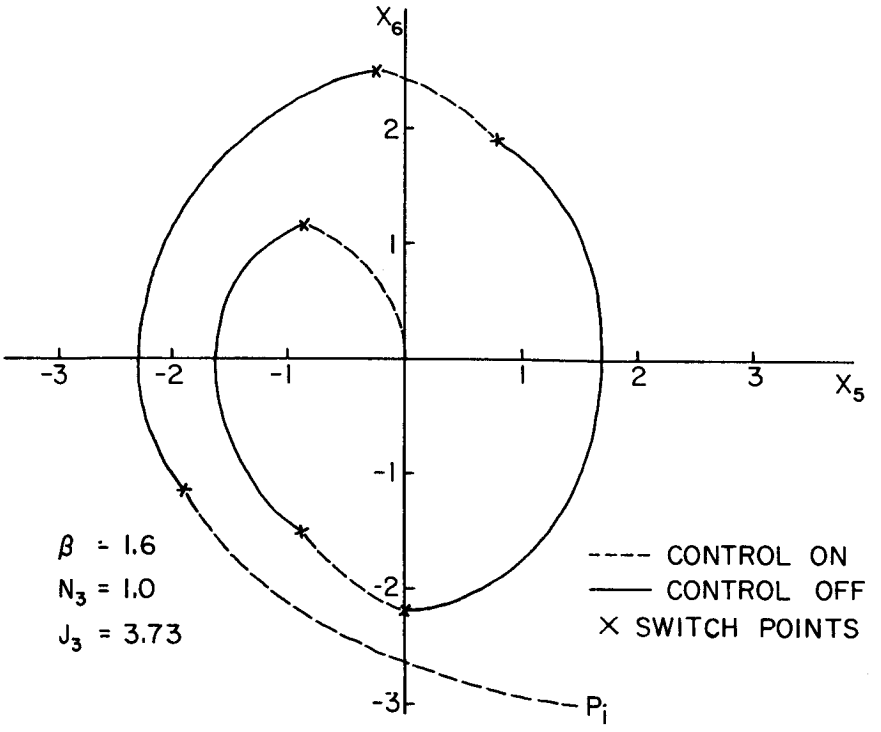

a. $\theta_o = \pi$, $\tilde{T} = 2\pi\beta$

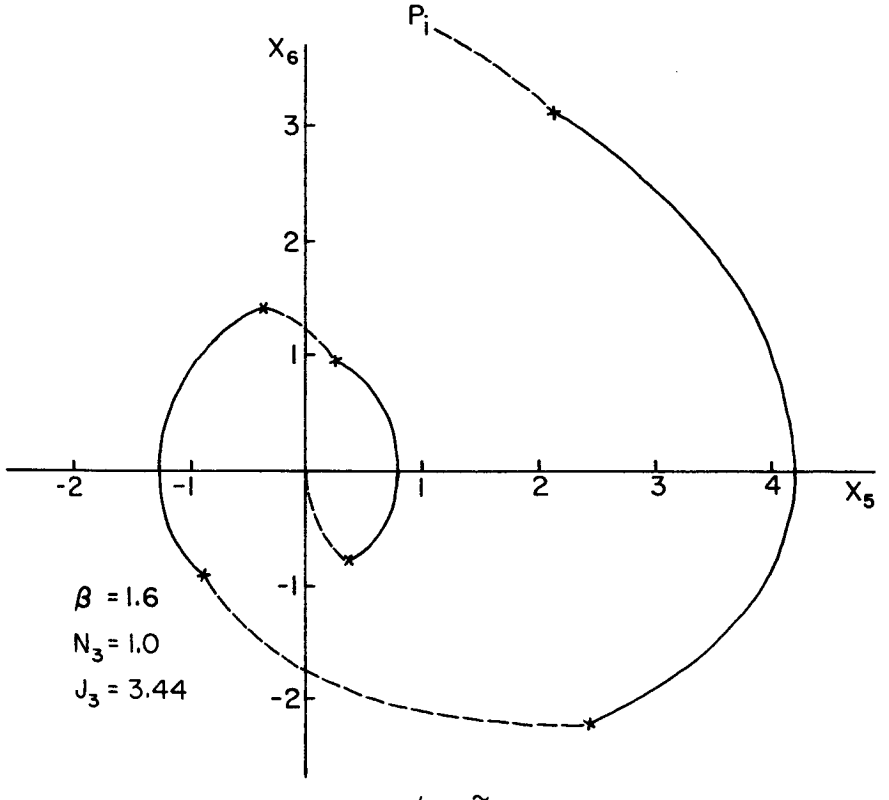

b. $\theta_o = 3\pi/2$, $\tilde{T} = 2\pi\beta$

Figure 3.4 Reverse-Time Optimal Trajectories, e = 0.1 .

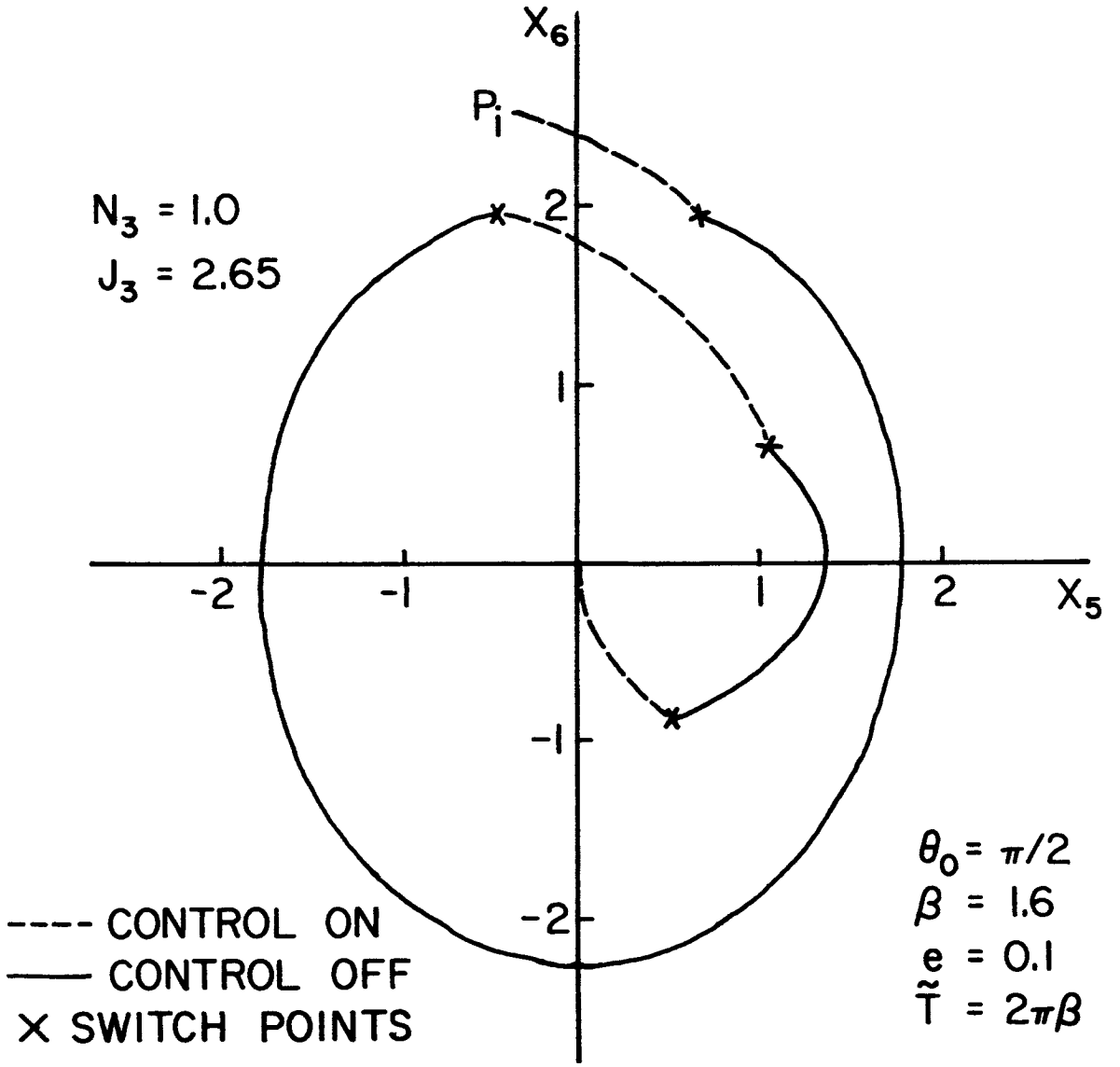

Figure 3.5 Reverse-Time Optimal Trajectory, Skipped Control Interval.

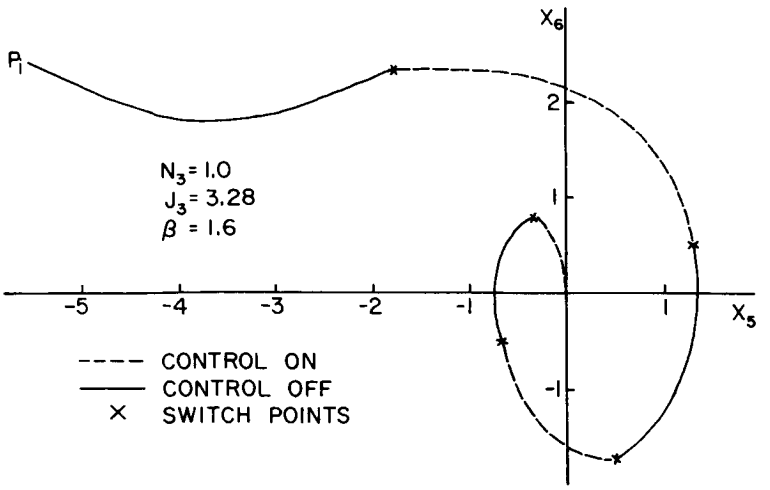

a. $\theta_o = 0$, $\tilde{T} = 3\pi\beta/2$

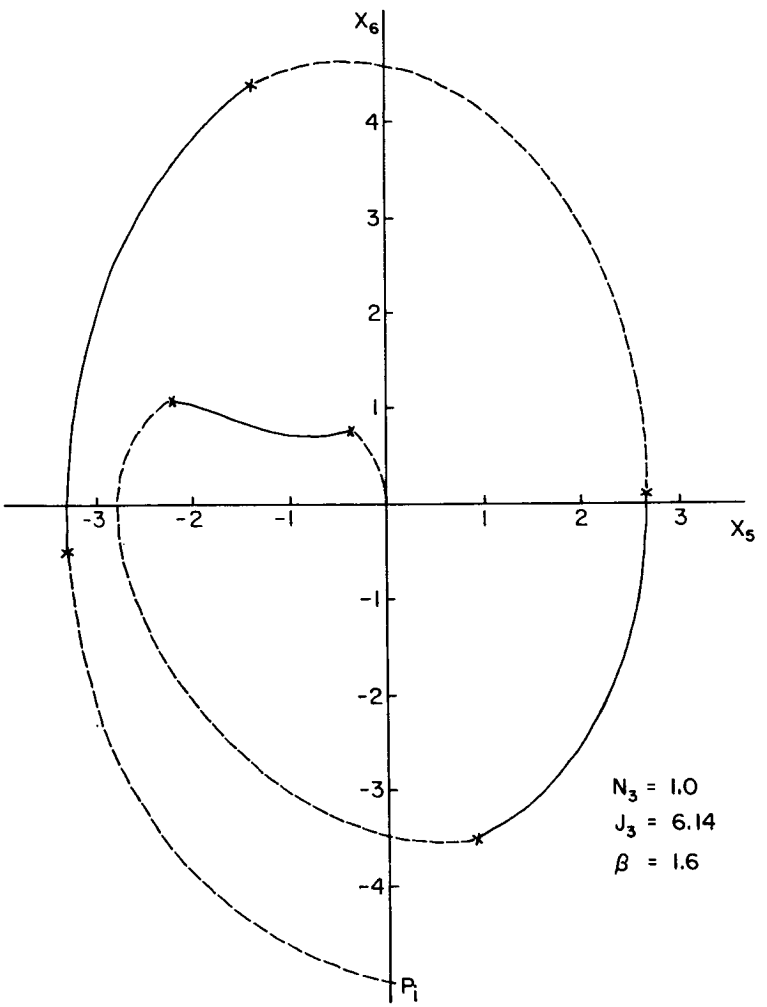

b. $\theta_o = \pi/2$, $\tilde{T} = 2\pi\beta$

Figure 3.6 Reverse-Time Optimal Trajectories, e = 0.2 .

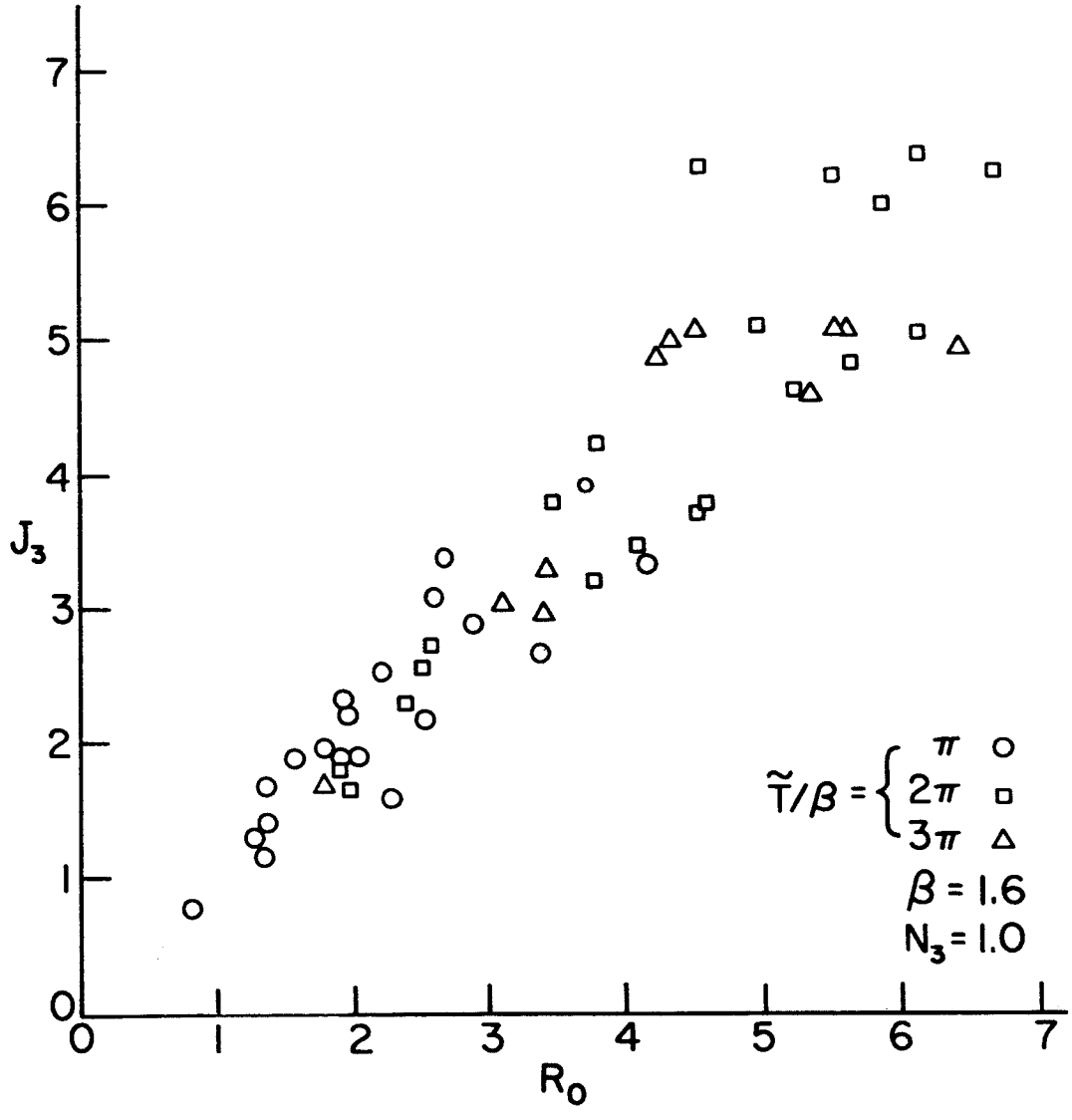

a. e = 0.1

Figure 3.7 Optimal Cost vs. Error Magnitude

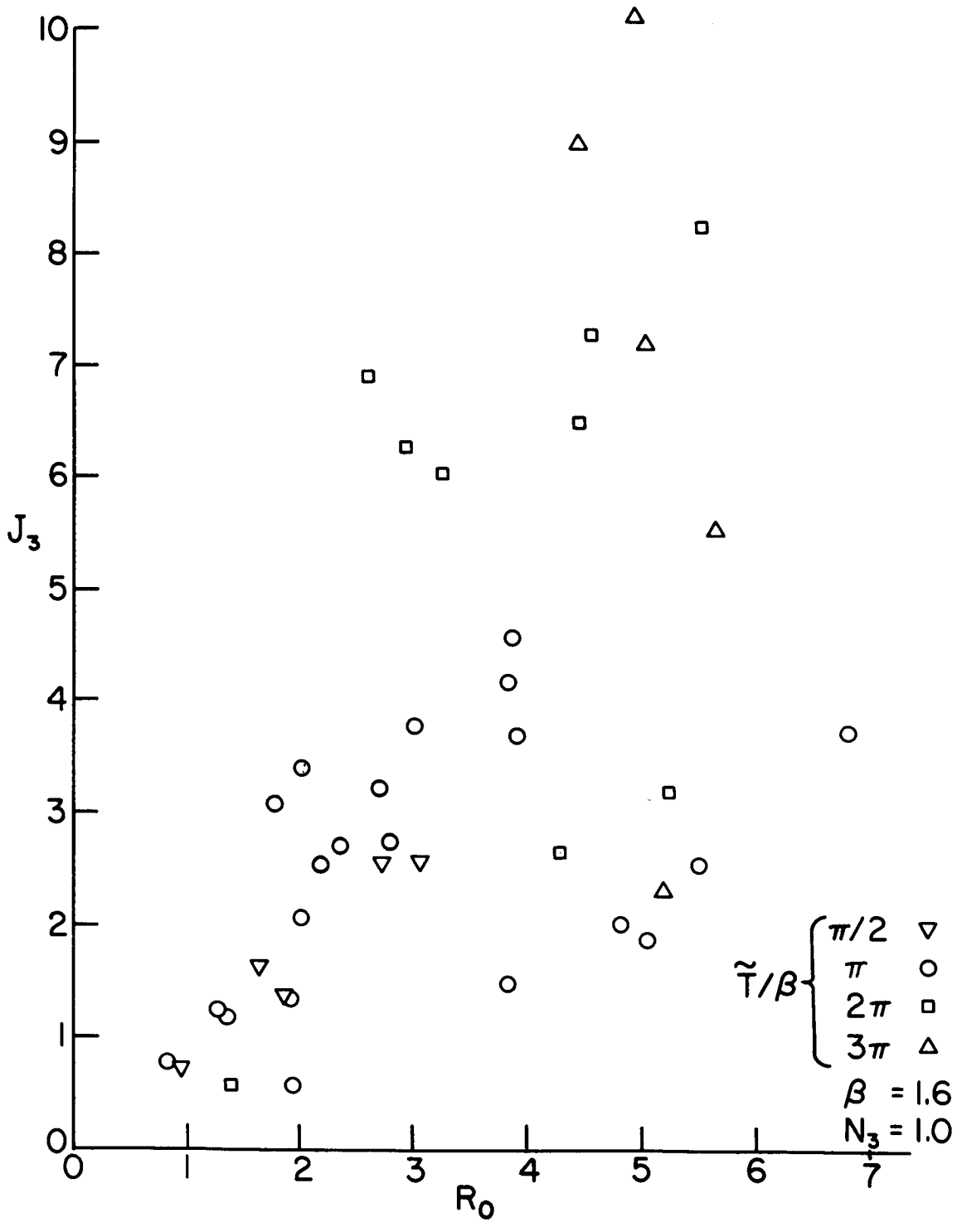

b. e = 0.2

Figure 3.7 (continued)

time and phase plane location do not appreciably affect the cost for a given error magnitude. Also, the symbols indicating the three solution times show, in most cases, the expected effect: a decrease in fuel consumption for an increase in time for a given initial error. Figure 3.7b shows that these statements are no longer true when the eccentricity is increased to 0.2. Now, in many cases the cost is not proportional to the time of solution for a given error magnitude (this is readily apparent at $R_o = 0.3$ in Figure 3.7b), so the cost is appreciably affected by the time of the occurrence and the phase plane location of the initial error. This behavior is largely due to the uncontrolled motions that have nearly constant velocity for an extended period of time, as in Figure 3.2b. Depending on its direction, this type of motion can greatly help or hinder the controller (see Figure 3.8).

Figure 3.9 shows the control-on intervals in the upper half of the phase plane for runs with an eccentricity of 0.1. (The intervals in the lower half are symmetrical with respect to the origin since the adjoint and system equations are linear and piecewise linear, respectively.) Since the control is a time-varying function of the state, no simple switching curve is apparent in this figure. However, many of the switch-on points lie very nearly on a parabola, particularly in the vicinity of the origin. The points that do not lie near this parabola are approximately half on one side of it and half on the other. In a similar plot for runs with an eccentricity of 0.2 the switch points were much more scattered except very near the origin where they again were clustered

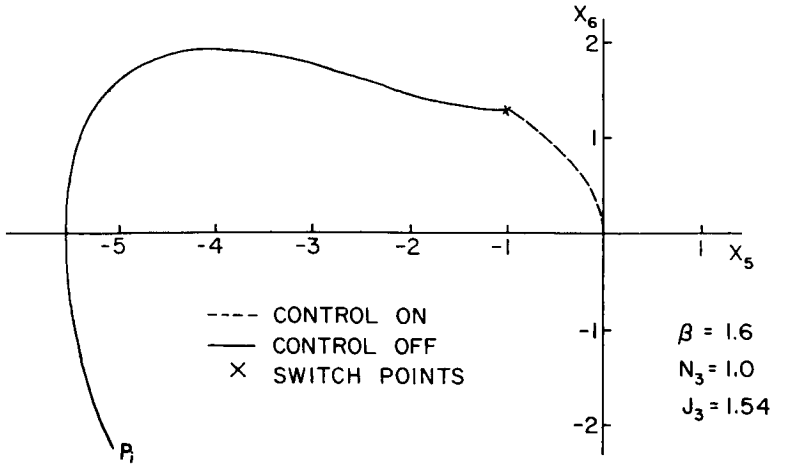

a. Controller Helped; $\theta_o = -\pi/2$, $\tilde{T} = \pi\beta$

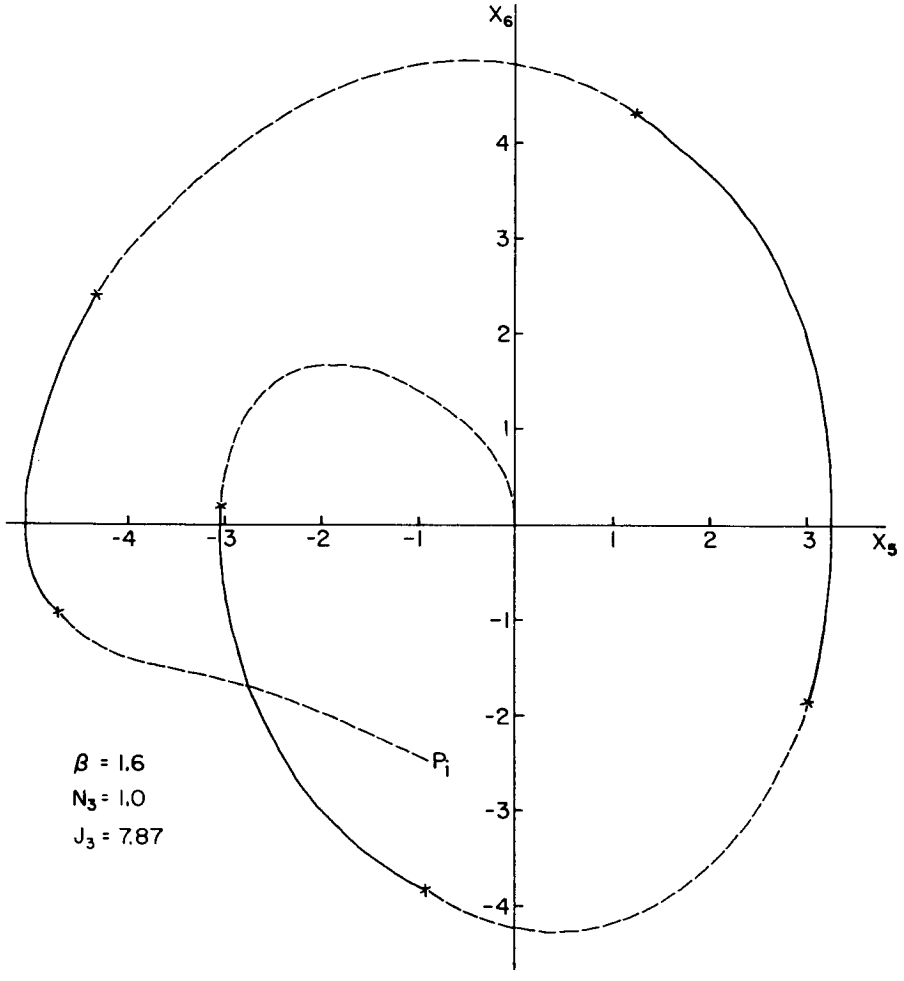

b. Controller Hindered; $\theta_o = 3\pi/4$, $\tilde{T} = 9\pi\beta/4$

Figure 3.8 Reverse-Time Optimal Trajectories, e = 0.2

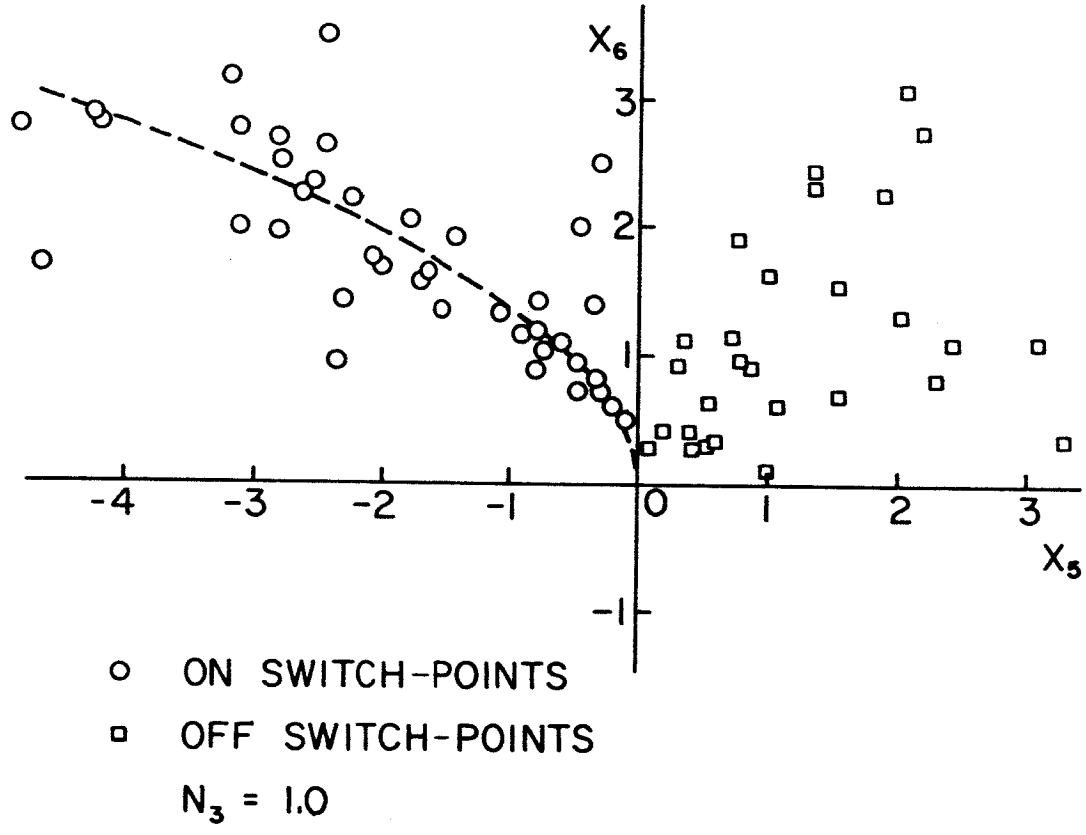

a. Optimal Switch Points, e = 0.1

Figure 3.9 Optimal Switching

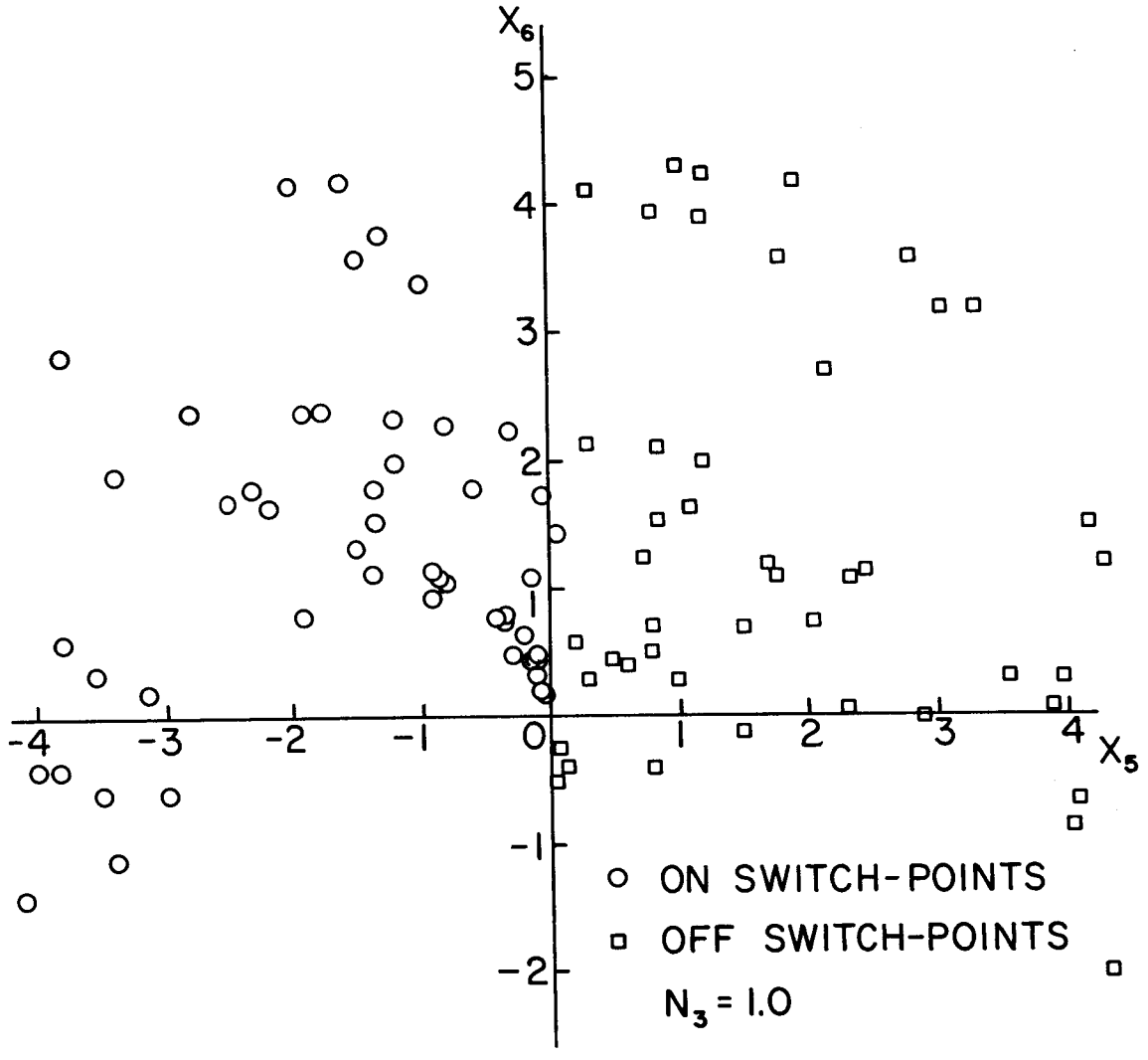

b. Optimal Switch Points, e = 0.2

Figure 3.9 (continued)

along a parabola. Since the last switch point for an optimally controlled motion always lies on a trajectory that passes through the origin, it is logical that these points would lie on a curve having approximately the shape of an arc of a circle or a parabola.

The above considerations make it apparent that it will be considerably more difficult to realize a near optimal controller for eccentricities around 0.2 than for smaller eccentricities.

C. Suboptimal Pitch Control

Further study of the adjoint initial conditions and the switching points for various initial and final times failed to reveal the state and time dependence of the optimal switching curves. Thus, the characteristics of the optimal control that were discussed in the preceding section will now be used as a basis for developing a suboptimal pitch control system.

1. Selection of the System

As discussed in the last section, many of the optimal "switch-on" points occurred on or near a parabola through the origin of the phase plane. Also, Figure 3.9 shows that in many cases the length in time of the control-on intervals is longest while the error magnitude is large. (The intervals are of constant length in time for the $1/(s^2+1)$ plant.) Thus, a parabola appears to be a good choice for the switch-on portion of the suboptimal switching curve.

The switch-off points are much more scattered than the switch-on points, so a choice for this portion of the switching curve is not so obvious. Other considerations must be taken into account. One of these

is that besides being efficient the control system should be as simple as possible, i.e., easy to realize. Computer realization of the switching curves is greatly simplified if the curves are symmetric with respect to the phase plane axes and are constant with time. For this reason, and because it fits the switch-off points about as well as any other simple curve, a parabola will also be used for the switch-off portion of the suboptimal switching curve. Therefore, the chosen suboptimal pitch control system has the form

$$u_3 = \begin{cases} -N_3 \, CST \, x_6 & \text{for } x_6^2 > b|x_5| \\ 0 & \text{for } x_6^2 < b|x_5| \end{cases} \qquad (3\text{-}11)$$

where b is a constant whose value is yet to be determined. The phase plane switching curves for this system are shown in Figure 3.10. The computer realization of this control system is described in Appendix C.

2. Optimization of the System Parameter

Ten representative optimal solutions for disturbances of various magnitudes (see Table 2) that occurred at five different locations on the orbit, as shown in Figure 3.11, were selected from the many reverse-time solutions. These ten solutions were used to determine the best value for the suboptimal-control-system parameter b. An initial choice for b was made by curve fitting a parabola to Figure 3.9a such that it passed through the largest concentrations of optimal switching points. The resulting value for the parameter was 2.0. To determine the merit of this choice, each of the ten initial conditions of Table 2 was controlled using the suboptimal control system with various values of b near and at the initial choice. These values ranged from 0.5 to 2.5 in steps of

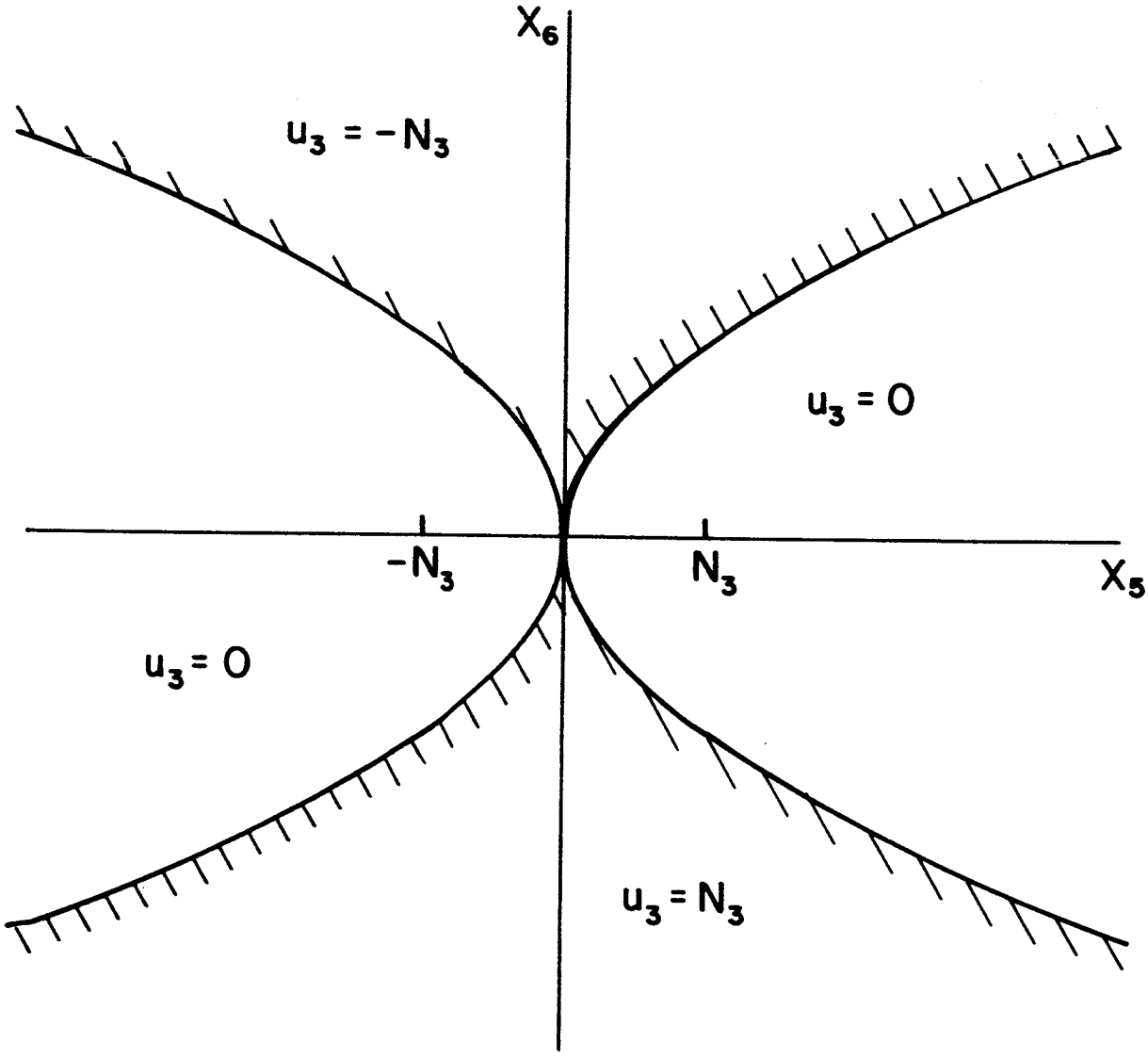

Figure 3.10 Suboptimal Switching Lines

TABLE 3.2

REPRESENTATIVE TEST RUNS $e = 0.1$ and $\beta = 1.6$

Run	θ_o	$\tilde{T}/\beta$	X_{50}*	X_{60}*	$\bar{p}(\tilde{\tau}_f)$*
1	0	π	1.70	- 0.33	(0,1.5)
2	π	2π	1.45	- 2.98	(0,1.5)
3	π	π	3.20	- 0.23	(0,1.5)
4	0	2π	- 0.05	- 4.53	(.5,1.0)
5	$\pi/2$	π	1.01	0.73	(.5,1.0)
6	$3\pi/2$	2π	- 0.85	- 3.60	(.5,1.0)
7	$3\pi/2$	π	0.67	1.84	(.5,1.0)
8	π	2π	0.36	- 2.48	(.5,1.0)
9	$3\pi/4$	π	1.46	1.37	(.5,1.0)
10	$3\pi/4$	2π	1.11	- 3.06	(.5,1.0)

* The scaling is such that $N_3 = 1.0$

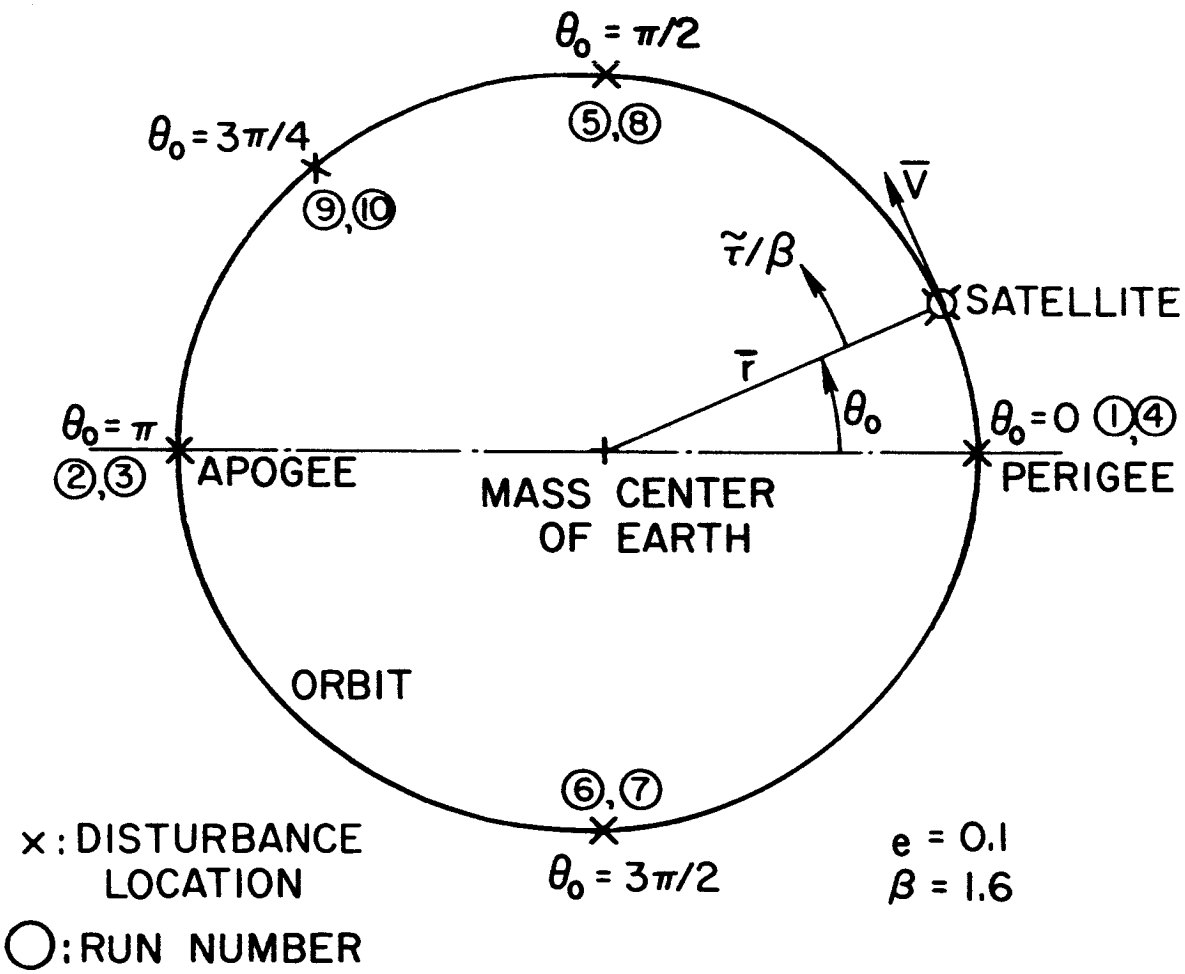

Figure 3.11 Orbit Locations of Representative Disturbances.

0.25. In each case the cost and control-time was compared to the optimal solution; the results are presented in Figure 3.12.

Figure 3.12 shows that in only one case, case (5), was the control system quite inefficient; the increase in cost over the optimal was never less than twenty percent*. In two cases, (cases (3) and (9)), the system was very efficient; for some values of b the cost was less than for the optimal solution. (The time of solution was, however, somewhat longer.) In the remaining test cases reasonably good efficiency can be obtained by the proper choice of the parameter b. In making this choice, both cost and time of solution must be considered. Figure 3.12 also shows that in most cases the cost decreases and the time increases as b is increased. However, for the larger values of b the increase in time is much more significant than the decrease in cost. The desired control times were chosen when the reverse-time optimal solutions were run, and, therefore, the suboptimal solutions should have approximately the same control times. Taking this into account, the best performance of the suboptimal control system was obtained when b was equal to 1.75. This is quite close to the original choice found from Figure 3.9.

3. Comparison to the Optimal Control

With the selected value of b, the average increase in cost over the optimal for the test runs was only 9.0 percent. Also, the control times were in most cases approximately equal to those for the optimal solutions. To further check the performance of the suboptimal

---

* The large jump in cost in case (5) is due to the increase in control time. The additional uncontrolled interval occurred at a bad time so the error grew considerably before the control was again turned on.

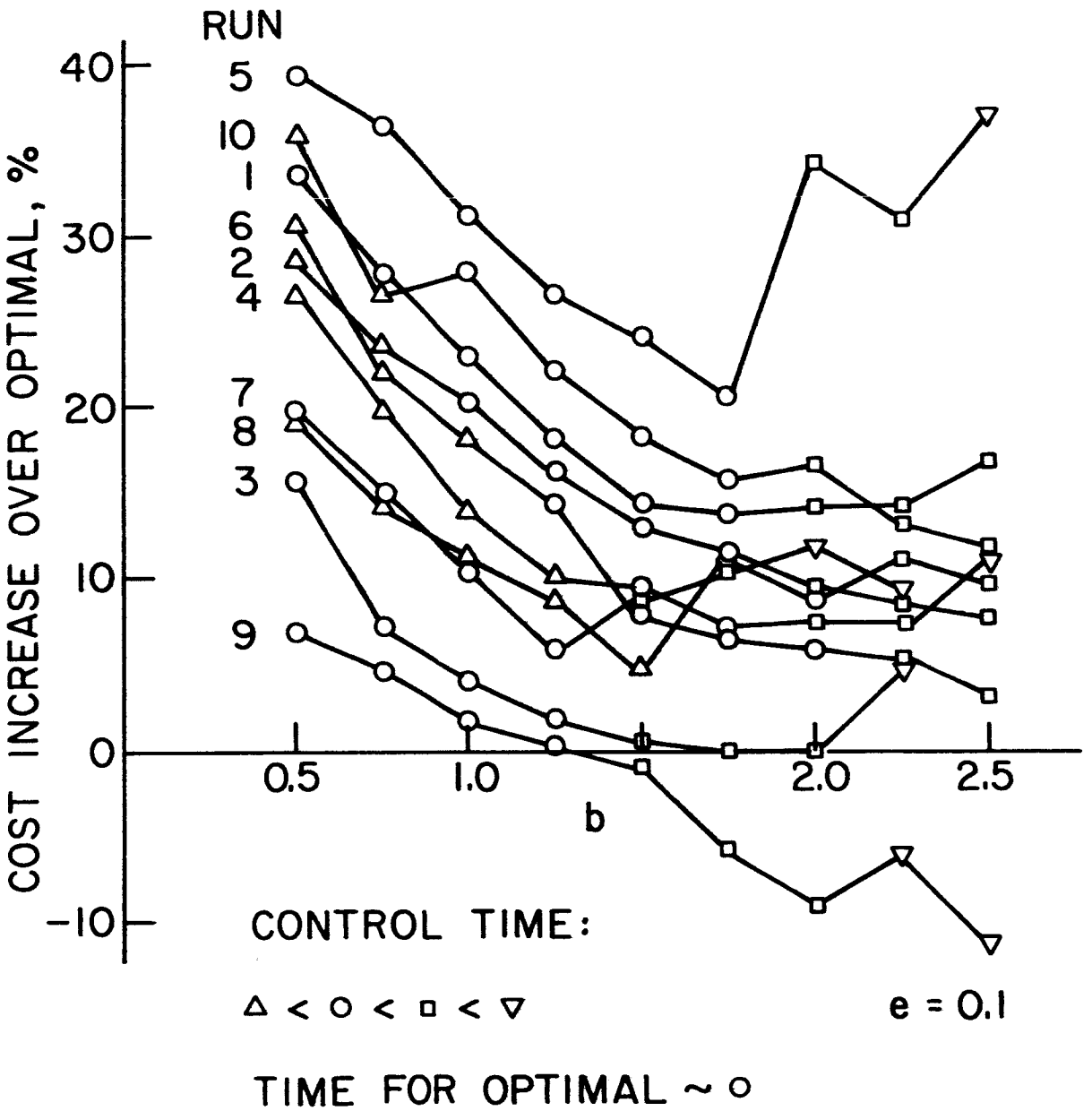

Figure 3.12 Cost Increase vs. Control Coefficient

control system it was used to control a large variety of initial conditions. Figure 3.13 is a plot of cost J versus initial error magnitude R_o for these runs. The shaded region is the region which contained practically all such points for the reverse-time optimal runs (see Figure 3.7). Since most of the suboptimal solutions lie within the same region as the optimal solutions, the overall performance of the suboptimal control system compared to the optimal control system is very good.

Direct comparisons of optimally and suboptimally controlled trajectories with the same initial conditions, as in Figure 3.14 show that the phase plane locations of the switching points for the two control systems do not differ a great deal. They also show one reason for the increase in cost with the suboptimal system. In 70% of the test cases the error magnitude during control was kept smaller by the suboptimal system than by the optimal system, as shown in Figure 3.14 Since this is a desirable characteristic, the additional fuel consumption of the suboptimal system is not entirely wasted.

Additional requirements on the controller, such as minimizing the error during control, naturally force it to expend more fuel. Thus, in effect the control system (3-11) is also a near optimal pitch control system for a performance criterion of the form:

$$J = \int_{t_o}^{t_f} (|u| + k|R_o|)dt \qquad (3\text{-}12)$$

where $k < 1$, i.e., the fuel consumption is weighted more heavily than the error magnitude.

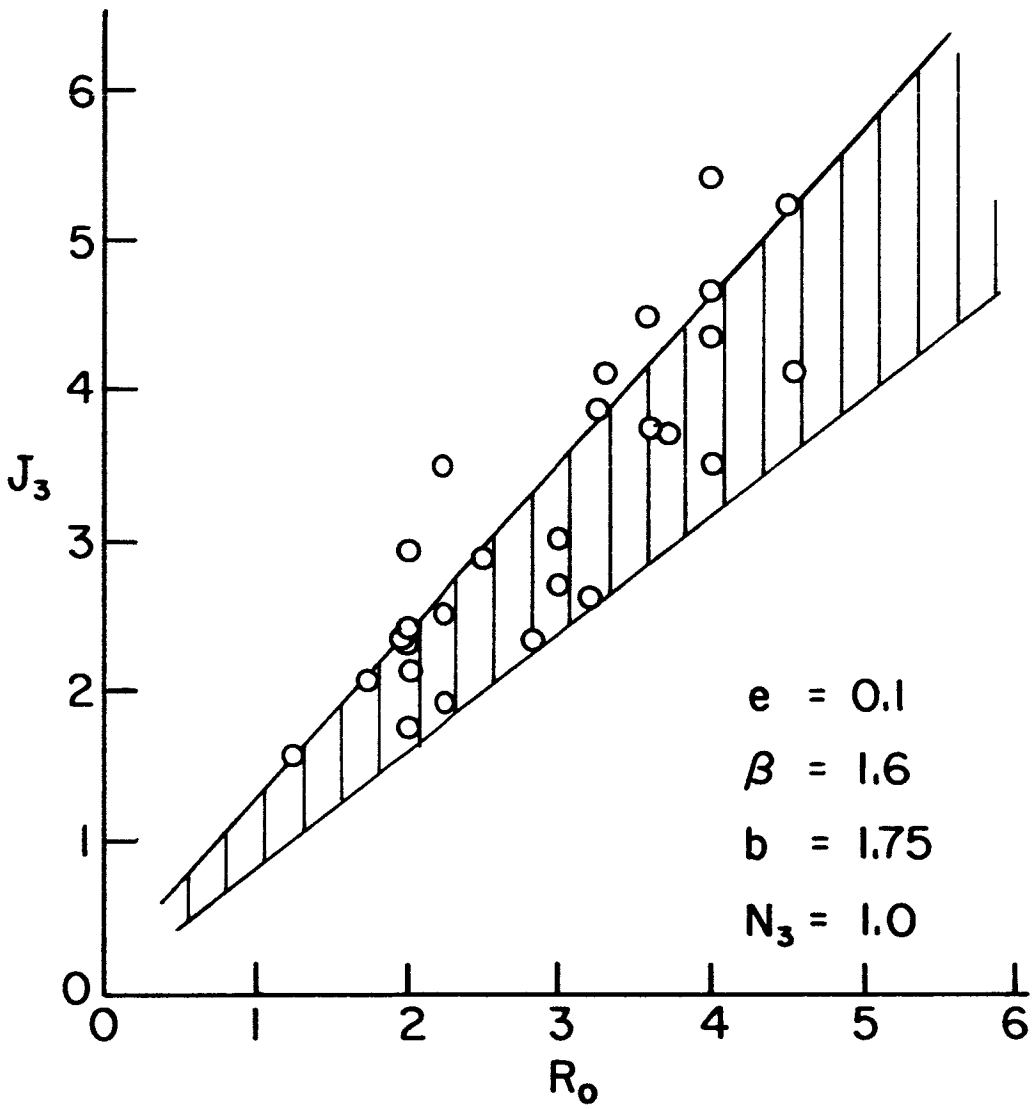

Figure 3.13 Suboptimal Cost vs. Error Magnitude.

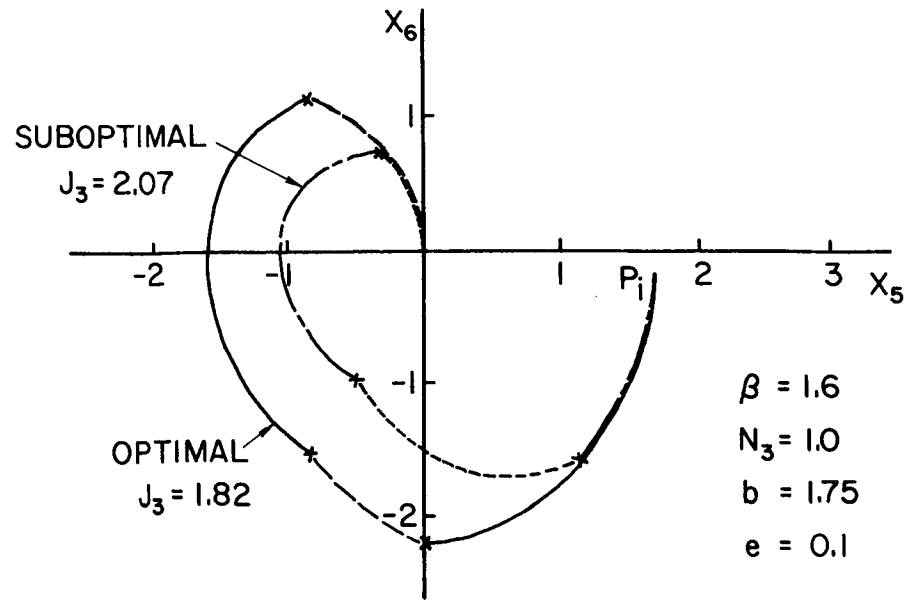

a. $\theta_o = 0$, $\tilde{T} = \pi\beta$

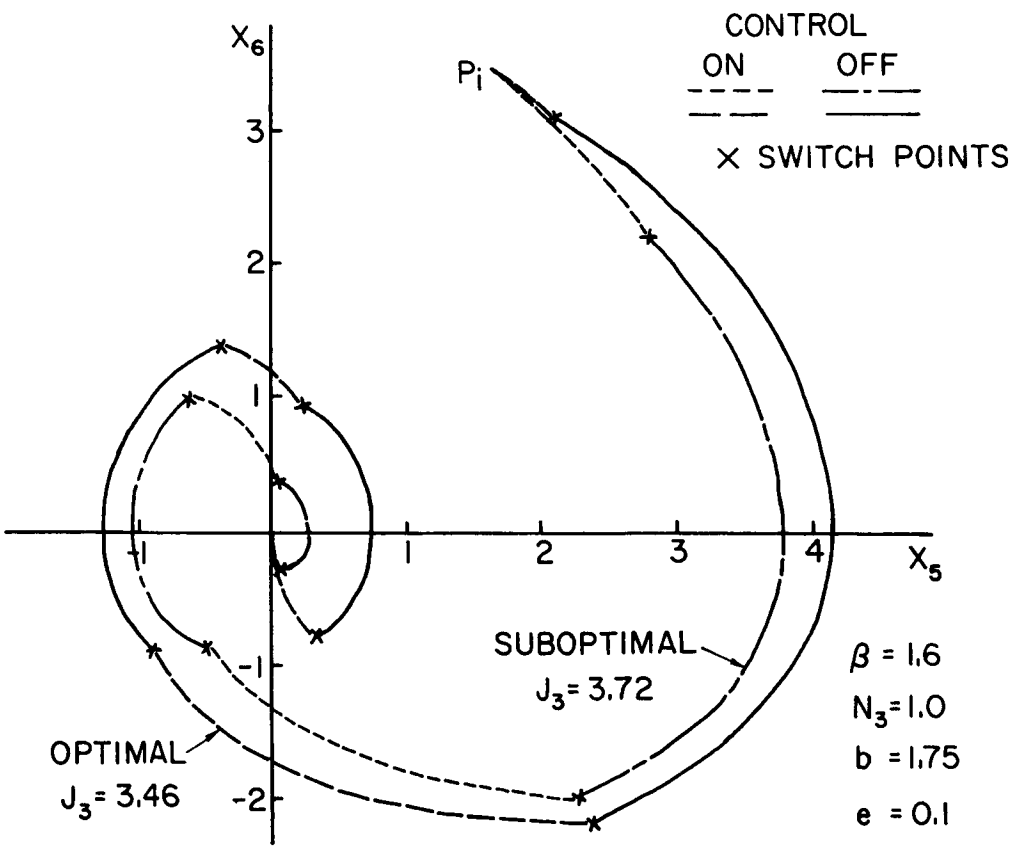

b. $\theta_o = -\pi/2$, $\tilde{T} = 2\pi\beta$

Figure 3.14 Comparison of Optimal and Suboptimal Trajectories.

4. Comparison to Another Suboptimal Control

The selected suboptimal control system (3-11) has the advantage of being very simple. However, there is another coast-type control system that is perhaps slightly simpler. The switching lines are straight, i.e., instead of squaring x_6, its absolute value is found. This "sector" system has the form:*

$$u_3 = \begin{cases} -N_3 \, \text{SGN} \, x_6 & \text{for} \quad |x_6| > k|x_5| \\ 0 & \text{for} \quad |x_6| < k|x_5| \end{cases} \tag{3-13}$$

A single value of k was chosen for all initial times and states since an invariant control system was desired. Using the initial conditions of the representative reverse-time trajectories of Table 2, the value of k that gave the best average efficiency for the desired control times was found to be 2.0. With this value of k the sector system had an average increase in cost over the optimal of 12%, only 3% greater than the parabola system, as shown in Figure 3.15. This figure also shows that when either system was very efficient, the other was too. However, for initial conditions that were difficult to control, i.e., for which near optimal cost could not be obtained by a simple control system, the sector system performed considerably worse than the parabola system (see Figure 3.15). Thus, the parabola system is more capable of allowing for the variations in the pitch behavior. In addition, when the efficiencies of the two systems were approximately equal, the control-time with the

---

* Flügge-Lotz and Craig [25] show that this system is optimal with respect to a minimum-fuel performance criterion for the $1/(s^2+1)$ plant if the control time is restricted to a special set and k is a specified function of the initial error.

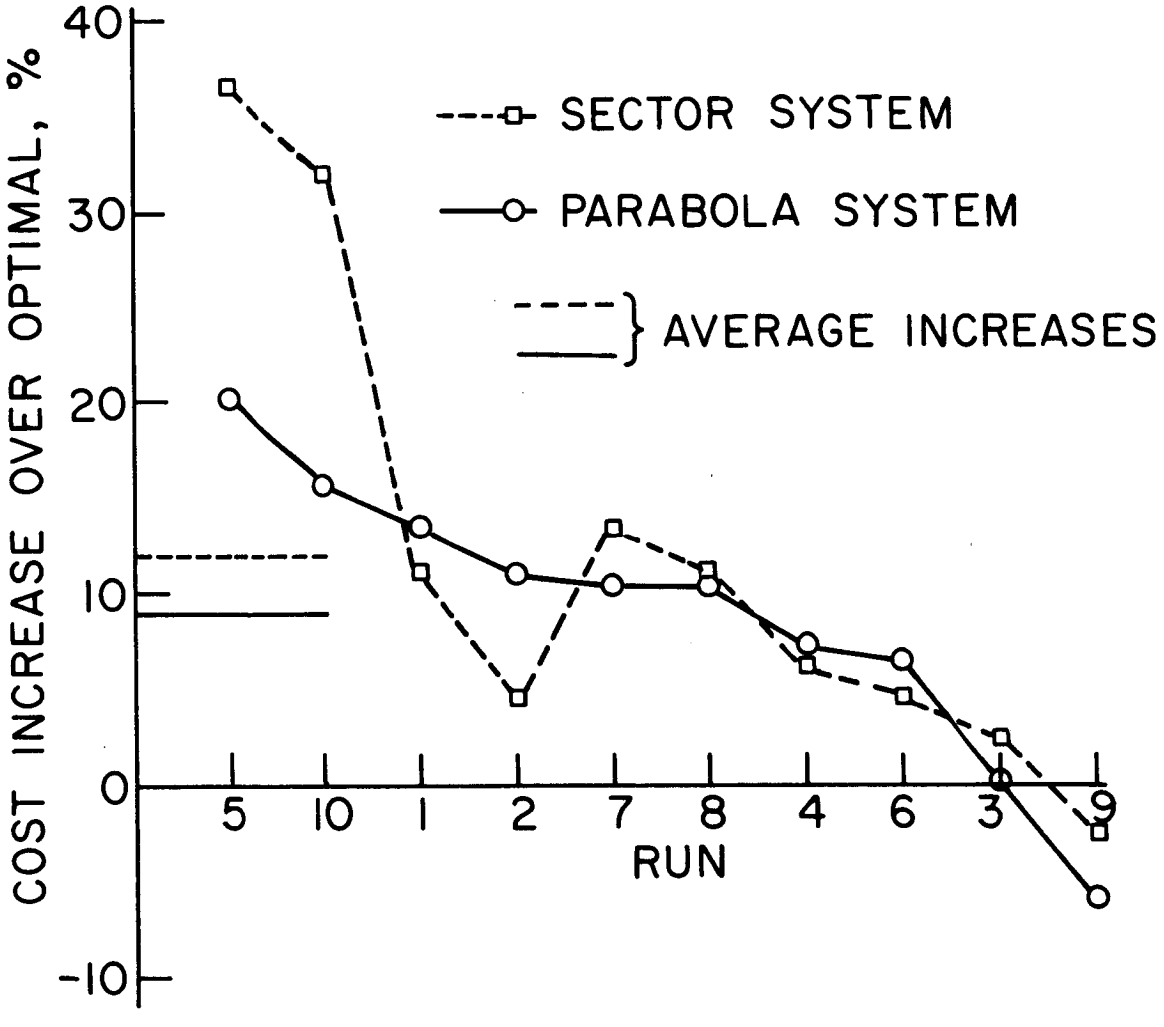

Figure 3.15 Cost Comparison for Two Suboptimal Systems.

sector system was the same or greater, but never smaller, than the control-time with the parabola system.

Another reason why the sector system is not as desirable as the parabola system for this application is illustrated in the examples of Figure 3.16. In these examples, as in 80% of the cases that were compared, the parabolic switching curves resulted in a smaller error magnitude during control than the sector switching lines. This is due to the fact that with the parabola system the control is on for longer intervals when the error is large than when it is small, while for the sector system the intervals are approximately constant. In the remaining 20% of the cases the error magnitude during control was approximately the same.

The decrease in average cost, along with the decrease in error magnitude during control, definitely makes the slight increase in complexity of the parabola system over the sector system worthwhile.

5. Extension of the System

The above development of a suboptimal control system was limited to values for the inertia parameter k_3 and the orbital eccentricity e of 0.85 and 0.1, respectively. The chosen system must now be extended for control of satellites of other shapes and satellites in orbits of other eccentricities.

a. Other Satellite Shapes. The inertia parameter k_3 has a possible range of minus one to plus one, but the negative values should be eliminated for stability reasons. As k_3 approaches zero, the effect of the gravity gradient term diminishes and the pitch equation approaches the form

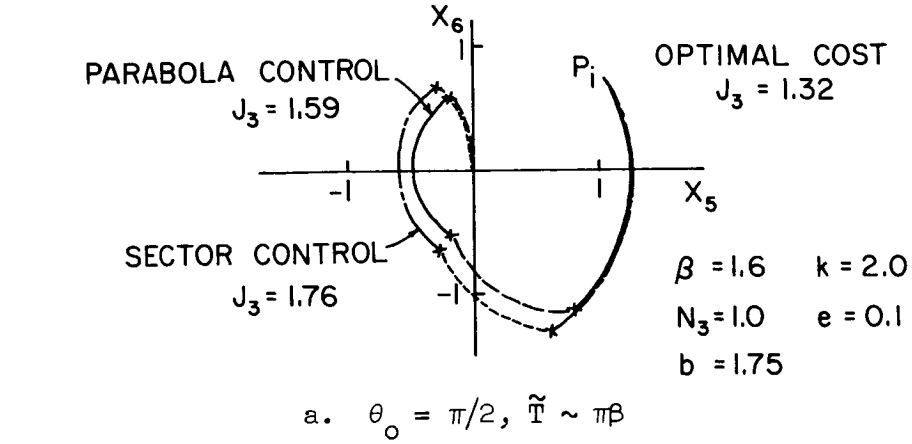

a. $\theta_o = \pi/2$, $\tilde{T} \sim \pi\beta$

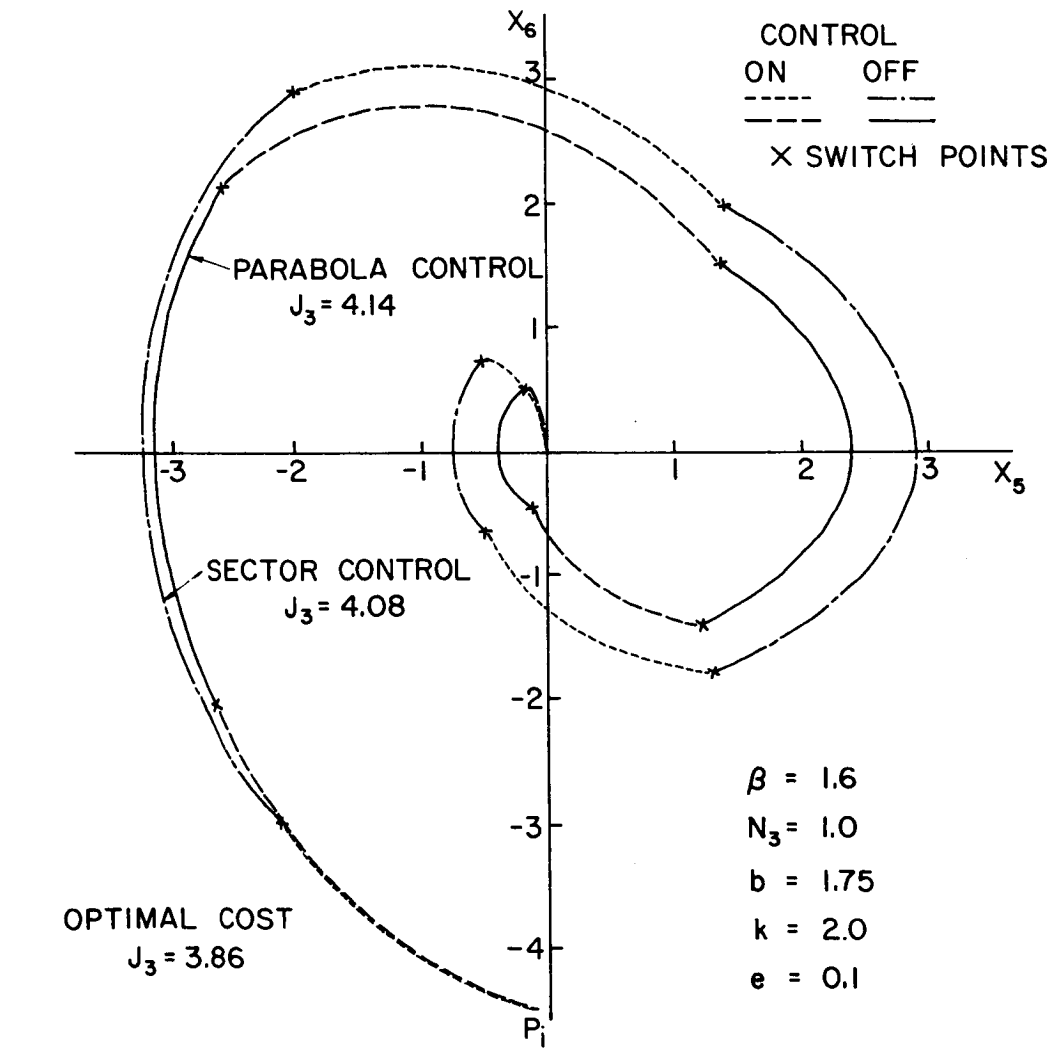

b. $\theta_o = 0$, $\tilde{T} \sim 2\pi\beta$

Figure 3.16 Trajectory Comparisons for Two Suboptimal Systems.

$$\ddot{x} = u + f(t) \tag{3-14}$$

where $f(t)$ is small. For this equation the optimal control is much different from that for Equation (3-1), as is expected from comparing minimum-fuel optimal control for $\ddot{x} = u$ to that for $\ddot{x} + x = u$ (see Craig [7]). Thus, the devised suboptimal control cannot be expected to work satisfactorily for small k_3. Analog computer solutions verified this since the suboptimal cost was as much as 80% greater than the optimal cost when k_3 was near zero.

The suboptimal control system is also unsatisfactory for $k_3 = 1/3$ since for this value of the inertia parameter the Mathieu equation, and consequently the linearized pitch equation, is unstable. Analog computer solutions showed that with this value of k_3 the system was sometimes unable to reduce the error to zero; a limit cycle resulted instead.

Therefore, in the following k_3 will be limited to the range $0.5 \leq k_3 \leq 1.0$. This means that the satellites which are being considered are those whose roll and pitch moments-of-inertia are nearly equal and are a fair amount larger than their yaw moment-of-inertia.

For k_3 within this range the behavior of the system does not vary a great deal. Figure 3.17 shows that near the origin the optimal trajectories are almost identical. (The trajectory that does differ from the rest is one for which $k_3 = 1/3$.) Thus, only the larger initial errors show a significant change in the performance of the suboptimal control system. Consequently, these are the only initial conditions for which the best value of the control parameter b might change. For

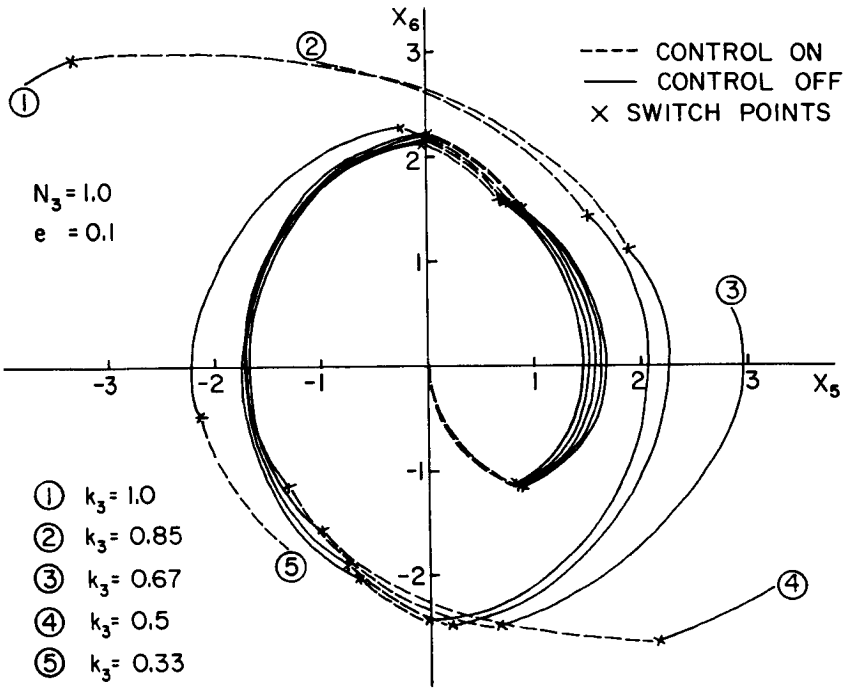

a. $\theta_o = \pi$, $\tilde{T} = 2\pi\beta$

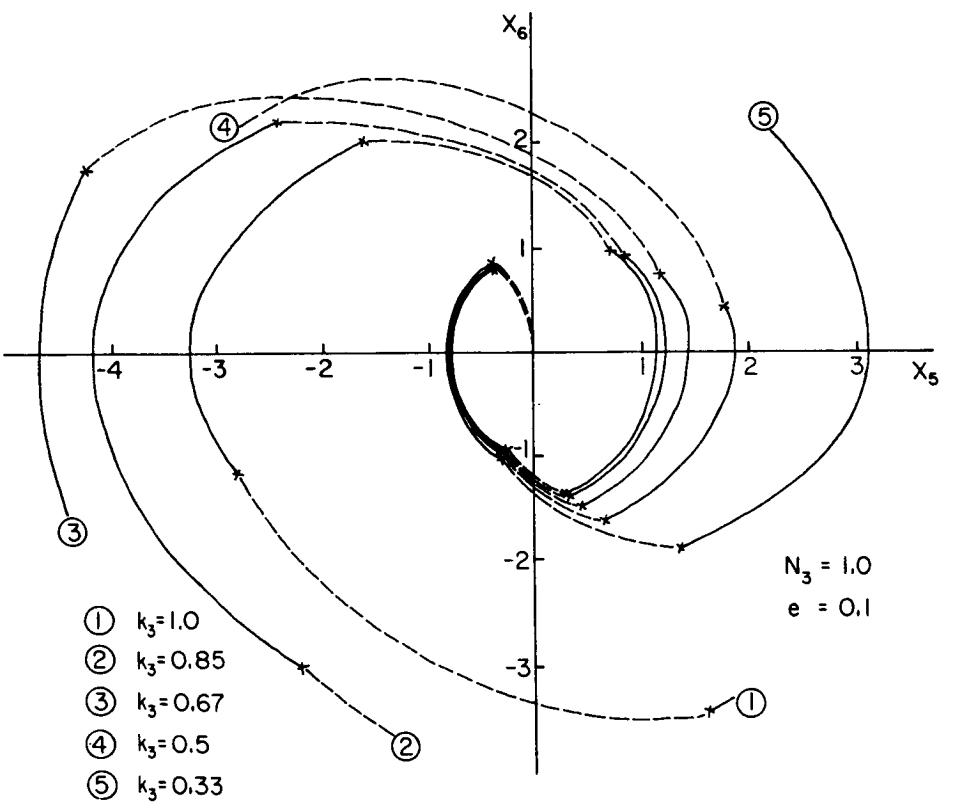

b. $\theta_o = 3\pi/2$, $\tilde{T} = 2\pi\beta$

Figure 3.17 Reverse-Time Trajectories for Various Satellite Shapes, e = 0.1 .

these initial conditions, the same procedure as before was used to determine the best value of b for several values of k_3 in the range $0.5 \leq k_3 \leq 1.0$. Some individual cases changed appreciably in cost from that for $k_3 = 0.85$, but on the average the changes were small. The best value of b for all the tested values of k_3 was found to be the same, i.e., 1.75 . Thus, designing for a central value of k_3 produced a system that is near optimal for a fair range of satellite inertia properties.

b. Other Orbital Eccentricities. In deriving the linear time-varying attitude equations the assumption of small eccentricity was made. The approximations that were used should be reasonably accurate for eccentricities up to about 0.2. As shown in section III-B, the behavior of the optimal control for eccentricities this large was sometimes quite different from the behavior for eccentricities around 0.1. Thus, the suboptimal control system that was developed for eccentricities around 0.1 cannot be expected to work exceptionally well for eccentricities around 0.2.

Forward-time runs on the analog computer were used to determine just how well the control system performed for $e = 0.2$. It was found that for most initial conditions, the system performed quite well. However, there were some initial conditions for which the system appeared unstable, i.e., the error magnitude grew too large for the linearized equations to be valid (see Figure 3.18). This "unstable" behavior was found to occur for eccentricities larger than 0.15 and was caused by the nearly-constant velocity behavior of the pitch equation that was

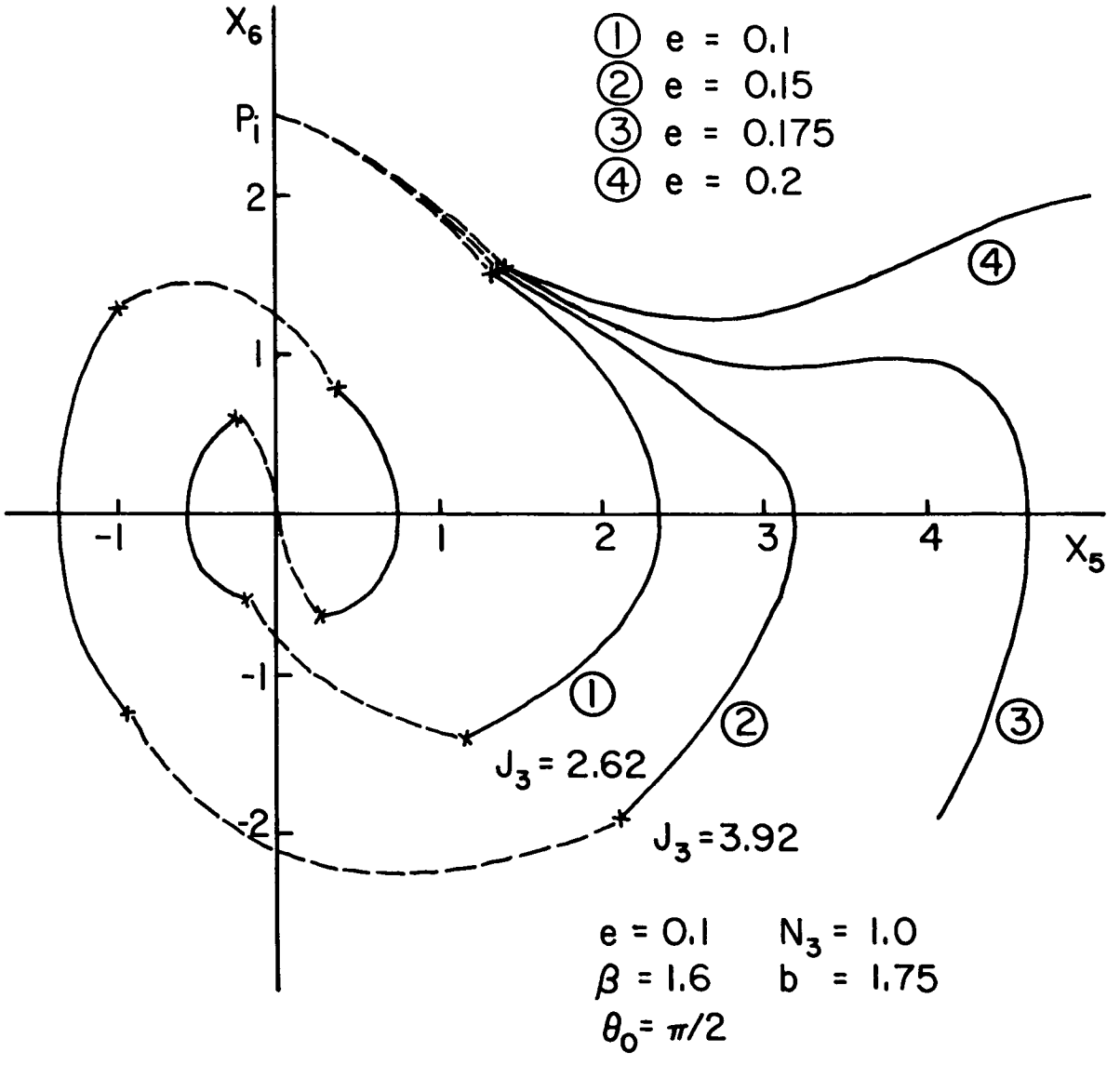

Figure 3.18 Instability due to Increased Eccentricity.

previously mentioned. This instability could not be prevented without a complete change in the form of the switching curves.

For eccentricities less than or equal to 0.15,the best values for the control system parameter b and the average increases in cost over the optimal with these values were determined using the analog computer. The results are shown in Figure 3.19. Again, in choosing b the control time, in addition to the fuel consumption, is taken into account. For the selected values these times are such that large errors are controlled in approximately two cycles in the pitch phase plane, which corresponds to about one orbit of the satellite.

Figure 3.19 shows that the performance of the suboptimal system improves and the best value of b increases as the eccentricity of the orbit decreases. For the larger eccentricities the gas jets need to be on more, i.e., b is smaller, in order to eliminate the error in the desired amount of time. Thus, the fuel consumption for a given error increases as the eccentricity increases. However, the rate of increase for the optimal control is smaller, and consequently the efficiency of the suboptimal system decreases as the eccentricity increases. The system has excellent performance for $e \leq 0.1$, reasonably good performance for $0.1 < e \leq 0.125$, and poor performance for $e > 0.125$. For the larger eccentricities ($e > 0.125$) it is apparent that the parabolic switching curves are no longer a good approximation to the optimal switching curves. Therefore, the suboptimal system is recommended only for eccentricities less than around 0.125.

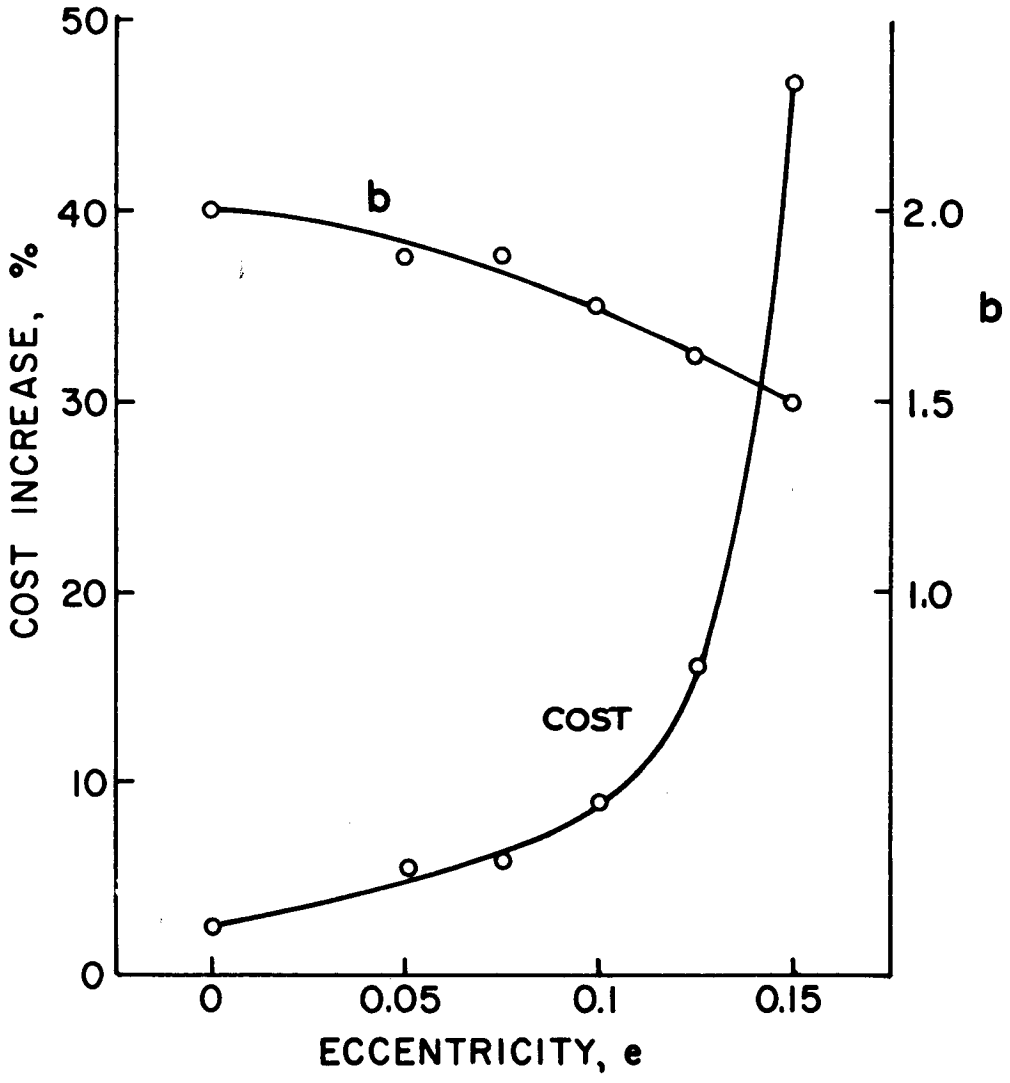

Figure 3.19 Cost Increase and Controller Coefficient vs. Eccentricity.

6. Discussion of the System

What has been developed in the above sections is a suboptimal pitch control system that is very simple, yet is quite efficient. The simplicity of the system allows for easy realization using analog elements, giving a continuous-feedback system. The performance of the system is good throughout fairly large ranges of the orbital eccentricity and the pitch inertia parameter: $0 \leq e \leq 0.125$ and $0.5 \leq k_3 \leq 1.0$. Also, the best value of the suboptimal-control-system parameter b changes very little with changes in the eccentricity and the inertia parameter within these ranges.

The fact that the best value of the parameter b changes very little with changes in the satellite and orbit parameters within the above ranges has significant practical value. The orbit of a satellite will change slowly unless adjustments are constantly made, and the moments-of-inertia of the satellite will change slightly because of fuel expulsion, extendable booms, etc. Thus, the exact values of the orbit and satellite parameters are frequently not known. Consequently, a system that is equally well suited for a range of these parameters is necessary.

Since the performance is also not greatly affected by small changes in the parameter b, the system is relatively insensitive to small amounts of sensor noise. Noisy measured values of the error and error rate are equivalent to random variations of the switching points about the nominal parabolic switching curve, i.e., small random variations in b. This is shown in Figure 3.20 where noise having a maximum

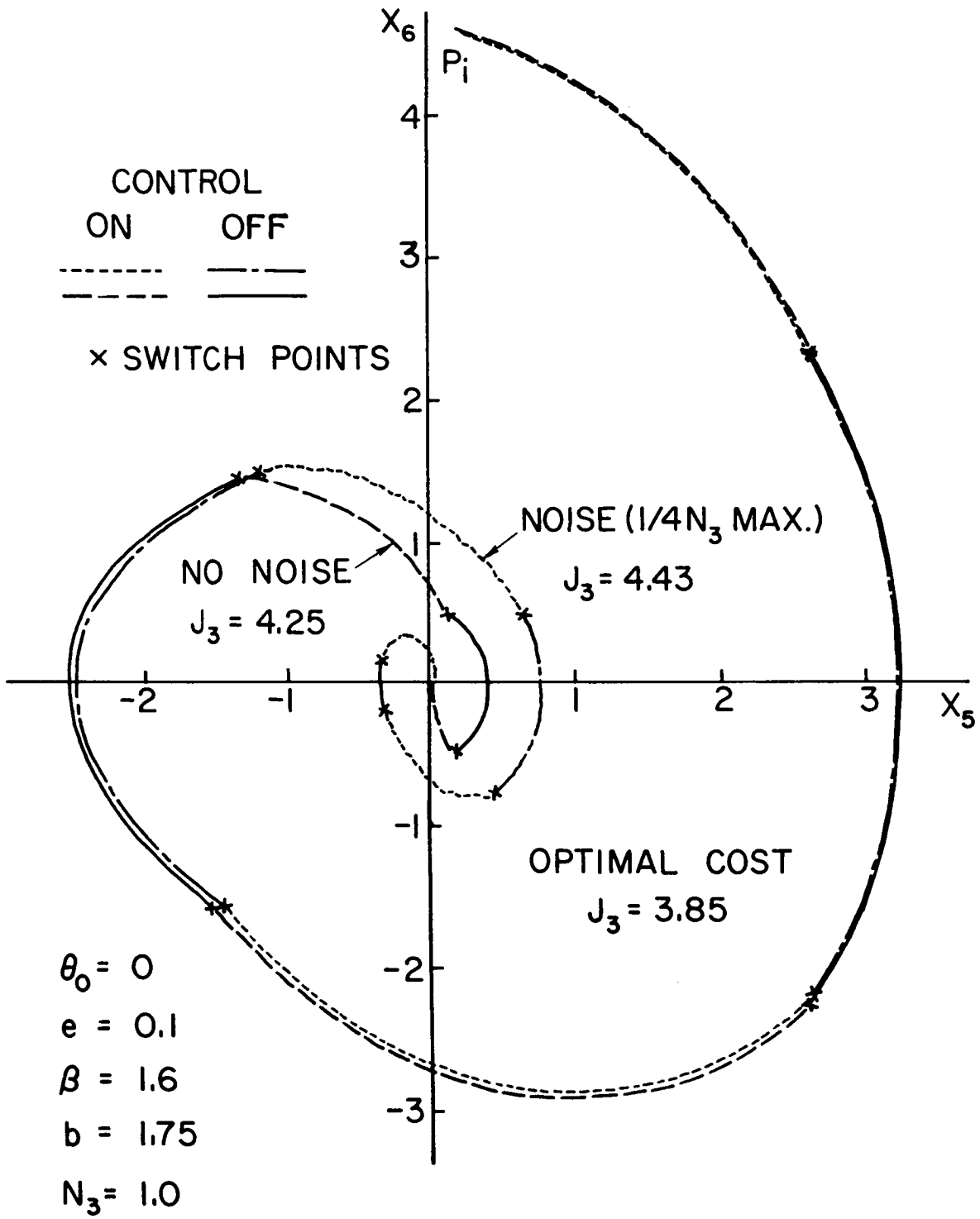

Figure 3.20 Example with Sensor Noise.

amplitude of $\frac{1}{4}N_3$ was added to the error rate x_6 before it was fed into the controller. As expected, the noise had little effect when the values of the state variables were large. When the origin was approached the switching points changed considerably, forcing the controller to take an extra half cycle to eliminate the error. However, the cost increased only 4.2 percent, which is quite good considering that the noise level in this example was quite high.

One problem in the control of the pitch attitude, that has thus far been neglected, is that the motion is forced. The forcing function was neglected since, as state before, it is fairly small and it does not affect the form of the optimal control as a function of time. In addition, neglecting it facilitated comparisons of the backward optimal and the forward suboptimal trajectories and costs, since then there was no difficulty getting all the way back to the origin. Because it is periodic and since a great many examples were considered, the effects of the forcing function, if it had been included, would have averaged out. Thus, the same suboptimal control system with the same efficiencies would have evolved. Consequently, there is no need to include the forcing function when considering acquisition control, as was done in this chapter.

However, when considering steady-state control, the forcing function becomes very important. Because of it, the desired end state is not an equilibrium state. Thus, the steady-state motion is a limit cycle about the origin of the error phase-plane. The size of the limit cycle is a function of the duration and timing of the control pulses

during each cycle and the magnitude of the forcing function, which is proportional to the eccentricity of the orbit. Obviously, the forcing function must be included when steady-state control is considered. This is what is done in Section B of Chapter V.

IV. YAW-ROLL ATTITUDE CONTROL

Complete three-axis control of the attitude of the satellite must be provided for the linearized versions of the attitude equations to be valid. The full non-linear attitude equations show that the motions about the three axes are coupled. Thus, only if the yaw and roll errors are held small can the previous results for the linearized pitch equation be used.

A. Linearized Yaw-Roll Equations

For the linearized equations the pitch motion is decoupled from the yaw and roll motions but the yaw and roll motions are still coupled. The linearized yaw-roll equations are (see Equations (2-32) and (2-41))

$$\bar{x}' = A_1(\tau)\bar{x} + B_1\bar{u}^* \tag{4-1}$$

where

$$\bar{x}^t = [x_1\ x_2\ x_3\ x_4] = [\theta_1\ \theta_1'\ \theta_2\ \theta_2']$$

$$\bar{u}^{*t} = [u_1^*\ u_2^*]$$

$$A_1(\tau) = \{a_{ij}\}\ , \qquad i,j = 1,2,3,4 \tag{4-2}$$

$$B_1 = \begin{bmatrix} 0 & 0 \\ 1 & 0 \\ 0 & 0 \\ 0 & 1 \end{bmatrix}$$

Under certain reasonable assumptions of eccentricity and satellite inertia properties these complicated and difficult-to-analyze equations can be reduced to a more workable form.

From considerations in the previous chapter on pitch control the eccentricity of the orbit will be limited to the range $0 \leq e \leq 0.125$. The satellite shape has already been assumed to be such that the nominal moment-of-inertia parameter values are $k_1 = 0.25$, $k_2 = -0.91$, and $k_3 = 0.85$. For these parameter values and small eccentricities some of the terms in Equation (4-1) are quite small. This is more readily apparent if a time scale change is made.* The dimensionless independent variable τ is changed to

$$\hat{\tau} = \alpha n t \tag{4-3}$$

where $\alpha^2 = -4k_2$. The matrix $A_1(\tau)$ then becomes

$$A_1(\hat{\tau}) = \begin{bmatrix} 0 & 1 & 0 & 0 \\ -\frac{k_1}{\alpha^2}(1+4eC) & 0 & -\frac{2e}{\alpha^2}S & \frac{1-k_1}{\alpha}(1+2eC) \\ 0 & 0 & 0 & 1 \\ \frac{2e}{\alpha^2}S & -\frac{1+k_2}{\alpha}(1+2eC) & -(1+3.25eC) & 0 \end{bmatrix} \tag{4-4}$$

where $C = \cos\left(\frac{\hat{\tau}}{\alpha}+\theta_o\right)$ and $S = \sin\left(\frac{\hat{\tau}}{\alpha}+\theta_o\right)$. Also, the control takes on the new form:

$$\bar{u}^t = [u_1 \; u_2] \tag{4-5}$$

where

$$u_i = u_i^*/\alpha^2 , \quad i = 1,2 \; .$$

---

* The actual purpose of the time scale change is to put the equations in a form that is better suited to analog computer realization.

For the nominal values of the moment-of-inertia parameters and an eccentricity of 0.1, the coefficients of the entries in $A_1(\hat{\tau})$ have the following values: $k_1/\alpha^2 = 0.069$, $2e/\alpha^2 = 0.055$, $(1+k_2)/\alpha = 0.047$, and $(1-k_1)/\alpha = .393$. Thus, a reasonable approximation to the yaw-roll set of equations is formed by neglecting the terms containing the first three of the above four coefficients. These terms are only about one-twentieth the magnitude of the dominant terms. The simplified yaw-roll equations are:

$$\bar{x}' = \tilde{A}_1(\hat{\tau})\bar{x} + B_1\bar{u} \tag{4-6}$$

where

$$\tilde{A}_1(\hat{\tau}) = \begin{bmatrix} 0 & 1 & 0 & 0 \\ 0 & 0 & 0 & \frac{1-k_1}{\alpha}(1+2eC) \\ 0 & 0 & 0 & 1 \\ 0 & 0 & -(1+3.25eC) & 0 \end{bmatrix} \tag{4-7}$$

Thus, the simplified yaw motion is that of a $1/s^2$ plant with a not-too-large forcing function due to the roll motion. The simplified roll motion is not affected by the yaw motion. The roll equation has very nearly the same form as the linearized, unforced pitch equation. The only difference is in the magnitude of the coefficient of the cosine term and that β is replaced by α . These differences are small, so a roll control system similar to the pitch control system will be considered. Noting the inertia properties and orientation of the satellite and the direction of the gravity gradient, the above characteristics of the small attitude motion are not surprising.

B. Optimal Yaw-Roll Control

With the change in the time scale the cost functional for the yaw-roll system of equations becomes

$$J_{1,2} = \int_{\hat{\tau}_o}^{\hat{\tau}_f} (|u_1| + |u_2|)d\hat{\tau} \tag{4-8}$$

Thus, as shown in Chapter II the optimal control with respect to this minimum-fuel performance criterion must satisfy the relations

$$u_i = N_i \text{ CST } p_{2i} , \qquad i = 1,2 \tag{4-9}$$

where $N_i = N_i^*/\alpha^2$ and the adjoint vector $\bar{p}$ now satisfies the equation

$$\bar{p}' = - \tilde{A}_1^t(\hat{\tau})\bar{p} \tag{4-10}$$

In the adjoint system of equations the coupling is opposite to that in the system equations, (4-6). p_1 and p_2 are not affected by p_3 or p_4, but p_3 and p_4 are affected by p_1 and p_2. p_2 is a simple linear function of $\hat{\tau}$ of the form

$$p_2 = -p_1\hat{\tau} + p_{2_o} \tag{4-11}$$

where p_1 and p_{2_o} are constants. Consequently, the optimal control for the simplified yaw equation has at most two switchings and is very similar to that for the $1/s^2$ plant. The only difference is due to the roll forcing term in the yaw equation. This does not affect the form of the control as a function of time but causes a change in the phase-plane switching points to guarantee that the origin is still reached.

p_4 satisfies a normalized Mathieu equation with a forcing term due to p_1 :

$$p_4'' + \left(1 + 3.25e \cos\left(\frac{\hat{\tau}}{\alpha} + \theta_o\right)\right) p_4 = + \left(\frac{1 - k_1}{\alpha}\right)\left(1 + 2e \cos\left(\frac{\hat{\tau}}{\alpha} + \theta_o\right)\right) p_1 \qquad (4\text{-}12)$$

Thus, one expects a similarity of the roll control to the pitch control with variations that depend on p_1 .

1. Reverse-Time Solutions

The system and adjoint equations were simulated on the analog computer. Optimally controlled trajectories were then determined by running in reverse-time starting at the desired end-state, as was done for the pitch equation. By making a large number of runs with a variety of final adjoint states and orbit locations (initial conditions in reverse-time) a fair coverage of the possible initial yaw-roll states was made. Figures 4.1 and 4.2 are two representative examples of these many reverse-time optimal trajectories.

2. Characteristics of the Optimal Controls

Figures 4.1 and 4.2 exhibit the characteristics that are expected considering the form of the simplified yaw-roll equations. The yaw motion is approximately parabolic when the yaw control u_1 is on, and deviates in the coast intervals from x_2 = a constant only because of the coupling with the roll motion. When the roll error is zero the simplified yaw motion is exactly that of a $1/s^2$ plant. Figure 4.3 is a phase-plane plot of the optimal yaw switching points for a variety of reverse-time runs.

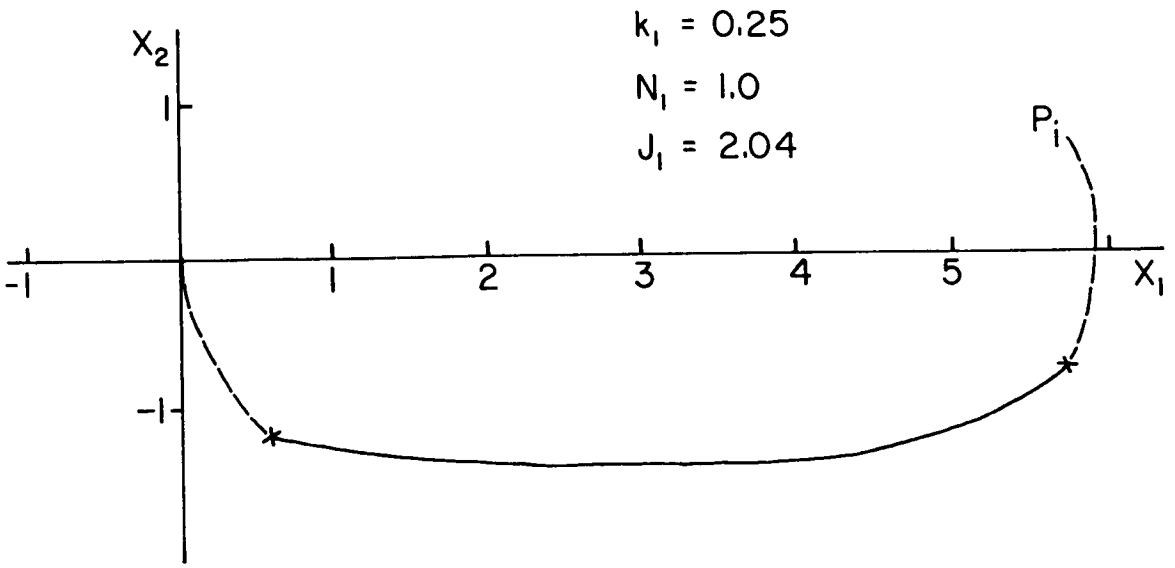

a. Yaw Motion

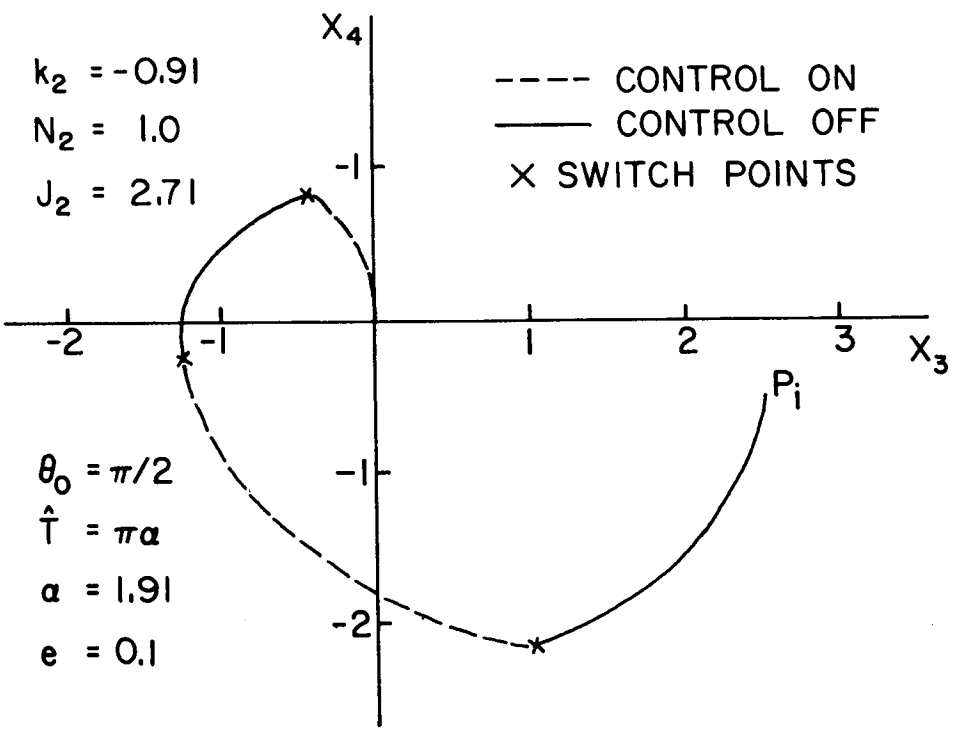

b. Roll Motion

Figure 4.1 Reverse-Time Optimal Trajectories

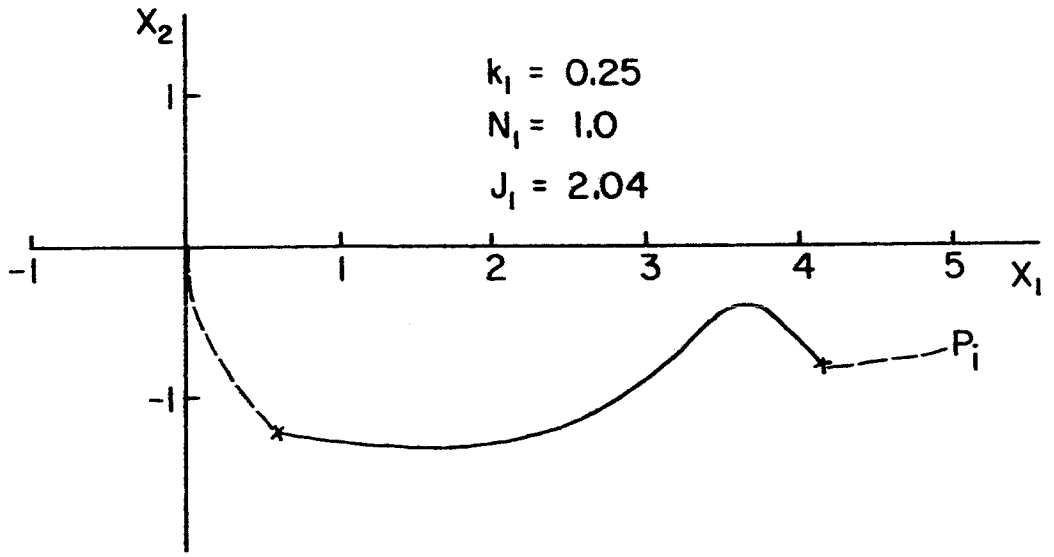

a. Yaw Motion

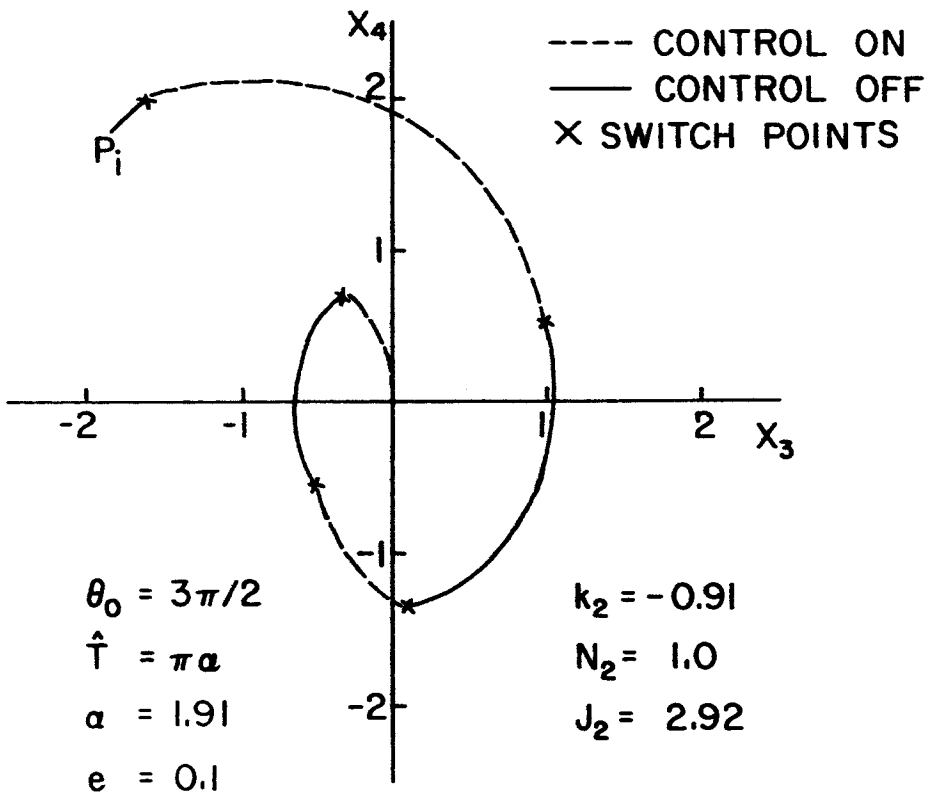

b. Roll Motion

Figure 4.2 Reverse-Time Optimal Trajectories

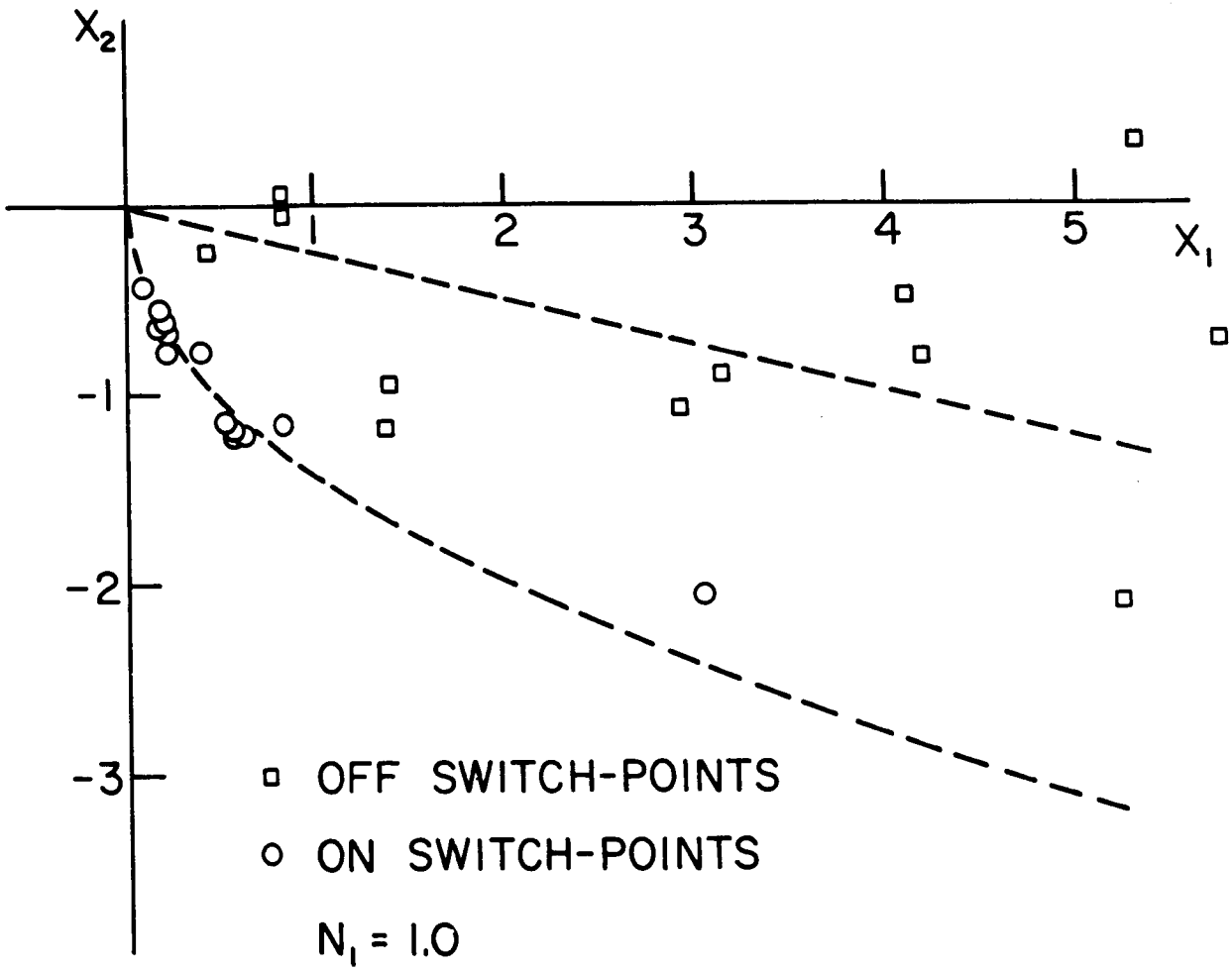

Figure 4.3 Optimal Yaw Switch Points.

The switch-on points lie on or near a parabola that is the zero trajectory when no cross coupling is present. The variations from the zero trajectory are not large because the cross-coupling term is not large. The switch-off points are not as uniformly located but are usually roughly on a horizontal line with the corresponding switch-on point. The coast portions of the trajectories are close to the x_1-axis in most cases because the selected times for solution are fairly long.

The roll phase-plane trajectories appear very much like those of the pitch motion. The same general characteristics, such as the locations of the control intervals and the switching points, are apparent. The main difference between the roll and pitch systems is that the equation for the roll adjoint, of which the control is a coast function, is non-homogeneous. The pitch adjoint satisfies the homogeneous form of the equation with only slightly different coefficients. Removing the forcing term in the roll adjoint equation, which is equivalent to using zero yaw control, was found to cause only small shifts in the switching points in the roll phase-plane, as shown in Figure 4.4. Thus, the pitch equation results should be extendable to the roll equation.

C. Suboptimal Yaw-Roll Control

The characteristics of the optimal controls that were discussed in the preceding section will now be used as a basis for developing a suboptimal yaw-roll control system, as was done in the last chapter for the pitch motion.

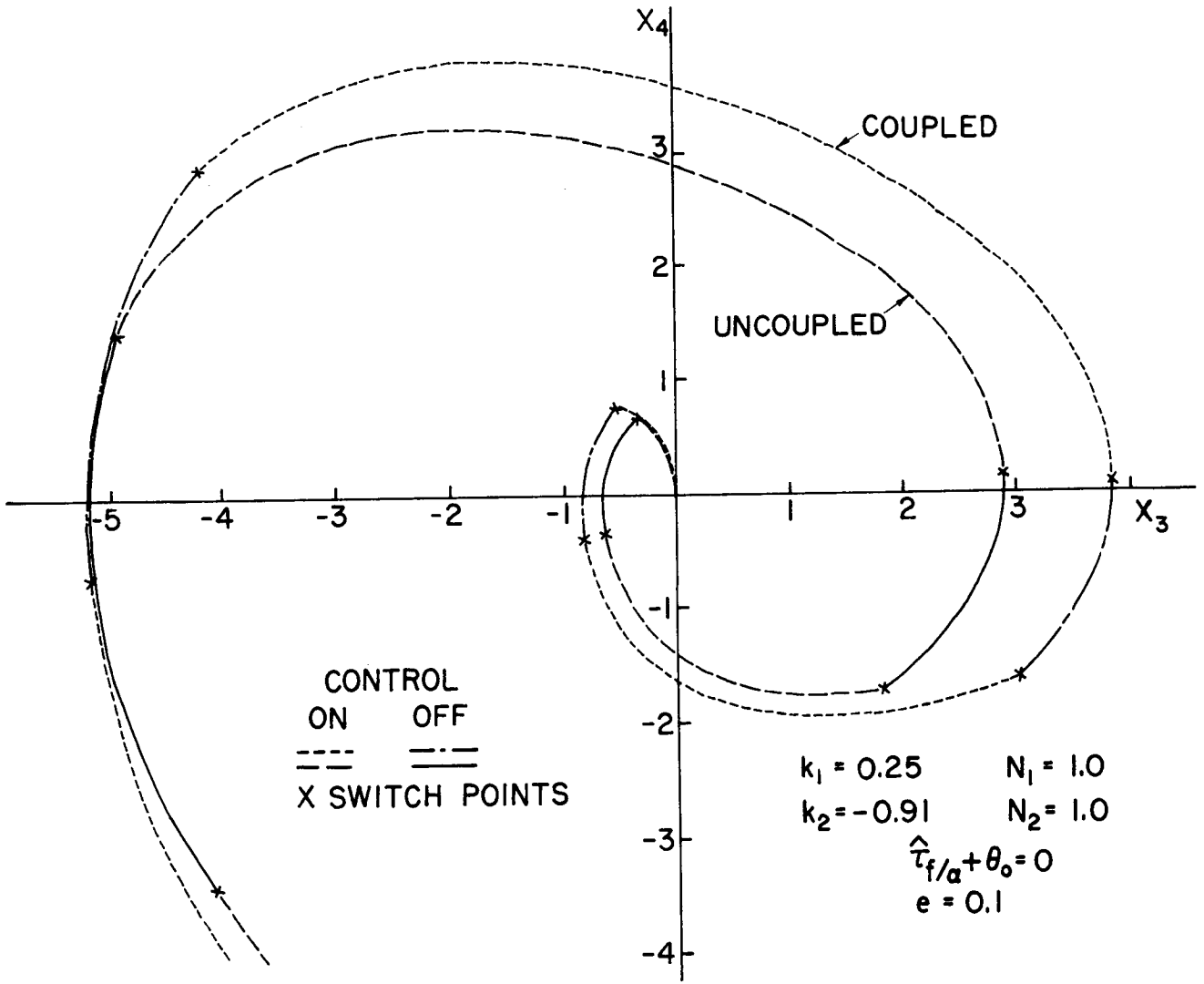

Figure 4.4 Optimal Roll Motion, Coupled and Uncoupled Adjoint.

1. Selection of the Systems

a. Yaw Control System. The optimal switching surfaces for the simplified yaw equation with the coupling neglected are known explicitly as a function of the state (see Flügge-Lotz and Craig [25] and Meditch [10]). With the coupling included the optimal trajectories have the same general characteristics -- parabolic trajectories when the control is on, relatively constant x_2 when the control is off, at most two switchings -- so a suboptimal control scheme should have similar switching surfaces. However, the optimal switching surfaces for the simple $1/s^2$ plant are not easy to generate, so an approximation to these curves is selected as the suboptimal yaw control scheme.

Rather than having a constant solution time for all initial conditions inside a minimum-time isochrone, as is true for the optimal switching curves, the yaw system is designed such that the solution time is roughly proportional to the error magnitude. This is accomplished by having the coast area in the phase plane an open rather than a closed region. From considerations of the $1/s^2$ optimal control, the on-switching curve is chosen to be the zero-trajectory parabola for no coupling. This is also the average zero-trajectory when coupling is present since the coupling term is approximately periodic. Further justification for the selection of this switching curve is that it is a good fit to the switching points shown in Figure 4.3.

The off-switching curve is chosen to be a straight line because it is easy to realize, it produces the desired shape of the coast area, and it is the best fit, for a simple curve, to the off-switch points of

Figure 4.3. Thus, the selected suboptimal yaw-control system has the following form:

$$u_1 = -\frac{1}{2}\,\mathrm{SGN}(x_2|x_2| + 2x_1) + \mathrm{SGN}(x_2 + cx_1) \qquad (4\text{-}13)$$

The phase-plane switching curves given by Equation (4-13) are shown in Figure 4.5. The computer realization of this control system is shown in Appendix C.

Based on the observed reverse-time optimal switching-points, the initial choice for the coefficient c in Equation (4-13) was 0.25. The merit of this choice was checked by simulating the system on the analog computer and using it to control various arbitrary initial conditions. It was found that the performance of the system could be improved, without increasing the solution time to a level above that for the optimal, by reducing the magnitude of c. Comparisons of the optimal and suboptimal trajectories showed that the lowest fuel consumption for control in the desired time was obtained with c equal to 0.10.* No improvement was obtained by changing the coefficient in the first signum function of Equation (4-13).

Except for some trouble cases that are discussed in the next section, the average increase in fuel consumption over the optimal for the system with these parameter values was 11.8%. Values for c greater than 0.10 reduced the coast time, and consequently, the control time, but they increased the fuel consumption. Values for c less than 0.1 showed the reverse effect in many, but not all, cases. The different behavior

---

* The control time for a yaw error of 0.4 radians and no roll error was $\hat{T}/\alpha = \pi$.

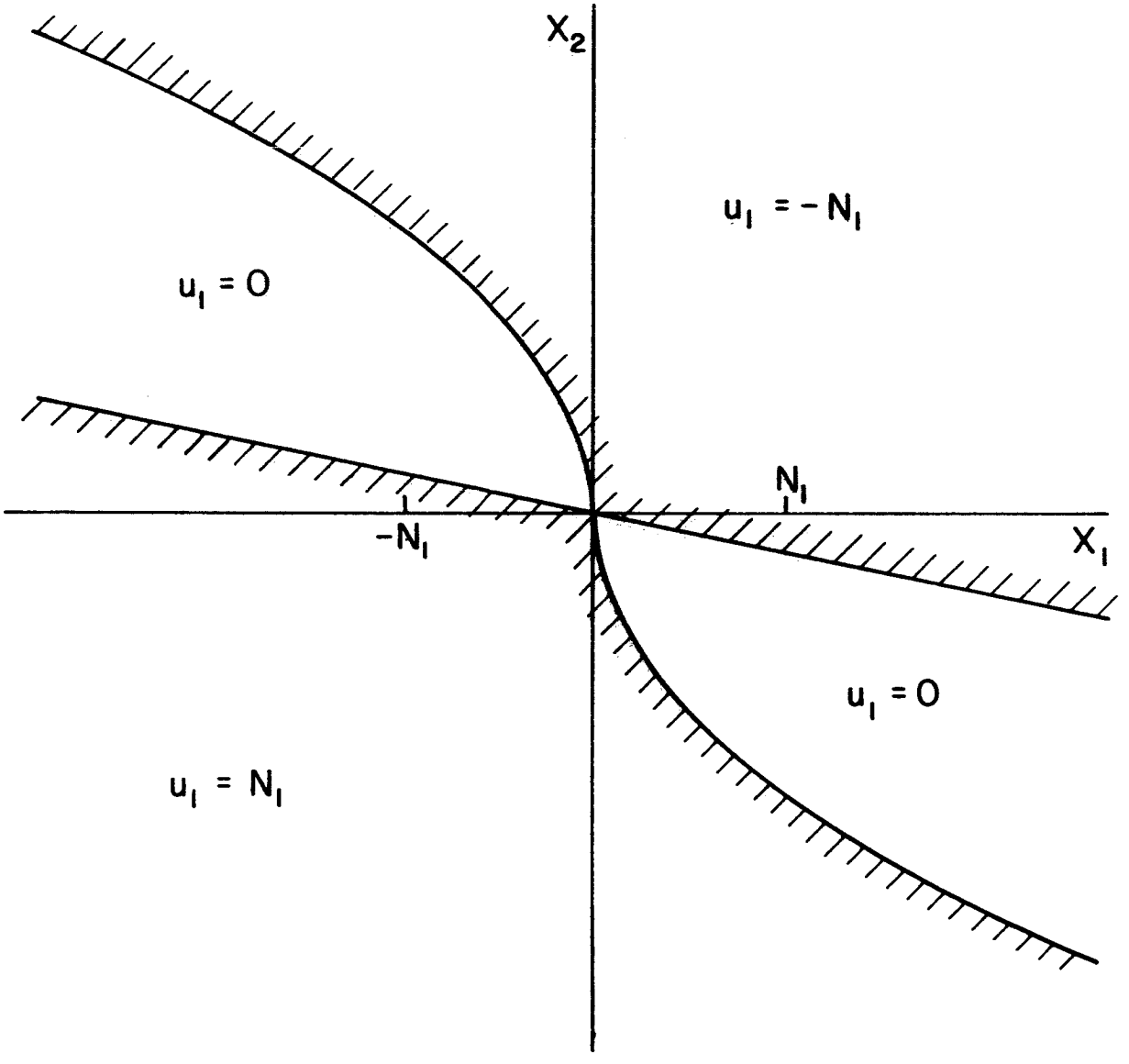

Figure 4.5 Suboptimal Yaw Switching Lines.

occurred when the coupling with the roll system had an adverse influence during the yaw coast-phase. Then, an additional half cycle of phase-plane motion was necessary to zero the error. This behavior also occurred for $c = 0.1$, as shown in Figure 4.6.

b. Roll Control System. As discussed above, the system and optimal-control equations for the simplified roll equation are essentially the same as those for the pitch equation. Also, comparisons of the reverse-time optimal trajectories showed that the switching characteristics of the two systems were indeed very similar. Thus, the suboptimal roll control system is chosen to be of the same form as the suboptimal pitch control, i.e.:

$$u_2 = \begin{cases} -N_2 \, \mathrm{SGN}\, x_4 & \text{for } x_4^2 > a|x_3| \\ 0 & \text{for } x_4^2 < a|x_3| \end{cases} \tag{4-14}$$

The best choice for the parameter a can be determined from the results of the last chapter. The difference between the modified pitch equation and the simplified roll equation is in the coefficient of the gravity-gradient terms. For the pitch equation the coefficient is $1 + 3e \cos(nt+\theta_o)$ while for the roll equation it is $1 + 3.25e \cos(nt+\theta_o)$. These can be made equivalent by defining

$$\epsilon = 1.08e \tag{4-15}$$

and substituting this into the roll equation. Thus, the best value of the parameter a for various values of e is found by making a small-scale change in the eccentricity axis of Figure 3.19. Consequently, for an eccentricity of 0.1 the roll system requires a slightly smaller parameter value (1.70) than the pitch system, and the average cost increase

over the optimal is slightly greater (~ 11%). Also, the maximum eccentricity for which the system is acceptable is reduced to about 0.115.

The above values that were obtained from Figure 3.19 were checked against the results obtained from analog-computer runs. The computer results showed that the best parameter value was indeed 1.70 and that the average increase in fuel consumption over the optimal was 11.2%.

2. Discussion of the System

The appearance of some suboptimally-controlled trajectories is shown in Figures 4.6, 4.7, and 4.8, which are solutions obtained from the analog-computer simulation of the yaw-roll system. For Figure 4.8 the system was run optimally in reverse-time to the initial condition and then suboptimally in forward-time. Thus, a direct comparison of the cost and solution-time was possible. For this particular example the solution-times were about equal, as in almost all the test cases, and the suboptimal system had an increase in fuel consumption of 7.1%. The average increase for the test runs was 11.5%. Also, in many cases, although not in this example, the roll controller exhibited the other desirable characteristics that the pitch controller showed, such as a smaller error magnitude during control than the optimal controller. Thus, even though the suboptimal yaw-roll control system is quite simple, its performance is near optimal.

The performance of the system is acceptable for eccentricities only slightly larger than 0.1, as mentioned above. However, for eccentricities less than 0.1 the efficiency of the suboptimal system increases as the eccentricity decreases. For the roll system this is readily

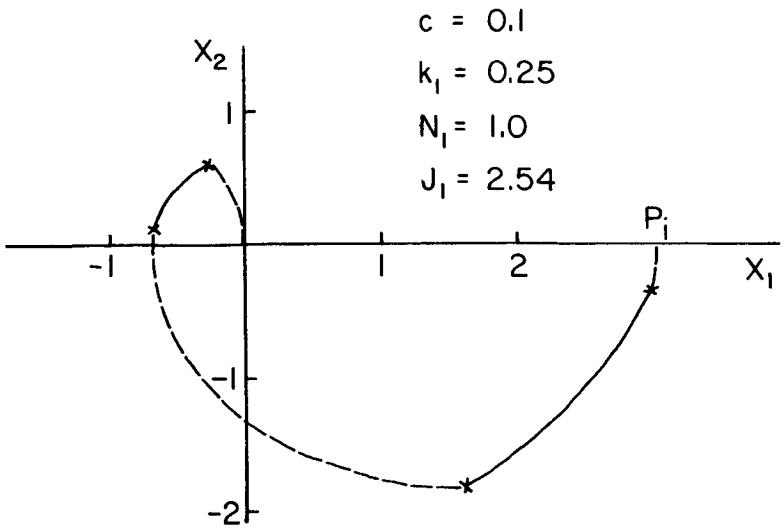

a. Yaw Motion

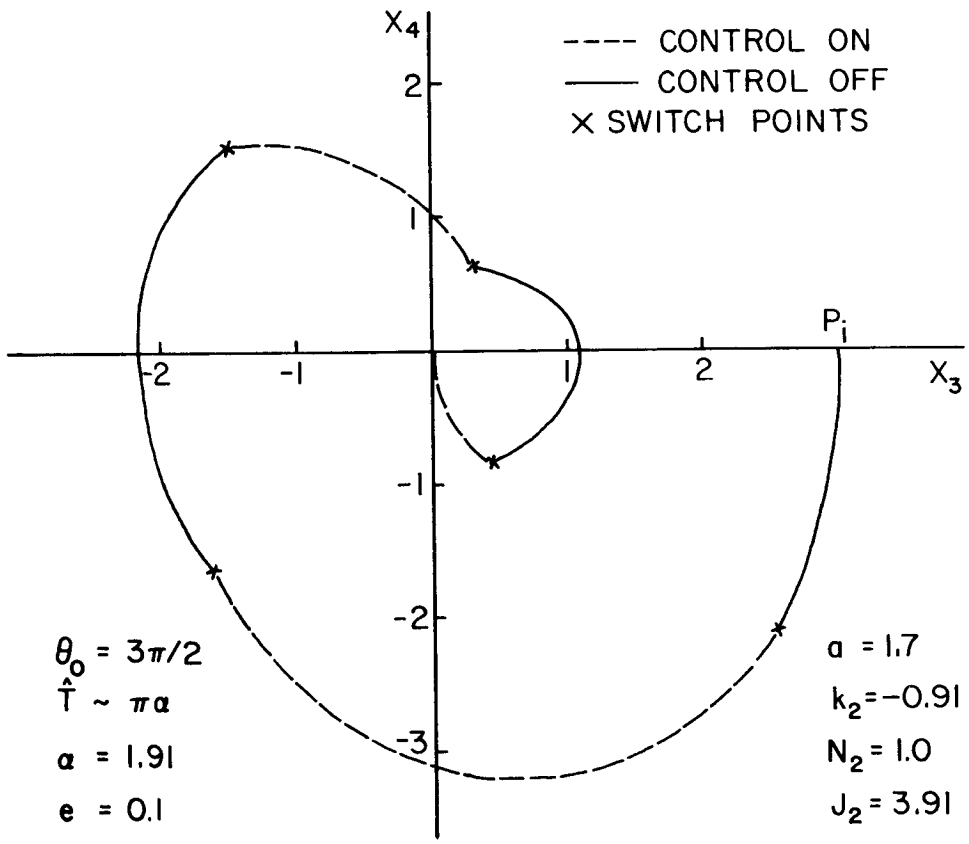

b. Roll Motion

Figure 4.6 Suboptimal Trajectories.

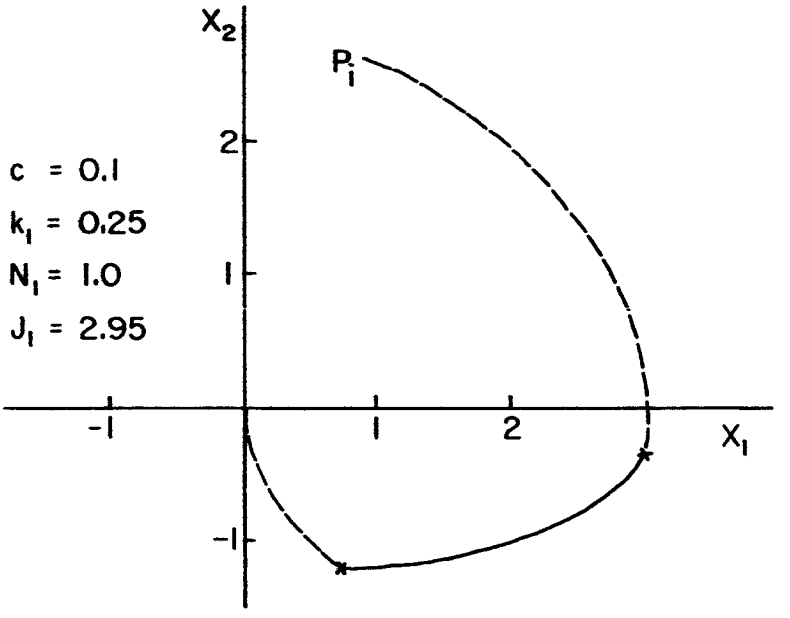

a. Yaw Motion

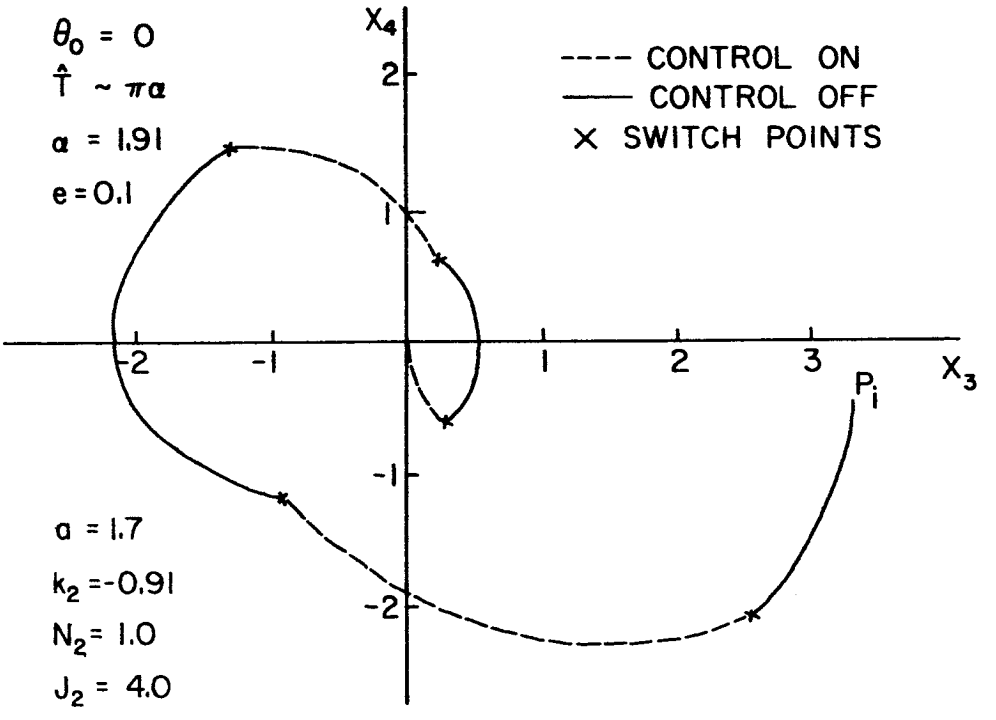

b. Roll Motion

Figure 4.7 Suboptimal Trajectories.

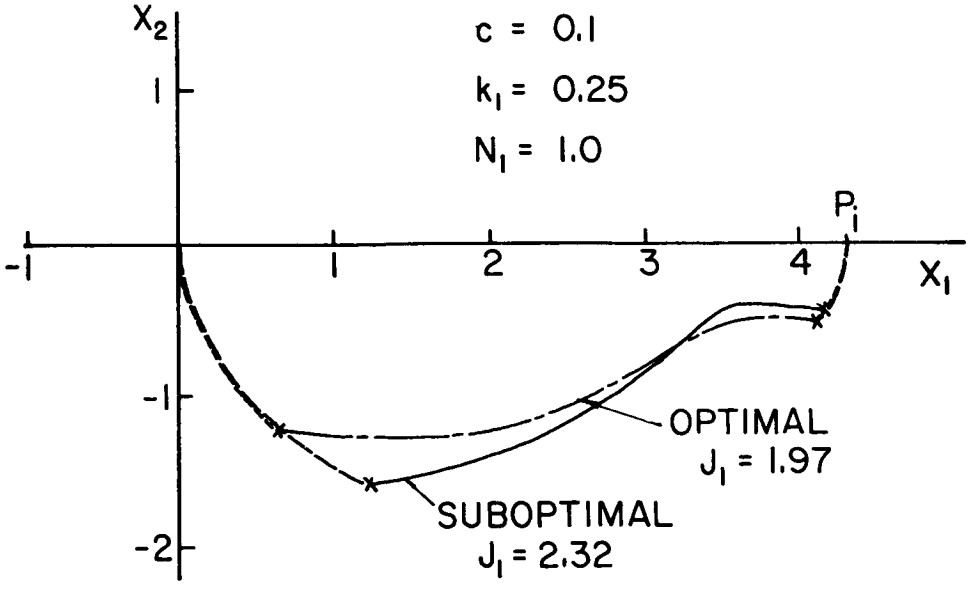

a. Yaw Motion

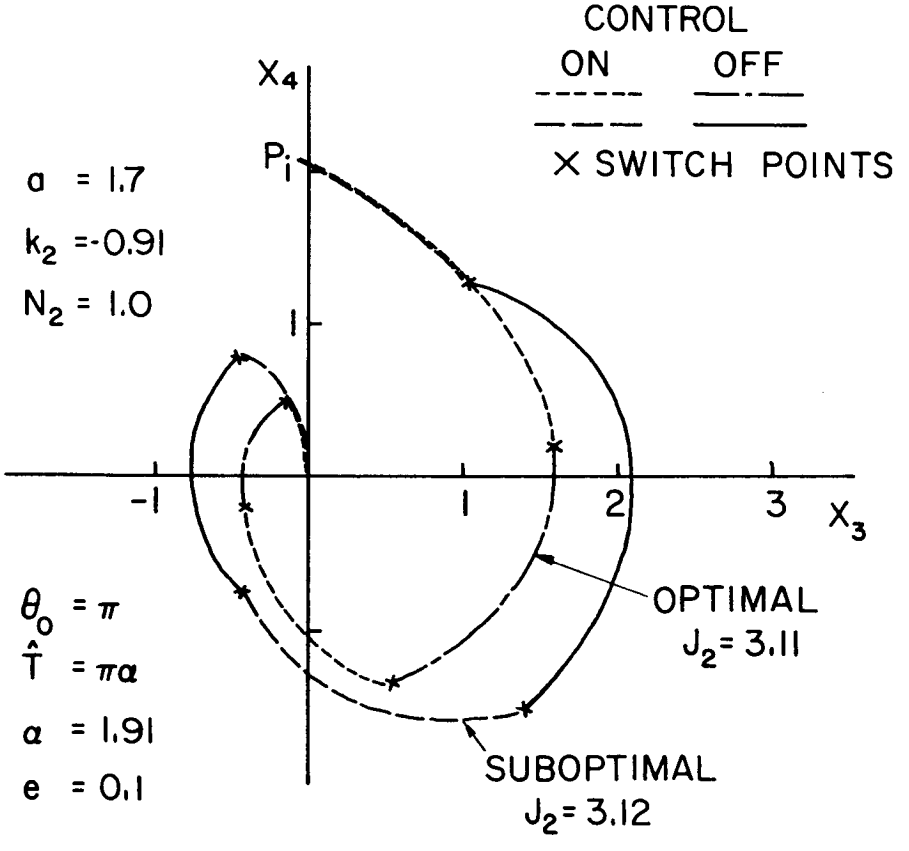

b. Roll Motion

Figure 4.8 Comparison of Optimal and Suboptimal Trajectories.

apparent from Figure 3.19 with the scale change of Equation (4-15). The only change in the yaw equation is that the variations in the forcing term decrease, so control is more easily accomplished. Thus, the yaw-roll control system is acceptable for eccentricities in the range $0 \leq e \leq 0.115$.

The satellite shapes for which the suboptimal system is acceptable must have inertia parameters such that the terms which were neglected to form Equation (4-6) remain small. Thus, the satellite must retain its basic inertia properties. Consideration of the terms that were neglected, shows that increasing the absolute value of k_2 and decreasing the absolute value of k_1 improves the approximations. In the other direction the dropped terms will be limited to a maximum value of one-tenth of the dominant terms. This restricts k_2 to a maximum value of -0.82 and k_1 to a maximum value of 0.27. These variations in k_2 do not affect the performance of the roll control system, as is discussed in Section C.5a of Chapter III. The variations in k_1 only cause small variations in the magnitude of the coupling term. This does not affect the performance of the yaw system to any significant degree. Thus, the suboptimal yaw-roll system is near optimal for satellites with inertia parameters in the ranges $0 \leq k_1 \leq 0.27$ and $-1.0 \leq k_2 \leq -0.82$.

A certain set of initial conditions was found to give the yaw-roll control system the appearance of being unstable. This behavior occurred when the initial roll error was relatively large, the initial yaw error-rate was opposite in sign to the roll error, and the initial time was such that the cosine term was positive and near maximum. When these conditions occurred the roll forcing term in the yaw equation was

larger in magnitude and opposite in sign to the yaw control. Thus, the apparent yaw control was of the wrong sign, which had the effect of driving the yaw state away from the origin. This behavior is shown in Figure 4.9. However, considering the unsimplified yaw equation it is apparent that under these conditions one of the terms that was dropped is growing large with a sense opposite to that of the roll forcing term. This could sufficiently reduce the effect of the roll term such that the apparent control remains the correct sign. As will be shown in the following chapter, this is indeed what occurs.

In this chapter a simple feedback control system for yaw-roll attitude control has been developed that is near optimal with respect to fuel consumption. It works very well for eccentricities around 0.1 or less and a small but realistic range of inertia properties. In the following chapter the system behavior will be checked using more accurate attitude equations.

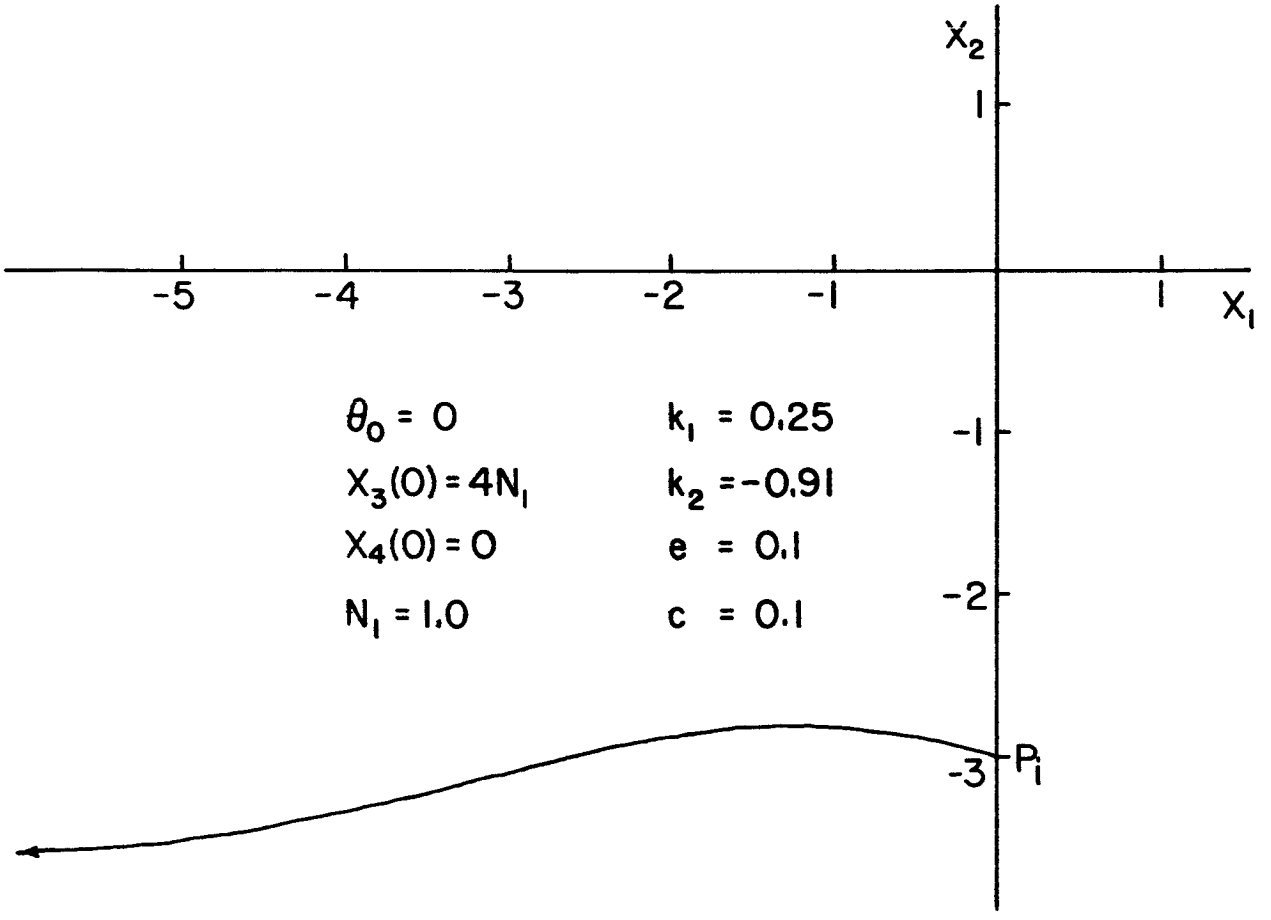

Figure 4.9 Unstable Yaw Motion

V. THREE-AXIS ATTITUDE CONTROL USING THE DEVELOPED SUBOPTIMAL SYSTEMS

To develop the near-optimal attitude control systems in the two previous chapters, the equations of the attitude motion of the satellite were linearized. For the linearized equations to be reasonable approximations, the motions that were discussed and controlled had to be limited to fairly small errors. In reality, there is no reason why the attitude errors would be limited to this range. Thus, to guarantee that the developed system is a workable design, its ability to control larger errors must be shown. Consequently, the nonlinear attitude and orbital equations, Equations (2-6), (2-7), (2-8), (2-11) and (2-12), must be used to describe the motion. In addition, the use of the nonlinear attitude equations will allow further investigation of the unstable behavior that was discussed in Chapter IV.

A. Suboptimal Acquisition Control

1. Digital Computer Simulation

The full nonlinear attitude equations were integrated on the Burroughs B5500 in Chapter II to investigate the uncontrolled motion. To study the controlled motion the control systems that were developed in Chapters III and IV were added to the computer program, which was not difficult because of the simplicity of the control systems. The computer program is outlined in Appendix C. Integrations were then performed for a variety of initial conditions. The Kutta-Merson integrating

procedure that was mentioned in Chapter II was used, and the results were plotted using a Calcomp plotter.

2. Examples of Controlled Motion

One set of initial conditions that was used was the one which produced the unstable motion in Chapter IV, i.e., negative velocity error in yaw, positive position error in roll, and an arbitrary error in pitch. The yaw motion for this example is shown in Figure 5.1. Initially the error grows as it did when the simplified linear equations were used. However, as was predicted in Chapter IV, terms that were neglected eventually dominate the trouble causing terms. Thus, while the error magnitude does grow larger than its initial value, the motion is stable.

The results of Chapters III and IV were obtained by using linearized and simplified attitude equations (Equations (3-8) and (4-6)). To check these results, several examples were run on the digital computer starting at initial conditions that were used in the previous chapters. Figure 5.2 shows the trajectories that were obtained by integrating the complete attitude and orbital equations with the initial conditions of Figures 3.14a and 4.7. The yaw and roll trajectories of Figure 5.2 are identical to those of Figure 4.7; the differences in appearance are due to changes in time and axes scaling. However, the two pitch trajectories (that in Figure 5.2 and the suboptimal portion of Figure 3.14a) are not identical. Up to point P in Figure 5.2, the differences are minor. They are due to the absence of the forcing function from the equations that were used to obtain Figure 3.14a. Beyond point P the forcing function dominates the motion, so the two trajectories are quite different.

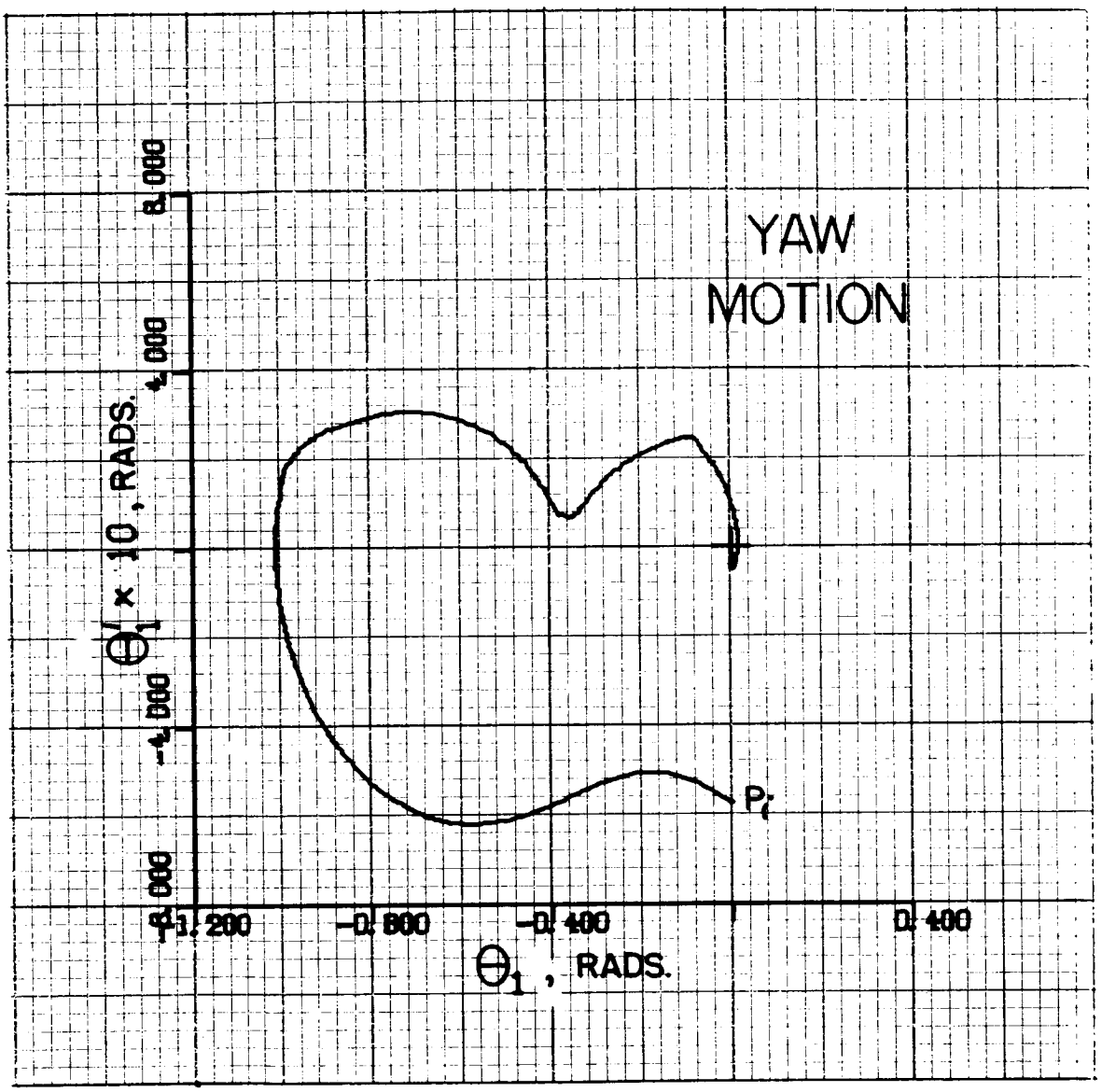

Figure 5.1 Yaw Motion, Unstable Trajectory of Chapter IV.

Thus, except for the presence of the steady-state pitch motion, the simplified linear equations, (3-8) and (4-6), gave quite accurate results over the range of errors for which they were used. In addition, the similarity of the two sets of results showed that the approximations which were made in Chapter II (expansion in terms of eccentricity and retention of only first-degree terms) gave accurate results over the range of eccentricity that was considered.

Figure 5.3 is a representative example of the runs that were made with large initial attitude errors. The errors are definitely outside the region where linearized equations are an acceptable approximation. The appearance of the phase-plane trajectories is quite different than that for the smaller errors in two of the phase-planes. However, no particular difficulty is encountered in eliminating the errors.* The fuel consumption for this particular example was an increase over that for the smaller errors in proportion to the increase in error. Thus, even though the appearance of the trajectories is quite different, there is good reason to believe that the efficiency of the suboptimal control system is about the same for this large error as for the smaller ones. In general, the fuel consumption for a given error magnitude varied more for the large errors than for the smaller ones. However, this is not surprising if one considers the shape of the cost versus error-magnitude plots, such as Figure 3.7a. The range of the cost steadily increases as the error magnitude increases.

---

* No steady-state pitch error is present because the auxiliary pitch control system that is described in the next section was included when this example was run.

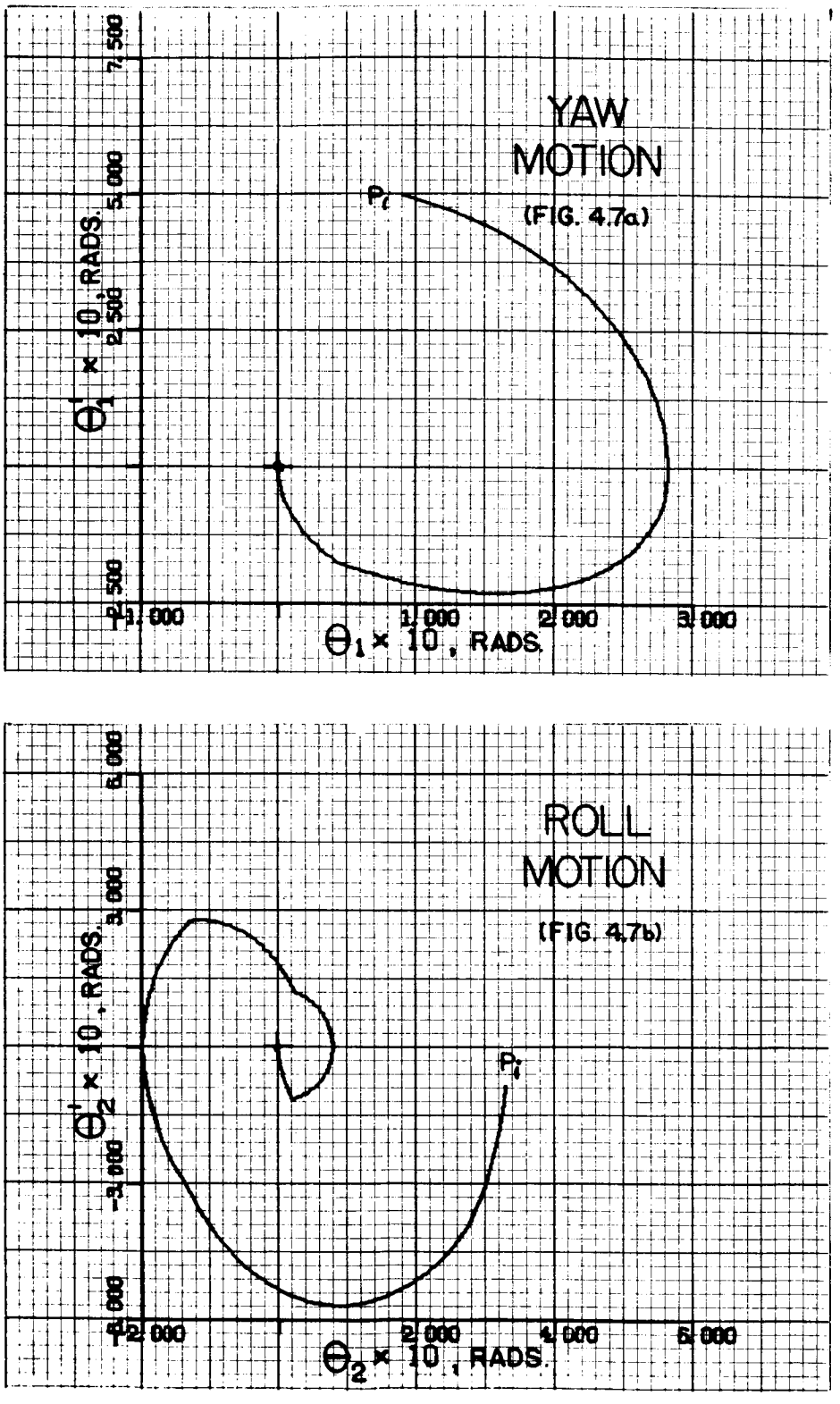

Figure 5.2 Controlled Motion, Initial Conditions of Figures 4.7 and 3.14a.

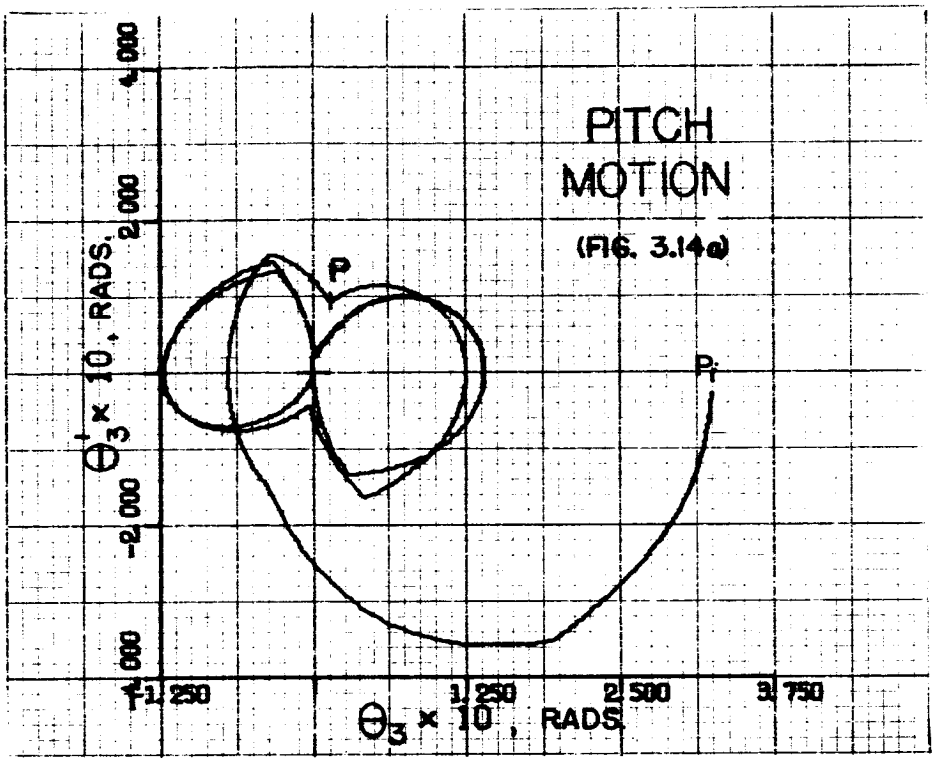

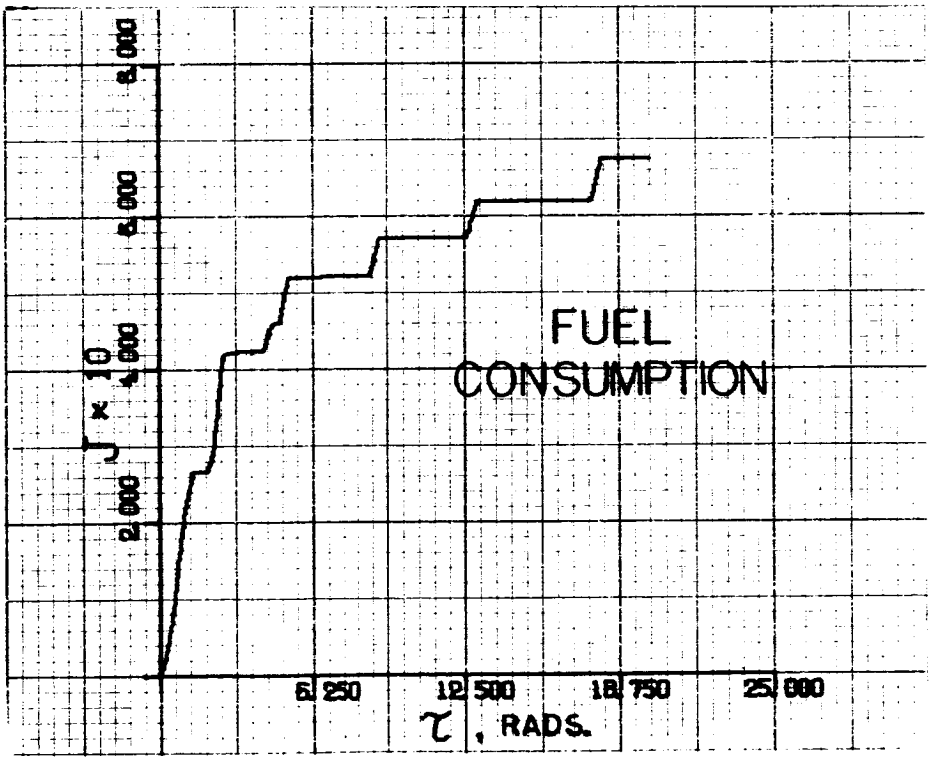

Figure 5.2 (continued)

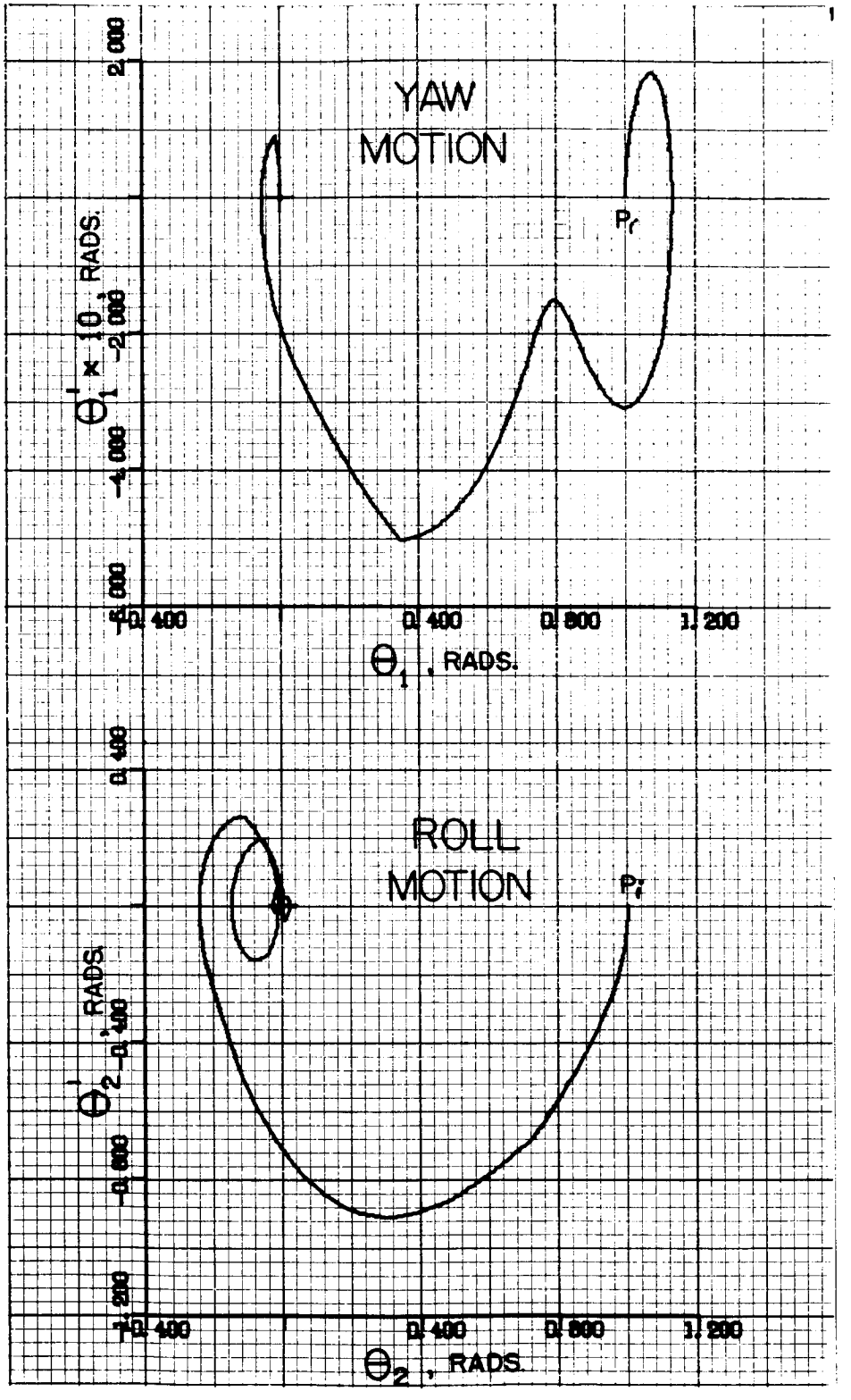

Figure 5.3 Controlled Motion, Large Attitude Errors.
Initial Values: $\theta_o = 0$, $\theta_1 = \theta_2 = \theta_3 = 1.0$ rad.

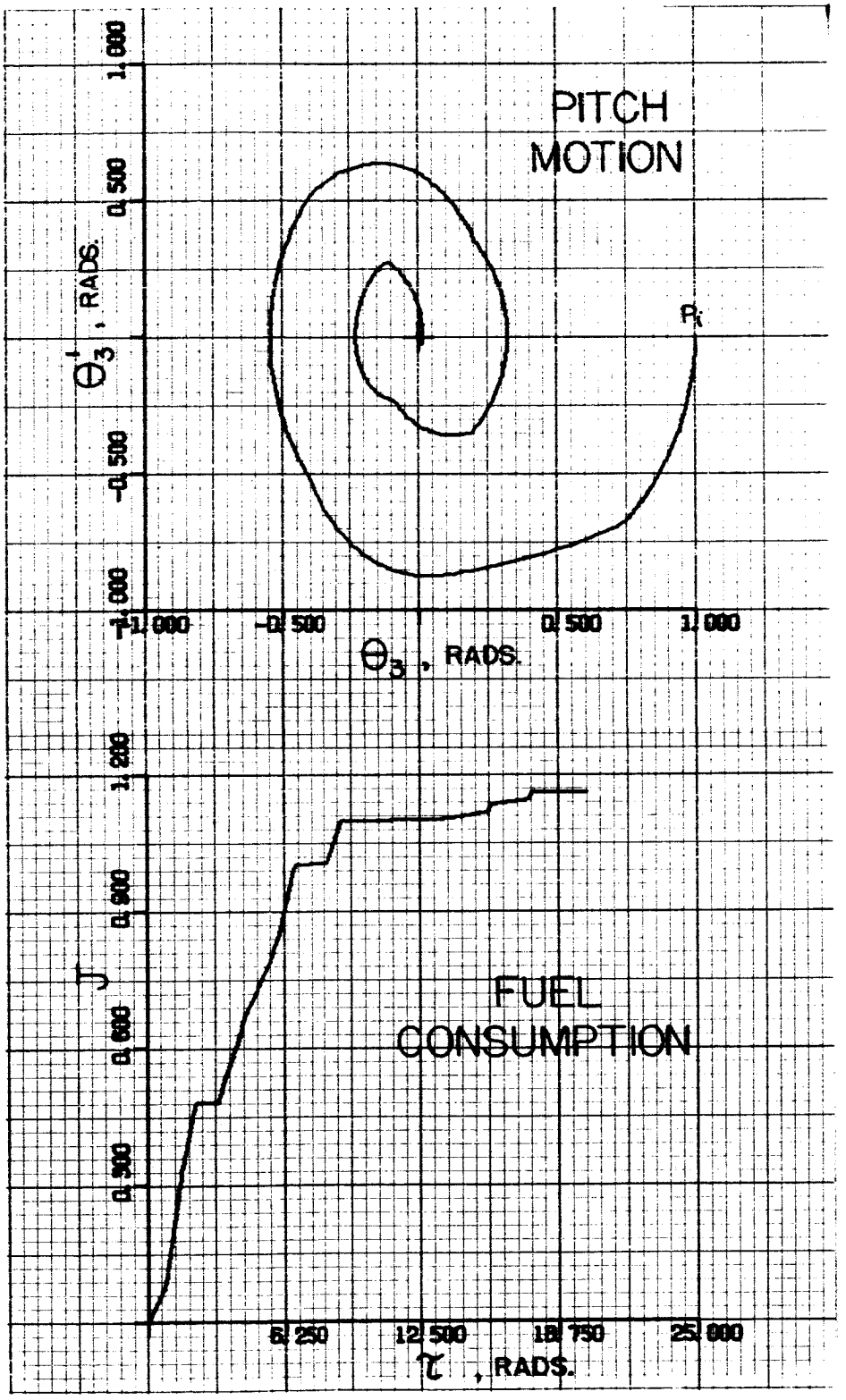

Figure 5.3 (continued)

From the above considerations it appears that the simple, efficient control system, that was developed in the previous two chapters, also works well for the acquisition control of large errors.

B. Steady-State Error Control

Acquisition is only one phase of the control problem. Once the desired attitude is attained, it must be held to within a small allowable error. For an earth-pointing satellite in an elliptic orbit, the desired attitude is not an equilibrium state because of the forcing function in the pitch equation. As shown in Chapter II the amplitude of the forced, uncontrolled motion can be as much as 12 degrees when the orbital eccentricity is 0.1.

1. Steady-State Yaw-Roll Control

Since the yaw and roll motions are not forced, their steady-state control is not as difficult as for the pitch motion. A simple yet effective solution is to leave small circular regions, about the origins of the yaw and roll phase planes, uncontrolled. The chosen satellite shapes are relatively stable with regard to the gravity torques. Thus, the attitude motion will remain inside the uncontrolled regions with little or no control effort, if there are no other outside disturbances.

For a test case the region was made 0.0063 radians in diameter, i.e., an allowable error of 10.8 minutes of arc. At 200 miles this amounts to a pointing error of 0.64 miles. Very little control effort was necessary to keep the roll error within this region. This is as expected since the motion is nearly that of a $1/(s^2+1)$ plant, i.e., circular phase-plane trajectories. The yaw motion, similar to that of a $1/s^2$ plant, is not

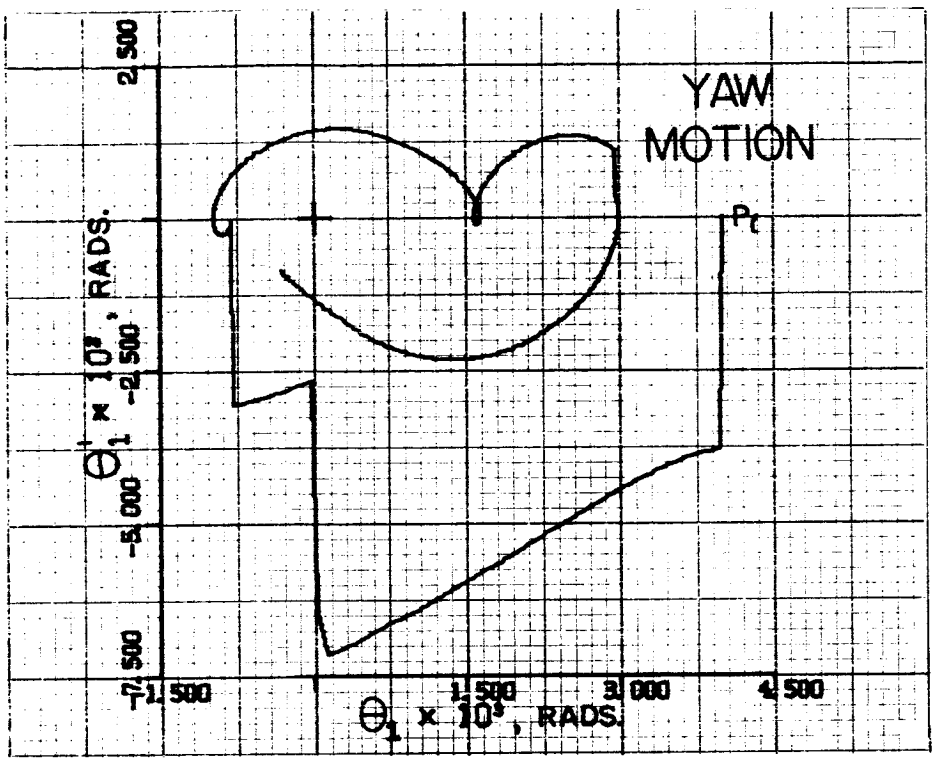

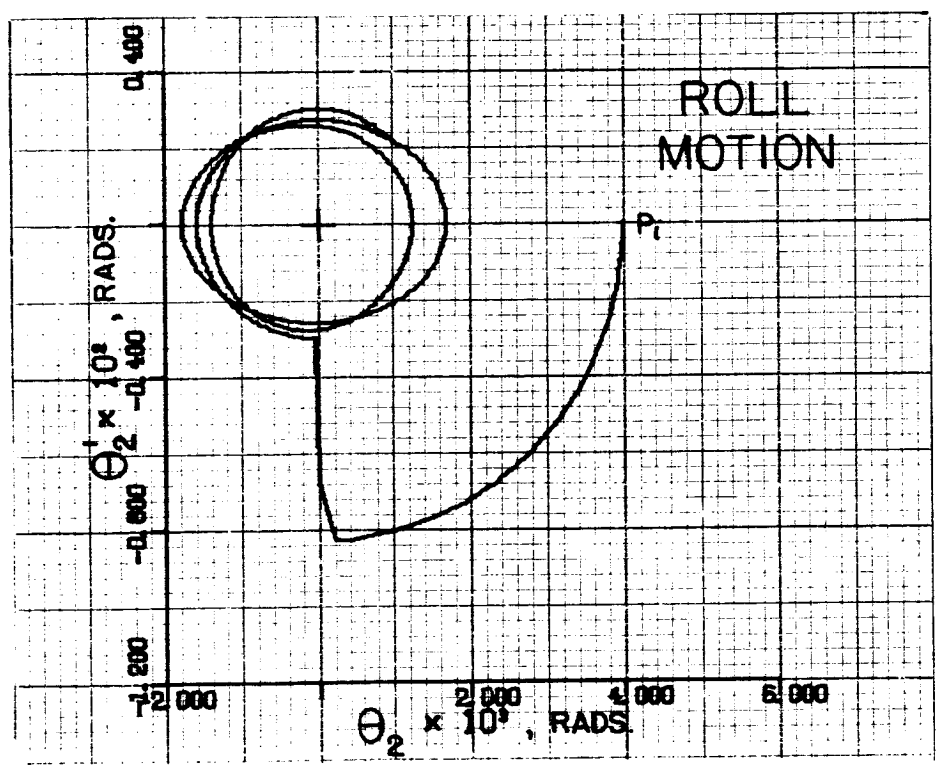

Figure 5.4 Steady-State Yaw and Roll Motions, $\theta_o = 0$.

as well behaved. Consequently, it required more steady-state control effort. However, the necessary control pulses usually occurred no more than twice per orbit and were very short in duration. Figure 5.4 shows the yaw and roll steady-state motions for one example. The control pulses are apparent.

The relative fuel consumption for acquisition and steady-state control is apparent in Figure 5.5. This particular fuel-consumption curve is for an example which had initial errors of $\theta_1' = 0.57$ rads , $\theta_2 = 0.76$ rads , and a small pitch error. The steady-state portion includes only the fuel consumption for yaw and roll control. No steady-state pitch control was employed. The figure shows that the fuel consumption for the yaw-roll steady-state control is very small, and quite satisfactory. Of course, the fuel consumption increases as the magnitude of the allowable steady-state error decreases. However, the error bound in the above example is probably small enough for many actual mission requirements.

2. Steady-State Pitch Control

Without any control the steady-state pitch motion is oscillatory with an unacceptable amplitude of up to 12 degrees. The pitch system that was developed in Chapter III will keep the error smaller ($\sim 7^\circ$) but at a high level of fuel consumption, as shown in Figure 5.6. Thus, an alternative method is necessary.

The forcing function in the linearized pitch equation is periodic. Thus, a momentum storage device, such as a reaction wheel, is a logical way to obtain the necessary control torques. Consequently,

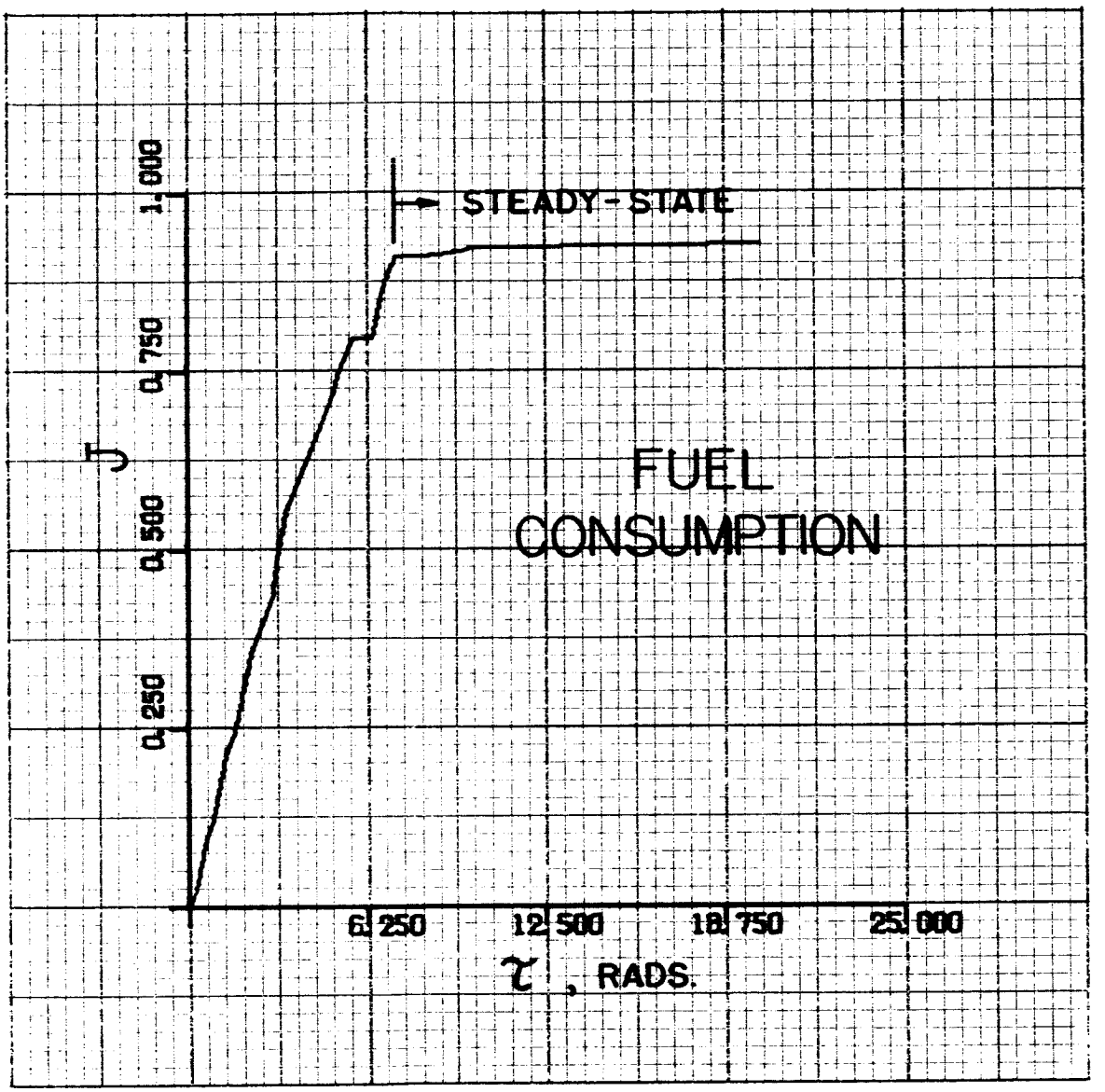

Figure 5.5 Yaw-Roll Fuel Consumption Curve,
Acquisition and Steady-State

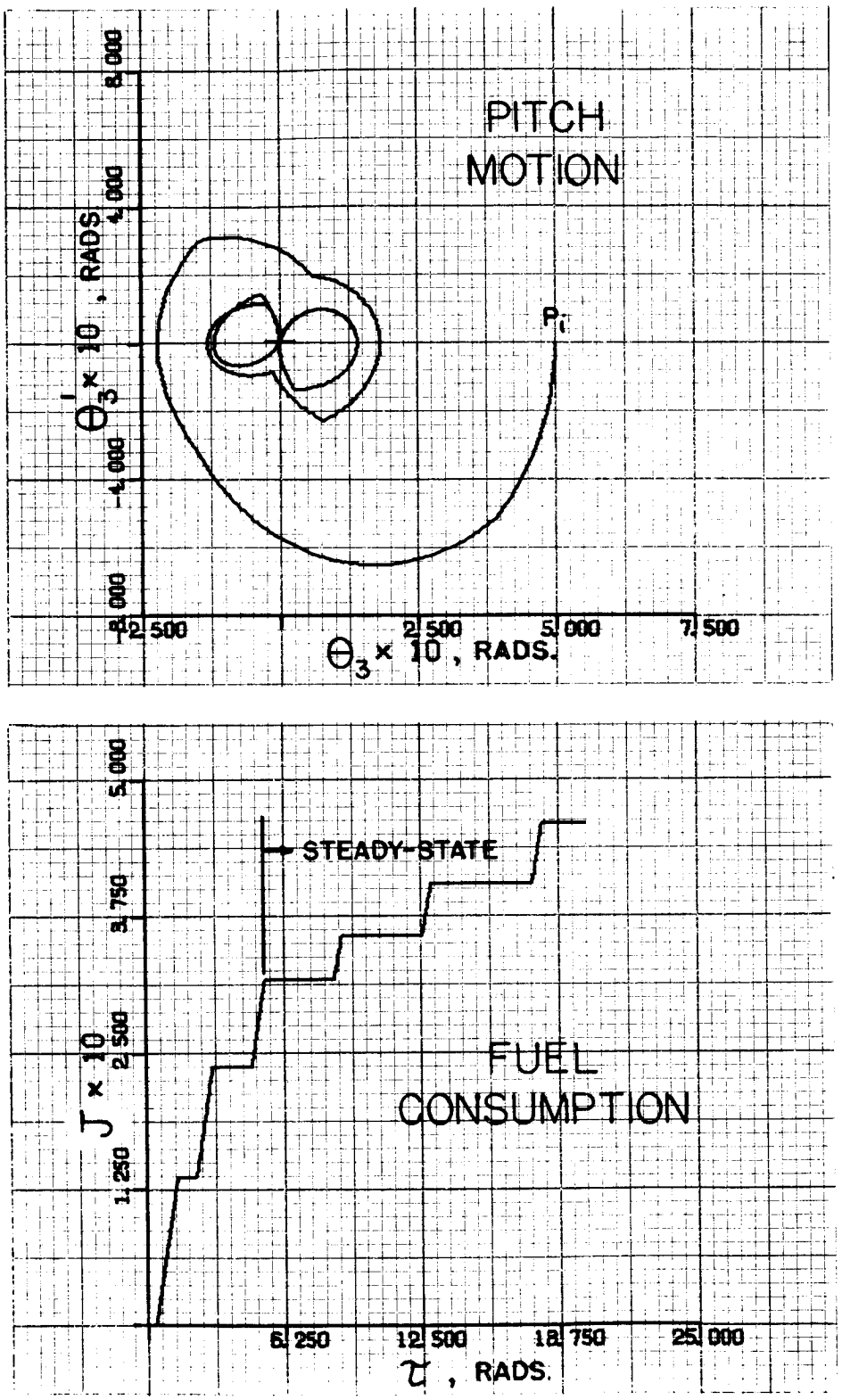

Figure 5.6 Pitch Steady-State Motion and Fuel Consumption, $\theta_o = 0$.

a small reaction wheel* was added to the pitch control system for steady-state control. The gas jets are used to control the error when the error is relatively large. When the error is reduced to a pre-selected magnitude, the control is switched from the gas jets to the reaction wheel. When a large error occurs the gas jets are again used. Appendix D describes the changes in the attitude equations due to the presence of the reaction wheel.

The complete system was integrated on the digital computer using the full nonlinear equations so that all coupling effects were included. The phase-plane trajectories for some arbitrary initial errors, that are outside the steady-state regions, are shown in Figure 5.7. Figure 5.8 shows the fuel consumption and the wheel speeds that were necessary to eliminate these errors. It is apparent that once the steady-state mode of operation begins, the fuel consumption is very small. Also, after the initial acceleration the wheel motion is approximately sinusoidal.

This combination reaction-wheel, gas-jet control system works well for most types of attitude errors. However, one problem remains. When a large error occurs and the gas jets take over, the reaction wheel continues to run at its angular velocity at the time of the disturbance. If the wheel speed is large, the coupling torques can cause the yaw and roll motions to become unstable (see Kane and Mingori [24]). One way to eliminate this instability is to brake the reaction wheel, when the large error occurs, until its speed is below a pre-selected threshold. The

---

* The moment of inertia J of the wheel is $10^{-5} \times I_3$.

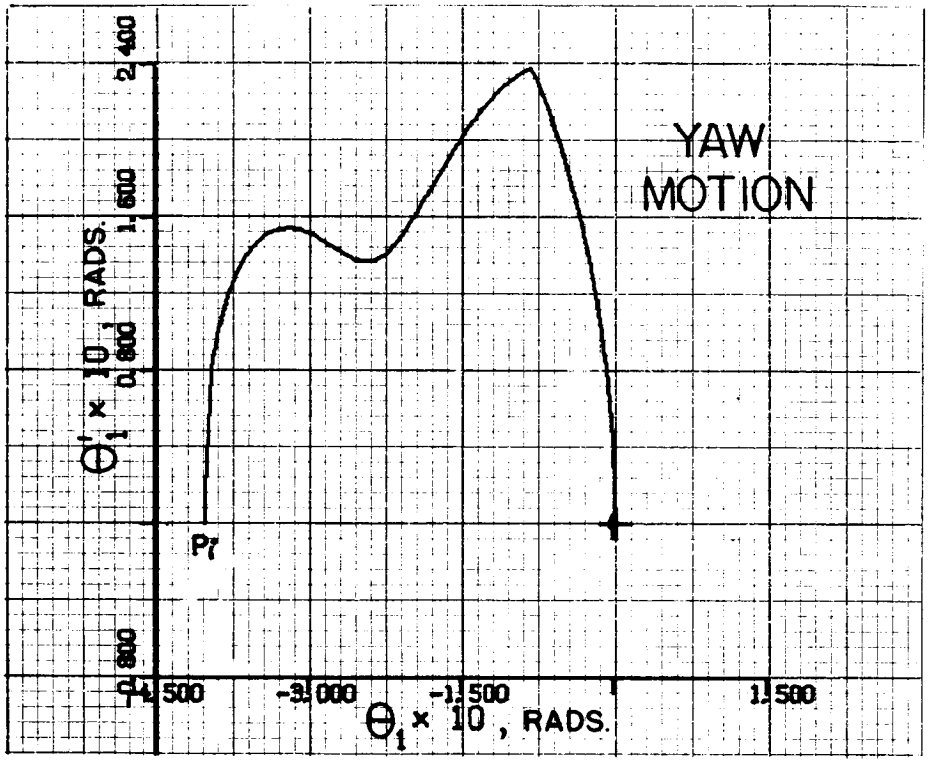

Figure 5.7 Controlled Motion with Pitch Reaction Wheel, $\theta_o = \pi/2$.

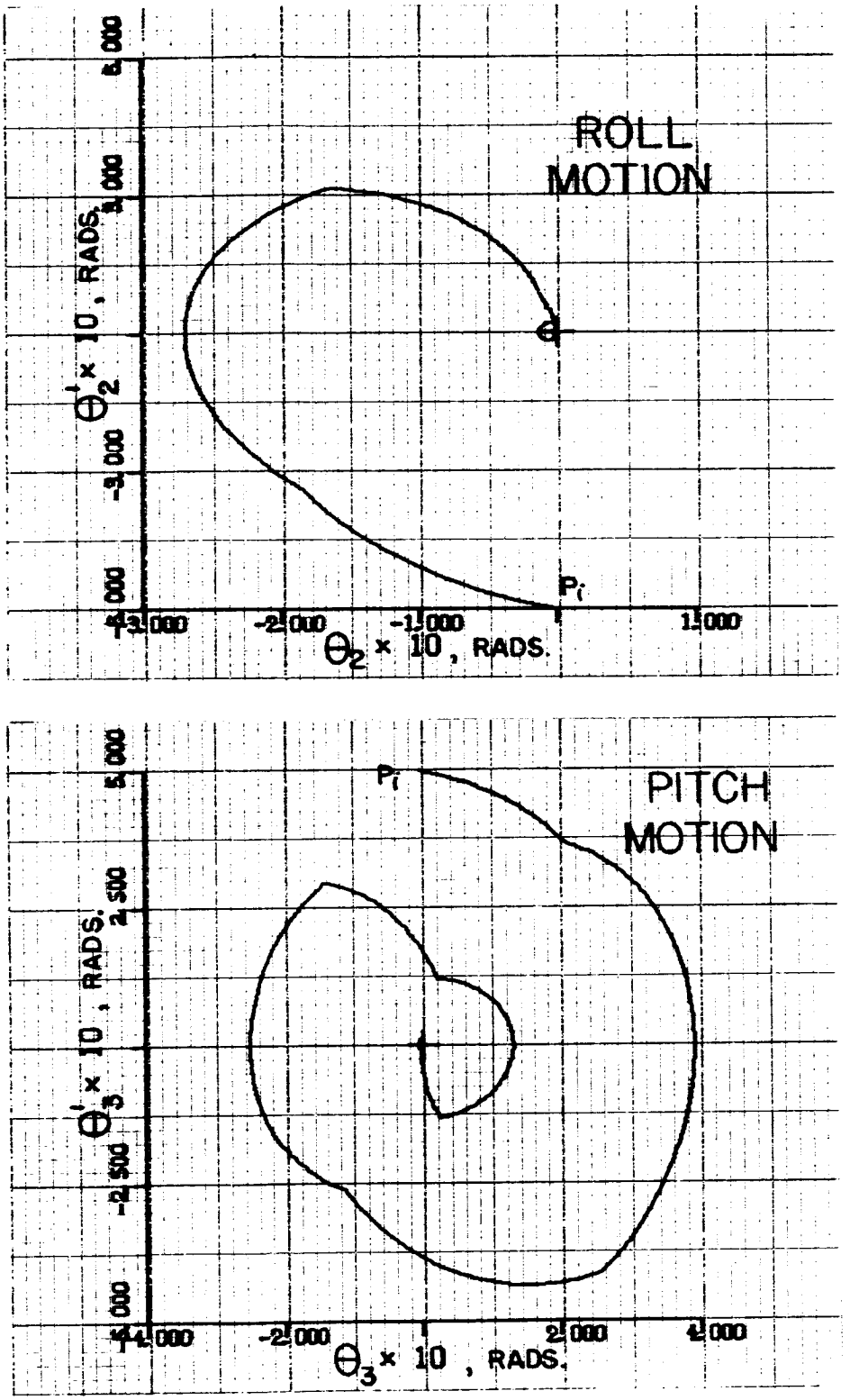

Figure 5.7 (continued)

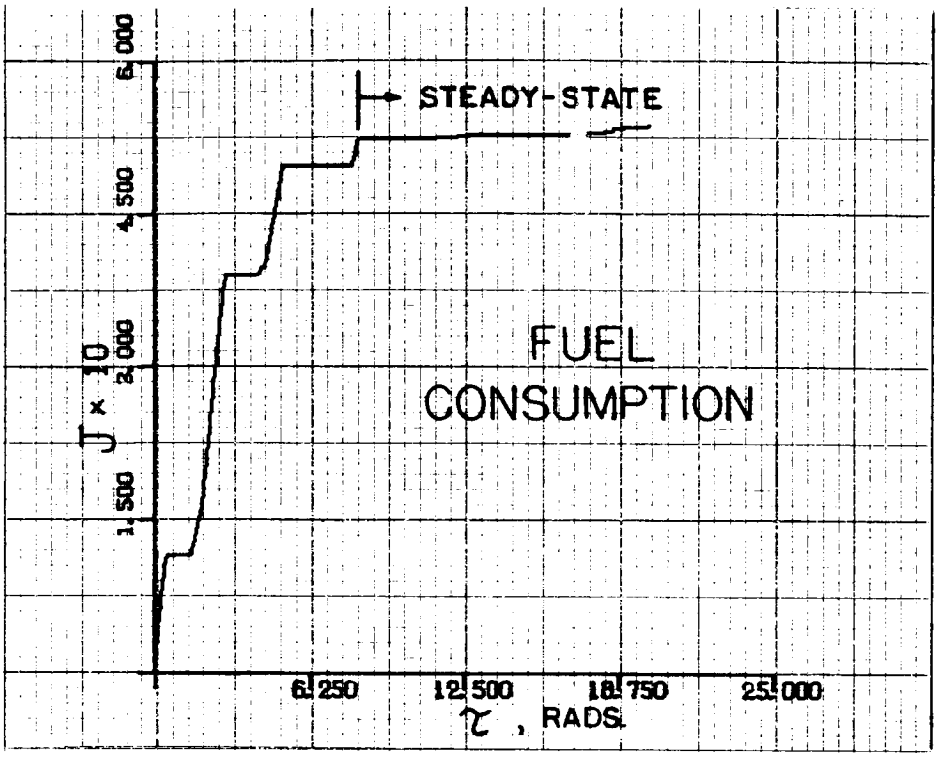

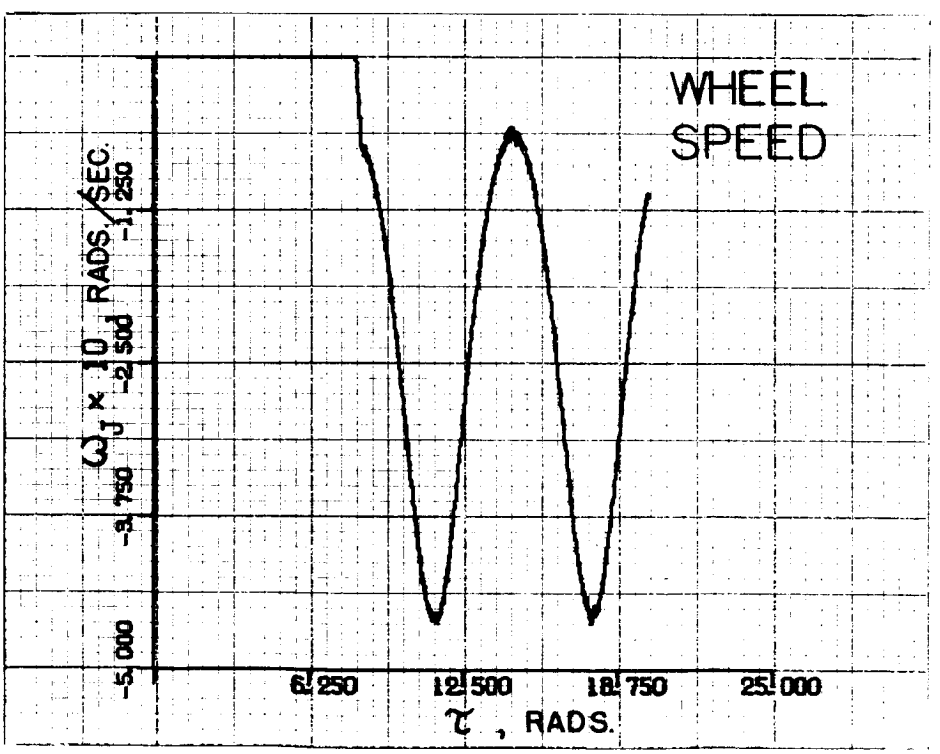

Figure 5.8 Fuel-Consumption and Wheel-Speed Curves for Figure 5.7.

pitch gas jets are used to compensate for the momentum transfer caused by the braking. The braking time is relatively short, so while the errors will grow due to the coupling torques caused by the spinning wheel, they will not become exceedingly large or unbounded. The additional fuel consumption will sometimes be quite large because of the braking and the growth in the errors. However, the portion used for braking is not wasted since this is necessary whenever the wheel saturates.

Figure 5.9 shows the phase-plane trajectories for the initial errors of Figure 5.7, but with an initial wheel angular velocity. The initial wheel speed is near the maximum that occurs in normal operation, such as in Figure 5.8. Figure 5.10 shows the fuel consumption and wheel speeds that occurred while controlling these errors. Due to the spinning wheel the fuel consumption is 21.9% greater than in Figure 5.8, but the control times are about the same. About 60% of the additional fuel was used to slow the reaction wheel, and, consequently, was not wasted. Thus, the increase in the fuel consumption due to the wheel motion was small. Since the wheel speed at the time of the disturbance will usually not be as large as for this example, the additional fuel consumption will often be even less. However, it is possible for the coupling torques to have a more adverse effect on the yaw and roll motions. Such a case occurred when the direction of the wheel velocity for the example of Figure 5.9 was reversed. In this case the spinning wheel caused the roll error to grow considerably before it was reduced. Consequently, the control time was increased 31% and the fuel consumption was increased 102%, not including that used to slow the wheel. However, a case such as this when all conditions are at their worst, is very unlikely. In most cases

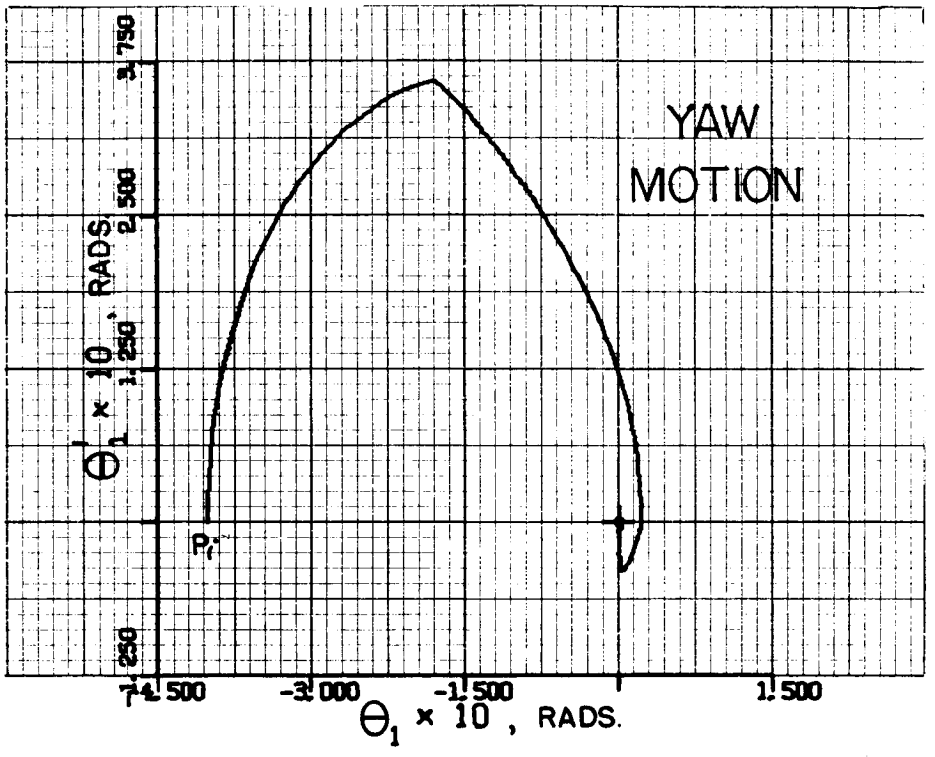

Figure 5.9 Controlled Motion, High Initial Wheel Speed, $\theta_o = \pi/2$.

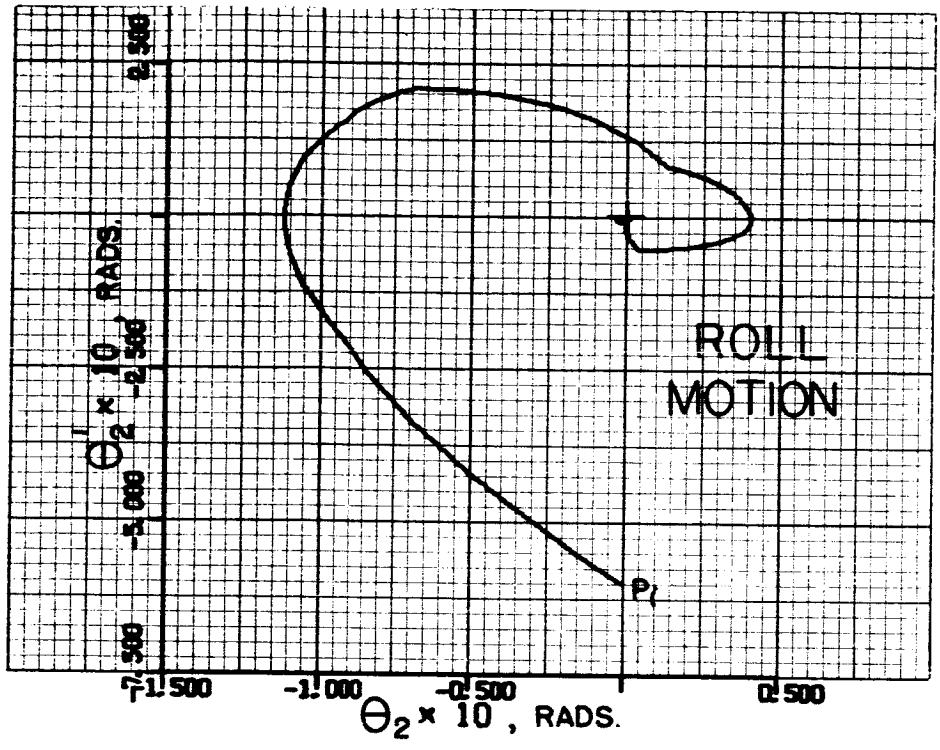

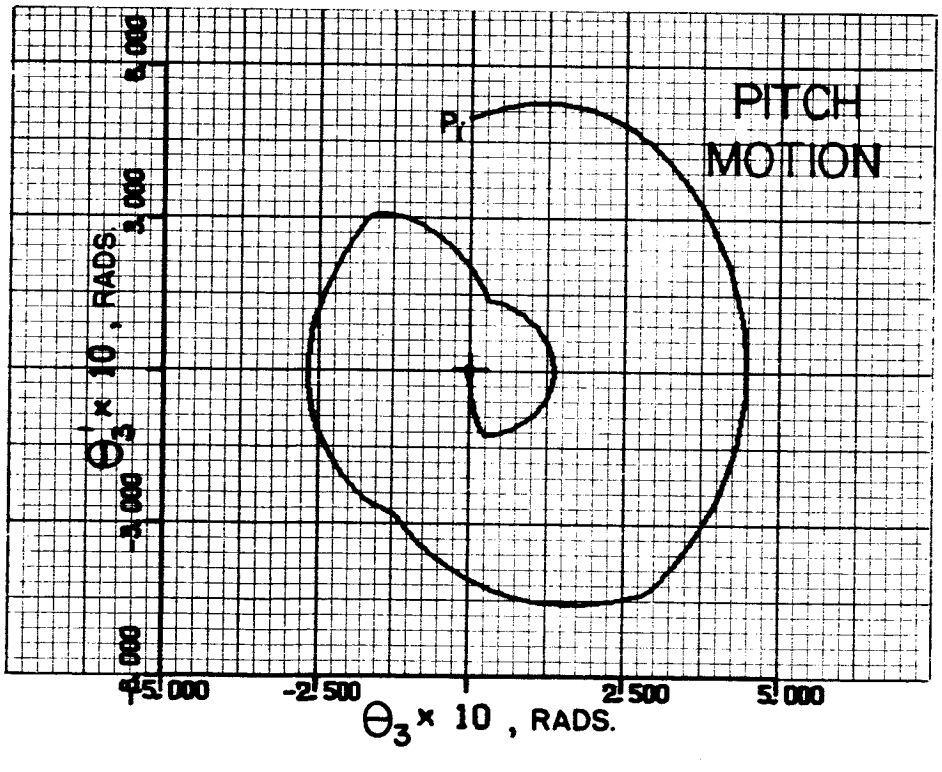

Figure 5.9 (continued)

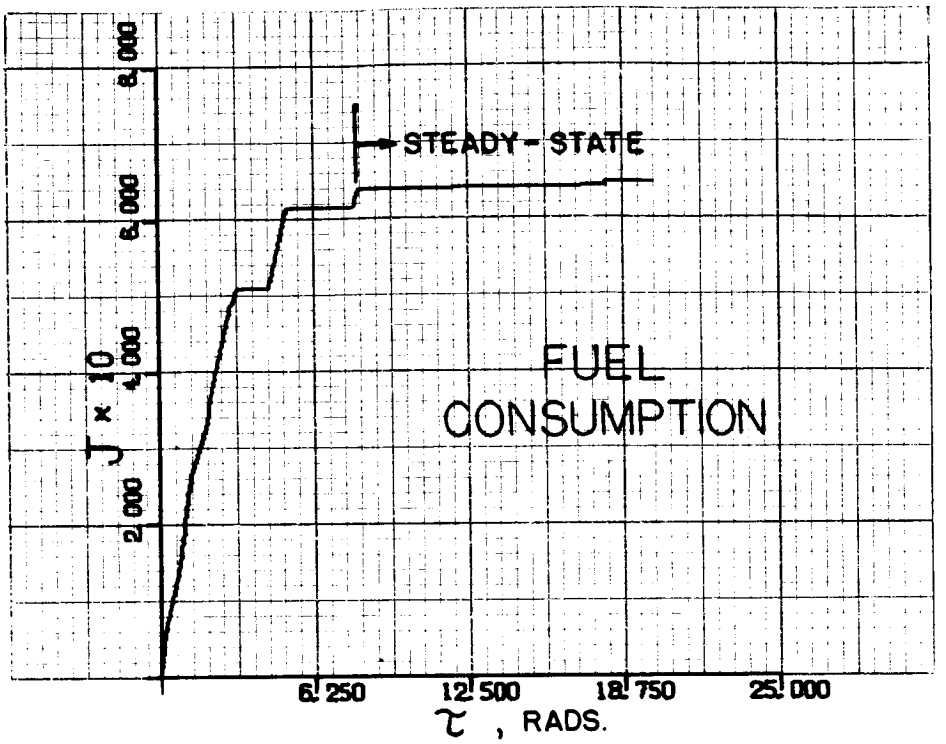

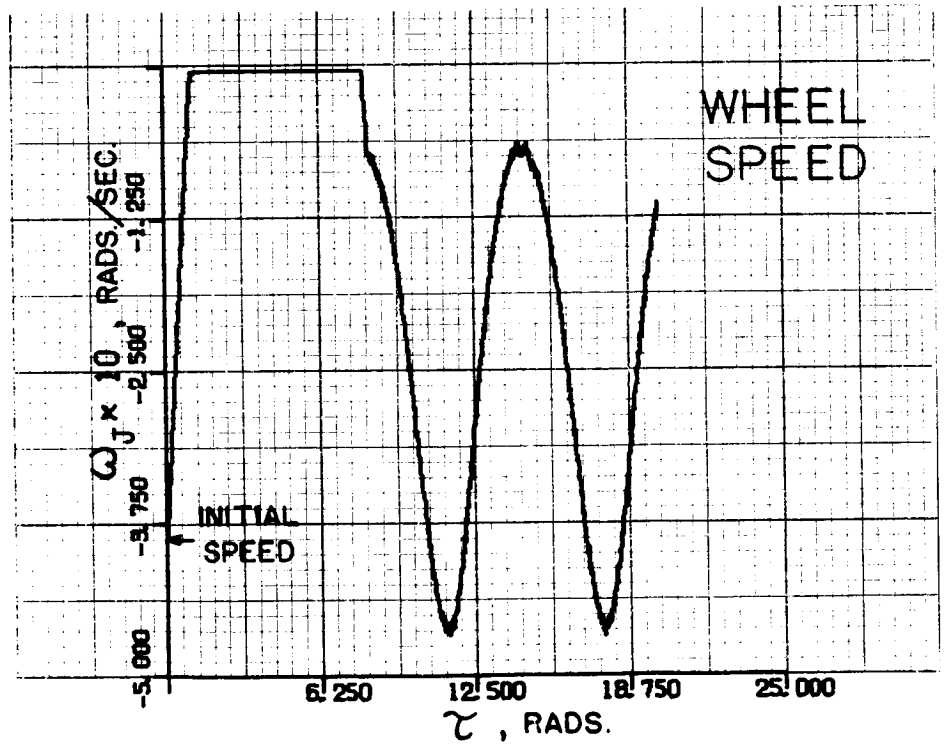

Figure 5.10 Fuel-Consumption and Wheel-Speed Curves for Figure 5.9.

the additional fuel consumption will not be large. Thus, while this steady-state system is definitiely not optimal, it is satisfactory.

C. Discussion of the System

In this chapter the suboptimal control systems, that were developed in the previous two chapters using linearized attitude equations, were checked using the more accurate nonlinear attitude equations. After modifications and additions to the control system to improve the steady-state performance, it was found to work quite well in most cases. The acquisition phase of control is near optimal for most small errors and many large errors when the residual wheel speed is small. The steady-state phase uses only a small amount of fuel and the power required to drive a small reaction wheel. Much of this power can be regained since the steady-state torque requirements are periodic. A block diagram of the complete attitude control system is shown in Figure 5.11.

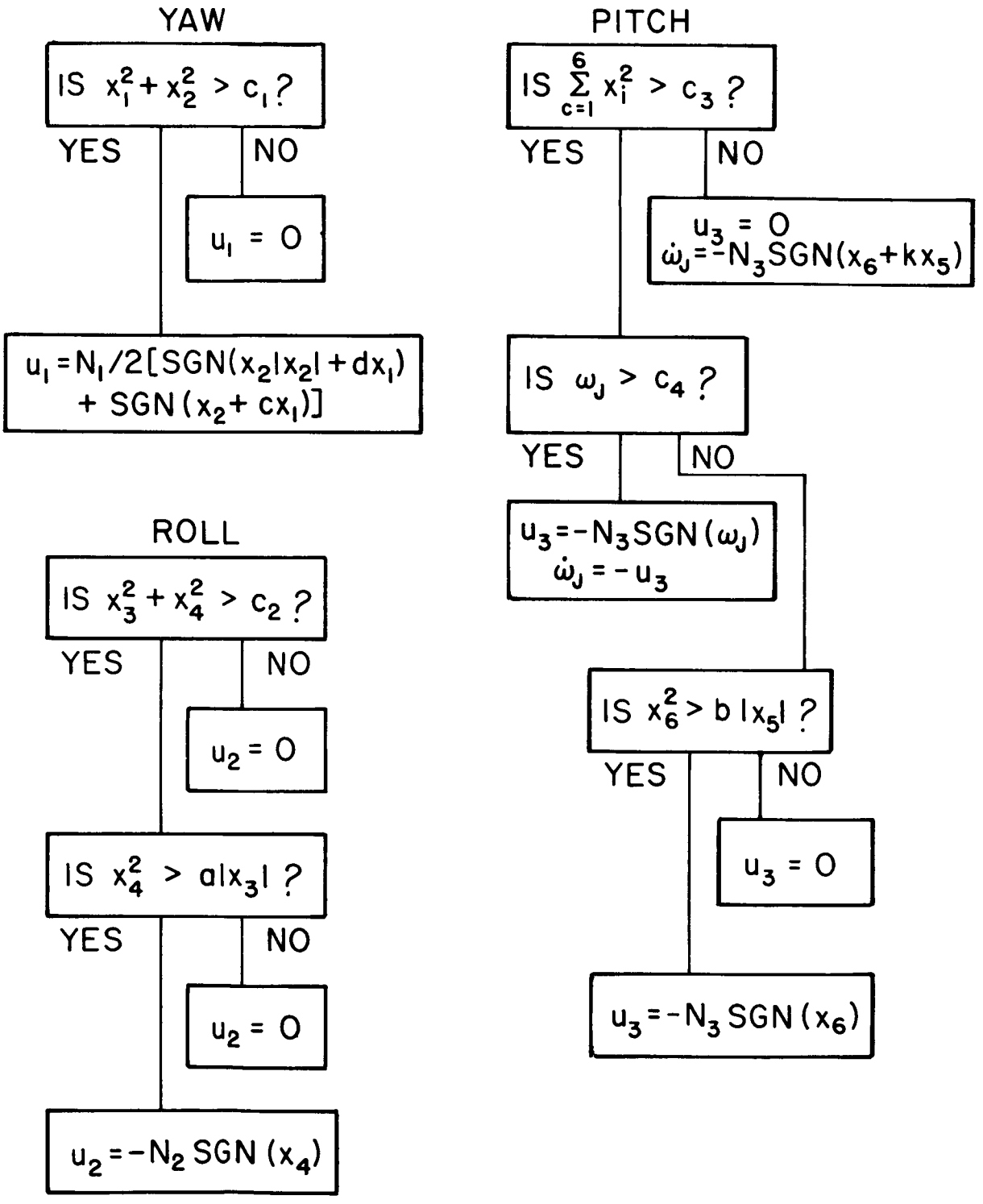

Figure 5.11 Block Diagram, Complete Attitude Control System.

VI. CONCLUSIONS

The problem considered in this paper is the attitude control of a satellite in an elliptic orbit. The satellite configuration is restricted to a limited range of inertia properties. Cold-gas jets that are bounded in thrust-level are used to supply the control torques. The criterion upon which the performance of the system is based is minimum fuel-consumption for reaching the desired attitude in a given time.

In Chapters III and IV a near-optimal continuous-feedback acquisition control system was developed using a combination of widely applicable and often simple procedures. First, Pontryagin's Maximum Principle was applied to determine conditions that the optimal control must satisfy. The system was then integrated in reverse-time starting at the desired final state and employing control as dictated by the Maximum Principle. This procedure is applicable to any system which does not possess inherent chatter, as discussed in Fuller [23].

For systems in which the optimal control function is discontinuous, e.g., minimum-time and minimum fuel-consumption, the phase-plane switching locations are readily apparent in the reverse-time trajectories. Curve fitting to the switching points for a large number of reverse-time trajectories was found to provide near-optimal switching curves. This procedure can be applied to any continuous-time system for which the reverse-time trajectories can be obtained. Since a simple near-optimal switching curve is usually desired, the procedure works best

for simple, linear, time-invariant systems. However, in this paper it was shown to work well also for a particular high-order, linear, time-varying system.

In Chapter V the control system was tested using the nonlinear attitude equations, which give a more accurate description of the actual attitude motion. In the acquisition phase of control the system performed very well, even for quite large errors. Several small modifications were made to the system to improve the steady-state performance. These included the addition of a small reaction wheel for steady-state pitch control. The resulting system was capable of limiting the steady-state errors to small magnitudes without large fuel or power requirements.

While the steady-state performance of the final system appeared quite good in most cases, it cannot be claimed that it is optimal or near optimal. Thus, further research related to this paper should be directed toward optimizing of the steady-state attitude control. Careful consideration should be given to selecting a performance criterion that weighs both error magnitude and control effort.

APPENDIX A

SATELLITE CONFIGURATION AND TORQUE LEVELS

The following data describe a fairly realistic satellite and mission. It serves to give physical meaning to the dimensionless parameters, errors, and torques that are used throughout the text.

The satellite is assumed to be in a slightly elliptic, near-earth orbit. The mission requires the satellite to be earth pointing, to within a small error, to facilitate information transfer. The orbit has an eccentricity of 0.1 and a perigee that is 200 miles above the earth's surface. Thus, the apogee is 1130 miles above the earth's surface and the satellite has an orbital period P of 1.74 hours. Its average orbital frequency, n, is 9.95×10^{-4} rads/sec.

The shape of the satellite is that of an elliptic cylinder with the following moment-of-inertia ratios: $I_1/I_3 = .12$ and $I_2/I_3 = .97$. To obtain these ratios the satellite is assumed to have moments-of-inertia of the following magnitudes:

$$\begin{aligned} I_1 &= 12 \text{ slug-ft}^2 \\ I_2 &= 97 \text{ slug-ft}^2 \\ I_3 &= 100 \text{ slug-ft}^2 \end{aligned} \tag{A-1}$$

With these moments-of-inertia and a vehicle weight of 500 lbs the satellite has an approximate radius of 1.24 ft. and a length of 4.26 ft. This requires a specific weight of 24.2 lbs/ft^3, which is probably

somewhat light. However, the actual satellite will have a smaller, denser instrument package with various protuding arms which provide the desired moments-of-inertia.

In deriving the equations of the attitude motion of the satellite, the gravity-gradient torque was included. For the terms due to this torque to be significant in the control problem, it is necessary that the control torques be very small, i.e., on the order of the gravity torque. Thus, it is assumed that the attitude control jets produce a reaction force of 10^{-5} lbs. This is possibly an order of magnitude smaller than present off-the-shelf items, but it is not unreasonable for the near future.* The gas jets are assumed to be on 3.5 ft moment-arms so that the magnitude of the control torques is 3.5×10^{-5} ft-lbs.

For the above control-torque magnitude and satellite shape, the dimensionless control bounds of Chapters III and IV have the following magnitudes:

$$N_3 = \frac{3.5 \times 10^{-5}}{3(I_2-I_1)n^2} = 0.14 \text{ radians}$$

$$N_1 = N_2 = \frac{3.5 \times 10^{-5}}{4(I_3-I_1)n^2} = 0.10 \text{ radians} \qquad \text{(A-2)}$$

One unit on the angular velocity axes of the figures in Chapters III and IV represents $0.14\beta n$ and $0.10n$ radians per second, respectively. Thus, the attitude angular velocities are on the order of the orbital angular velocity, i.e., 10^{-3} rads/sec.

---

* New developments, such as plasma jets, will certainly be capable of these low torque levels.

A representative value for the exhaust velocity of attitude control jets is 1500 ft/sec., i.e., a specific impulse I_{sp} of $1500/g = 46.5$ sec. Thus, the fuel weight-flow for the above jets is

$$\dot{w} = \text{Force}/I_{sp} = 2.15 \times 10^{-7} \text{ lbs/sec.} \qquad \text{(A-3)}$$

For this weight flow one unit on the fuel consumption curves in Chapter III represents

$$N_3 \times \dot{w}/\beta n = 1.88 \times 10^{-5} \text{ lbs. of fuel} \qquad \text{(A-4)}$$

and in Chapter IV represents

$$N_1 \times \dot{w}/\alpha n = 1.13 \times 10^{-5} \text{ lbs. of fuel} \qquad \text{(A-5)}$$

The scaling for the fuel consumption curves of Chapter V is $N_1 x\dot{w}/n$ or 2.15×10^{-4} lbs of fuel per unit. Based on these values, the yearly fuel-consumption for the attitude control system will be less than 10 lbs.

The pitch reaction wheel has a maximum torque level equal to that of the gas jets. Thus, its peak acceleration is 3.5×10^{-2} rads/sec^2. It can accelerate at this level for a maximum of about one-half orbit and in doing so will reach an angular speed of 110 rads/sec or about 1050 revolutions per minute. The maximum wheel speed for representative reaction wheels is 1800 rpm. The scaling for the plots of reaction wheel speed in Chapter V is such that one unit represents 100 rads/sec.

APPENDIX B

LIST OF SYMBOLS

Symbol	Definition
$A(\tau)$	matrix of coefficients of the linearized attitude equations
$A_1(\tau)$	first four rows and columns of $A(\tau)$
$\tilde{A}_1(\tilde{\tau})$	simplified and normalized $A_1(\tau)$
a	1) semi-major-axis of an ellipse; 2)roll-control-system parameter (see Eq.(4-14))
a_i	measure numbers of $\bar{e}_1$ in the $\bar{n}_i$ directions
a_{ij}	elements of the matrix $A(\tau)$
B	control coefficient matrix
B_1	first four rows and two columns of B
B_1, B_2, B_3	right-handed set of mutually-perpendicular coordinate axes
$\bar{b}_i$	unit vector directed along the B_i-axis
b	pitch-control-system parameter (see Eq.(3-11))
C	cosine of $(\hat{\tau}/\alpha + \theta_o)$
C_1, C_2, C_3	right-handed set of mutually-perpendicular coordinate axes
$\bar{c}_i$	unit vector directed along the C_i-axis
c	yaw-control-system parameter (see Eq.(4-13))
c_i	cosine of θ_i
CST	coast function
e	eccentricity of the orbit
$\bar{e}_i$	unit vector directed along the i-axis
$\bar{f}(\bar{x},\bar{u})$	vector function of $\bar{x}$ and $\bar{u}$, n-dimensional

Symbol	Definition
f_i	components of $\bar{f}$
G	universal gravitational constant
g	acceleration of gravity
$\bar{g}(\tau)$	vector forcing-function
$H(\bar{x},\bar{p},\bar{u})$	Hamiltonian function
H_n, H_{n+1}	H for n and n+1 dimensional systems
$\bar{H}_\omega$	angular momentum of the reaction wheel relative to the center of mass of the satellite
h	constant proportional to the angular momentum of the satellite considered as a particle rotating about the earth
I_{SP}	specific impulse of the gas jets
I	principal moment-of-inertia of the reaction wheel about a radial axis
I_1, I_2, I_3	principal moments-of-inertia of the satellite
J	1) cost functional; 2) principal moment-of-inertia of the reaction wheel about the spin axis
J_1, J_2, J_3	cost functional for the yaw, roll, and pitch axes
k	1) sector-control system parameter (see Eq.(3-13)); 2) cost-functional parameter (see Eq.(3-12))
k_1, k_2, k_3	moment-of-inertia parameters, $k_i = (I_k - I_j)/I_i$
$\ell(\bar{x},\bar{u})$	integrand of the cost functional
M	mass of the earth
$\bar{M}$	external moment on the satellite, excluding the control
M_i	components of $\bar{M}$ in the $\bar{n}_i$ directions
N_i^*	bound on $\lvert u_i^* \rvert$
N_i	bound on $\lvert u_i \rvert$
$\bar{n}_1, \bar{n}_2, \bar{n}_3$	unit vectors directed along the x, y , and z-axes

Symbol	Definition
n	average orbital angular velocity of the satellite
P	orbital period of the satellite (see Chap. V and App. A)
p	point in the phase-plane
$\bar{p}$	adjoint vector, n-dimensional
p_i	1) components of $\bar{p}$; 2) initial point in the phase-planes
R	local-vertical reference frame
R_o	initial pitch-error magnitude
R_1, R_2, R_3	torques about the x,y,z axes on the satellite due to the reaction wheel
$\bar{r}$	radius vector from the center-of-mass of the earth to the center-of-mass of the satellite
r	length of $\bar{r}$
S	sine of $(\hat{\tau}/\alpha + \theta_o)$
s	Laplace transform variable
s_i	sine of θ_i
SGN	signum function
T_{op}	solution time for the optimal case
$T, \tilde{T}, \hat{T}$	solution times in terms of τ, $\tilde{\tau}$ and $\hat{\tau}$
t	time
t^*	reverse-time
$\bar{u}$	control vector, r-dimensional
u_i	1) components of $\bar{u}$; 2) normalized attitude controls
$\bar{u}^*$	attitude-control vector
u_i^*	components of $\bar{u}^*$
$\dot{w}$	weight-flow of gas from the reaction jets
x,y,z	body-fixed coordinate axes

Symbol	Definition
$\bar{x}$	state-variable vector, n-dimensional
x_i	components of $\bar{x}$
y	dummy variable
1,2,3	coordinate-axes fixed in R
α	normalizing parameter, $\alpha^2 = -4k_2$
β	normalizing parameter, $\beta^2 = 3k_3$
δ,ϵ	Mathieu-equation parameters
ϵ	adjusted eccentricity for use of pitch results for roll system (see Eq.(4-15))
θ	angular position of the satellite in orbit
θ_o	θ at $t = 0$
$\theta_1,\theta_2,\theta_3$	nonclassical Euler angles
μ	gravitational constant of the earth
$\tau,\tilde{\tau},\hat{\tau}$	dimensionless independent variables, $\tau = nt$, $\tilde{\tau} = \beta nt$, $\hat{\tau} = \alpha nt$
τ^*	reverse dimensionless independent variable
$\bar{\omega}$	angular velocity of the satellite in an inertial frame
ω_i	components of $\bar{\omega}$ in the $\bar{n}_i$ directions
$\bar{\omega}_w$	angular velocity of the reaction wheel in an inertial frame
ω_J	angular speed of the wheel relative to the satellite
*	d/dt , differentiation with respect to time
'	$d/d\tau$, $d/d\tilde{\tau}$, or $d/d\hat{\tau}$
t	matrix transpose
-	vector
[]	matrix or vector

Symbol	Definition
$\lvert\ \rvert$	absolute value
o	initial
f	final

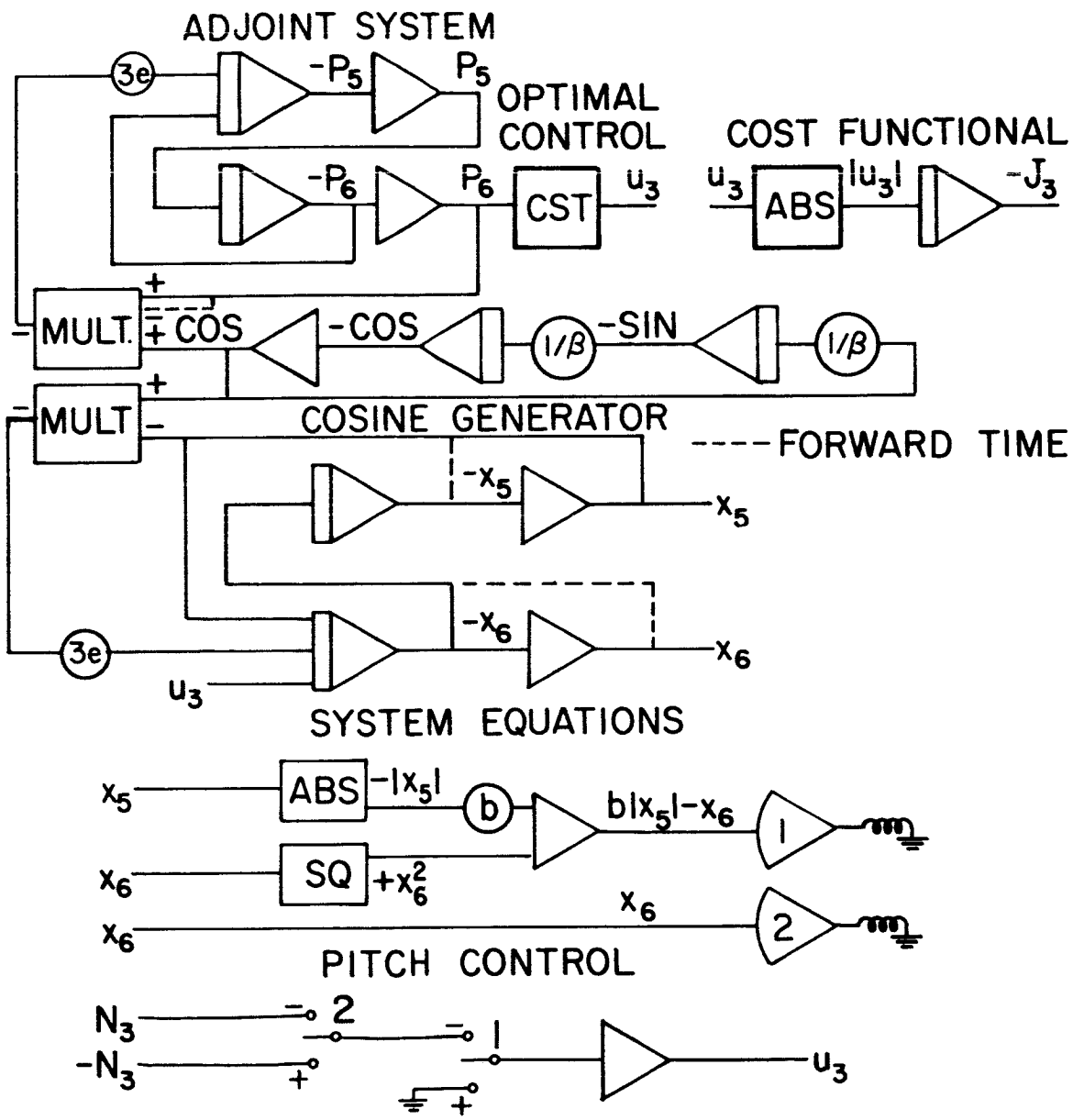

Figure C.1 Analog Computer Program, Pitch System.

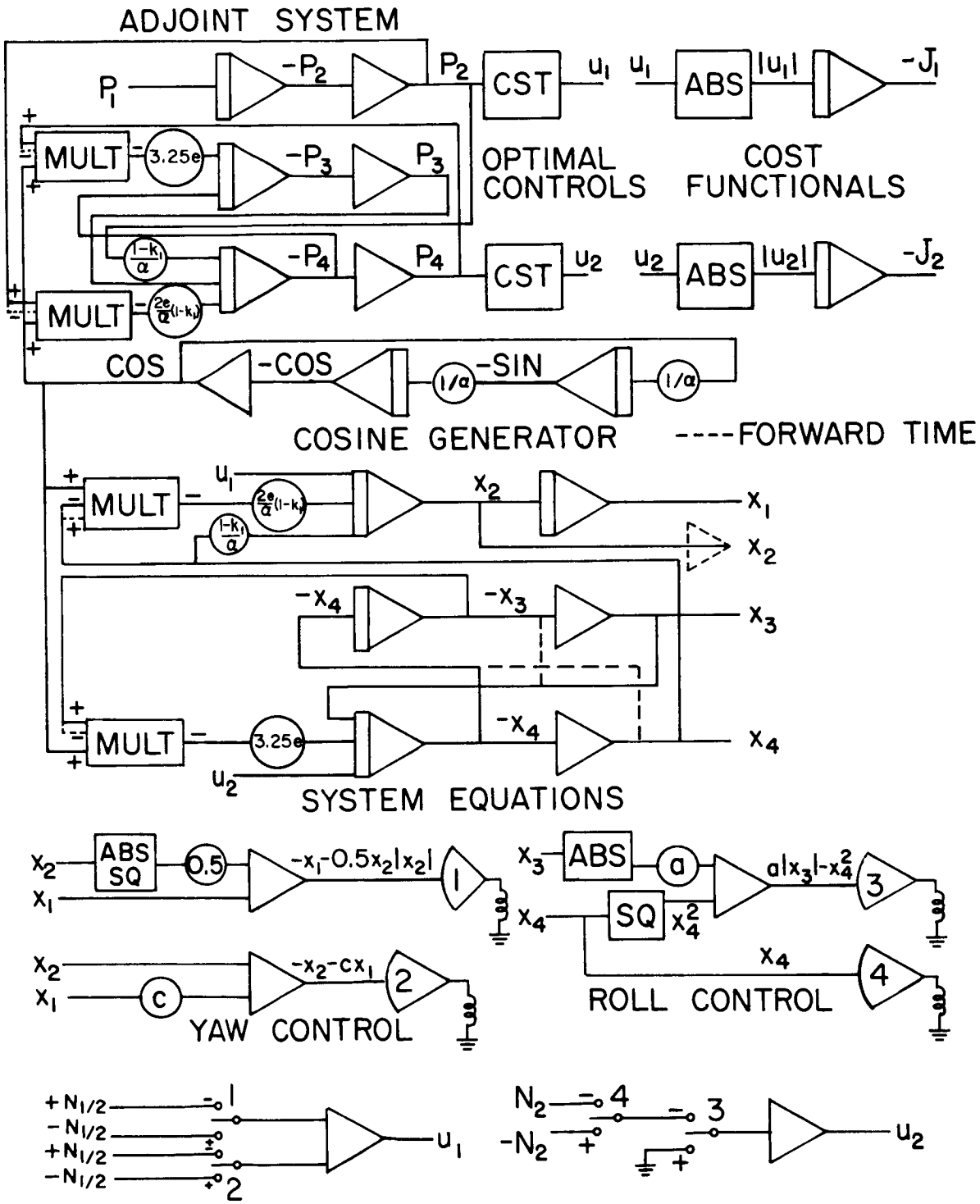

Figure C.2 Analog Computer Program, Yaw-Roll System.

KUTTA-MERSON INTEGRATING PROCEDURE

```
PROCEDURE KUTTAMERSON(N,X,H,Y,F,EPS,ERROR);VALUE N,H,EPS;INTEGER N;REAL
X,H,EPS;REAL ARRAY Y[0];PROCEDURE F;LABEL ERROR;BEGIN OWN REAL HC,FINAL,
H2,H3,H6,H8,ERR,TEST,T;OWN INTEGER I;OWN BOOLEAN DBL;LABEL L,KM,RETURN;O
WN REAL ARRAY Y1,Y2,F0,F1,F2[0:30];DEFINE FORI=FOR I:=1STEP 1UNTIL N DO#,
CONSTANTS=H2:=H/2.0;H3:=H/3.0;H6:=H/6.0;H8:=H/8.0#;IF N=0THEN BEGIN HC:=H;GO
TO RETURN END;IF H=0THEN GO TO RETURN;FINAL:=X+H;IF HC=0THEN HC:=H;IF EPS≠
0AND ABS(H)>ABS(HC)THEN IF SIGN(H)≠SIGN(HC)THEN H:=HC:=-HC ELSE H:=HC;T:=X+H
;X:=FINAL;CONSTANTS;L:FOR T:=T STEP H UNTIL FINAL DO BEGIN KM:F(T-H,Y,F0);
FORI Y1[I]:=F0[I]×H3+Y[I];F(T-2×H3,Y1,F1);FORI Y1[I]:=(F0[I]+F1[I])×H6+Y[I
];F(T-2×H3,Y1,F1);FORI Y1[I]:=(F1[I]×3.0+F0[I])×H8+Y[I];F(T-H2,Y1,F2);FOR
I Y1[I]:=(F2[I]×4.0-F1[I]×3.0+F0[I])×H2+Y[I];F(T,Y1,F1);FORI Y2[I]:=(F2[I]
×4.0+F1[I]+F0[I])×H6+Y[I];IF EPS≠0THEN BEGIN DBL:=TRUE;FORI BEGIN ERR:=ABS
(Y1[I]-Y2[I])×0.2;TEST:=ABS(Y1[I])×EPS;IF ERR>TEST THEN BEGIN H:=H2;T:=T-H2
;IF T+H=T THEN BEGIN X:=1;GO TO ERROR END;CONSTANTS;GO TO KM;END;IF 64.0×
ERR>TEST THEN DBL:=FALSE;END;IF DBL THEN BEGIN H:=2×H;CONSTANTS END DOUBLE
 H;END;FORI Y[I]:=Y2[I];END KUTTA MERSON LOOP;IF EPS=0THEN GO TO RETURN;H
C:=H;H:=FINAL-(T-H);IF ABS(H)>ABS(FINAL)×1.4551915228@-11THEN BEGIN T:=FINA
L;EPS:=0;CONSTANTS;GO TO L END;RETURN:END KUTTA MERSON;
```

EQUATIONS OF ATTITUDE MOTION

```
F[1] ← Y[2];
F[2] ← -2×E × SIN1 × (1+E×COS1)*3;
F[3] ← Y[4];
F[4] ← (-Y[6] × (Y[8]-Y[4]×SIN5-Y[2]×COS3×COS5)
   -Y[2]×SIN3 × (Y[4]×SIN5+Y[6]) + F[2] × COS3 ×
   SIN5 - (K1+K2) × 3×(1+E×COS1)*3 × COS5 ×
   SIN5×SIN7×COS7 - R × (P×K1×COS7 - Q×K2×
   SIN7) - 0.5×Y[10]×(J1×Q×COS7 + J2×P×SIN7)
   - G1×(-K2)×4.0×U1) ×SEC;
F[5] ← Y[6];
F[6] ← Y[4]×Y[6]×COS5 - Y[2]×COS3 × (Y[4]+Y[8]×
   SIN5) - F[2]×SIN3 - 3×(1+E×COS1)*3 × COS5
   ×SIN5 × (K1×SIN7*2 - K2×COS7*2) - R × (P×K1
   ×SIN7 + Q×K2×COS7) + 0.5×Y[10]×(J1×P×COS7
   + J2×Q×SIN7) + G2×(-K2)×4.0×U2;
F[7] ← Y[8];
F[8] ← Y[4]×COS5 × (Y[2]×SIN3 - Y[6]) - SIN5 ×
   (F[4] - Y[6]×Y[2]×COS3) - F[2]×COS3×COS5 - K3 ×
   (3×(1+E×COS1)*3 × COS5*2 × SIN7×COS7+P×Q)
   +G3×1.4×3.0×K3×(U3 + 10×E×RW3);
F[9] ← G1×ABS(U1) + G2×ABS(U2) + G3×ABS(U3)×1.4;
F[10] ← -G3×K3×3.0×1.4×10×E×RW3;
```

ATTITUDE CONTROL SYSTEM

```
U1 ← IF (Y[3]*2 + Y[4]*2) < C13 THEN 0 ELSE
   0.5×( SIGN(Y[4]×ABS(Y[4]) + C1×Y[3]) + SIGN(Y[4] + C12×Y[3]) );
U2 ← IF (Y[5]*2 + Y[6]*2) < C23 THEN 0 ELSE
   IF (Y[6]*2 - C2×ABS(Y[5])) < 0 THEN 0 ELSE -SIGN(Y[6]);
   ERRORSQ ← (Y[3]*2 + Y[4]*2 + Y[5]*2 + Y[6]*2 + Y[7]*2 + Y[8]*2);
U3 ← IF ERRORSQ < C34 THEN 0 ELSE IF ABS(Y[10]) > C36 THEN
   -SIGN(Y[10]) ELSE IF (Y[5]*2 - C3×ABS(Y[7])) < 0 THEN 0
   ELSE -SIGN(Y[6]);
RW3 ← IF ERRORSQ < C34 THEN -SIGN(Y[8] + C35×Y[7]) ELSE
   IF ABS(Y[10]) < C36 THEN 0 ELSE -U3;
```

Figure C.3 Digital Computer Program, Complete System.

APPENDIX D: ATTITUDE EQUATIONS WITH A PITCH REACTION-WHEEL*

With the addition of a reaction wheel, the satellite becomes two rigid bodies. Thus, to derive the attitude equations it is necessary to apply the angular momentum principle to each body and to include the interaction torques between them. In doing this it will be assumed that the reaction wheel is a perfect disc whose axis of rotation, the principal axis with the largest moment-of-inertia, is perfectly aligned with the pitch axis of the satellite.

The angular momentum principle is first applied to the satellite body. The result is Euler's equations with exactly the same form as in Chapter II, except that now the external moment about each axis is made up of the gravity gradient torque M_i plus the interaction torque of the reaction wheel on the satellite R_i , $i = 1,2,3$.

To determine the interaction torques, the angular momentum principle is applied to the reaction wheel. The angular velocity of the wheel in an inertial reference frame is

$$\bar{\omega}_w = \bar{\omega} + \omega_J \bar{n}_3 \tag{D-1}$$

where ω_J is the angular speed of the wheel relative to the satellite, and $\bar{\omega}$ and $\bar{n}_3$ are defined in Chapter II. The angular momentum of the wheel with respect to its center of mass, which is assumed to coincide with the center of mass of the satellite, is

---

* See Kane and Mingori [24].

$$\bar{H}_\omega = I(\omega_1\bar{n}_1+\omega_2\bar{n}_2) + J(\omega_3+\omega_J)\bar{n}_3 \qquad \text{(D-2)}$$

where $I = J/2$ *. When Equations (D-1) and (D-2) are substituted into the angular momentum principle, the following form of Euler's equations results:

$$\begin{aligned} I\dot{\omega}_1 + \omega_2(\omega_3+\omega_J)(J-I) &= M_{1\omega} - R_1 \\ I\dot{\omega}_2 + \omega_1(\omega_3+\omega_J)(J-I) &= M_{2\omega} - R_2 \\ J(\dot{\omega}_3+\dot{\omega}_J) &= M_{3\omega} - R_3 \end{aligned} \qquad \text{(D-3)}$$

where $M_{i\omega}$, $i = 1,2,3$, are the components of the gravity gradient torque on the wheel.

The Euler's equations for the wheel and the satellite are combined to eliminate the interaction torques R_i . Because of the symmetry of the wheel and the way in which it is mounted in the satellite, the gravity gradient torque is unchanged by the motion of the wheel with respect to the satellite. Thus, in the resulting set of equations the gravity gradient torques M_i are those on the combined body and wheel. The resulting equations are

$$\begin{aligned} I_1\dot{\omega}_1 + \omega_2\omega_3(I_3-I_2) + \omega_2\omega_J\frac{J}{2} &= M_1 \\ I_2\dot{\omega}_2 + \omega_1\omega_3(I_1-I_3) - \omega_1\omega_J\frac{J}{2} &= M_2 \\ I_3\dot{\omega}_3 + J\dot{\omega}_J + \omega_1\omega_2(I_2-I_1) &= M_3 \end{aligned} \qquad \text{(D-4)}$$

where the moments of inertia I_i are those of the combined body and wheel.

---

* The reaction wheel is assumed to be a disc.

By writing the components of the angular velocity $\bar{\omega}$ and the gravity gradient torque $\bar{M}$ in terms of the nonclassical Euler angles θ_i and solving for the angular accelerations $\ddot{\theta}_i$, the following set of equations is obtained from Equations (D-4):

$$\ddot{\theta}_1 = \text{(the right-hand side of Equation (2-6))} + \frac{1}{\cos\theta_2}\omega_J\frac{J}{2}\left(\frac{\omega_2\cos\theta_3}{I_1} + \frac{\omega_1\sin\theta_3}{I_2}\right) \tag{D-5}$$

$$\ddot{\theta}_2 = \text{(the right-hand side of Equation (2-7))} + \omega_J\frac{J}{2}\left(\frac{\omega_1\cos\theta_3}{I_2} - \frac{\omega_2\sin\theta_3}{I_1}\right) \tag{D-6}$$

$$\ddot{\theta}_3 = \text{(the right-hand side of Equation (2-8))} - \frac{J}{I_3}\dot{\omega}_J \tag{D-7}$$

Equations (D-5), (D-6), and (D-7) are the modified attitude equations that are used in Chapter V.

REFERENCES

1. DeBra, D. B., "The Large Attitude Motions and Stability due to Gravity, of a Satellite with Passive Damping in an Orbit of Arbitrary Eccentricity about an Oblate Body", Stanford University Ph.D. Thesis, May 1962, SUDAER Report No. 126.

2. Kane, T. R., "Attitude Stability of Earth Pointing Satellites", AIAA Journal, Vol. 3, No. 4, April 1965, pp. 726-731.

3. Nidey, R. A., "Gravitational Torque on a Satellite of Arbitrary Shape", American Rocket Society Journal, Vol. 30, No. 2, February 1960, pp. 203-204.

4. DeBra, D. B., and Delp, R. H., "Rigid Body Attitude Stability and Natural Frequencies in a Circular Orbit", Journal of the Astronautical Sciences, Vol. 8, No. 1, Spring 1961, pp. 14-17.

5. Pontryagin, L. S., Boltyanskii, V. G., Gamkrelidze, R. V., and Mishchenko, E. F., The Mathematical Theory of Optimal Processes, edited by L. W. Newstadt, Interscience Publishers, New York, 1962.

6. Rozonoer, L. I., "L. S. Pontryagin's Maximum Principle in the Theory of Optimal Systems - Parts I and II", Avtomatika i Telemekhanika, Vol. 20, 1962, pp. 1288-1302 and 1405-1421.

7. Craig, A., and Flügge-Lotz, I., "Investigation of Optimal Control with a Minimum-Fuel Consumption Criterion for a Fourth-Order Plant with Two Control Inputs; Synthesis of an Efficient Suboptimal Control", ASME Journal of Basic Engineering, Vol. 87, Series D, No. 1, March 1965, pp. 39-57.

8. Flügge-Lotz, I., and Marbach, H., "The Optimal Control of Some Attitude Control Systems for Different Performance Criteria", ASME Journal of Basic Engineering, Vol.85, Series D, June 1963, pp. 165-176.

9. Cannon, R. H., Jr., "Some Basic Response Relations for Reaction-Wheel Attitude Control", American Rocket Society Journal, Vol. 32, No. 1, January 1962, pp. 61-74.

10. Meditch, J. S., "On Minimum-Fuel Satellite Attitude Controls", IEEE Transactions on Automatic Control, Vol. AC-9, No. 2, April 1964.

11. Hubbs, R. A., "Adaptive Quasi-Optimum Switching Surfaces for Contactor Control Systems", Stanford University Ph.D. Thesis, April 1962.

12. Hayashi, Chihiro, Forced Oscillations in Non-Linear Systems, Revised and Enlarged Edition, McGraw-Hill Book Co., Inc., New York, 1964.

13. Goldstein, Herbert, Classical Mechanics, Addison-Wesley Publishing Company, Inc., Reading, Massachusetts, 1950, pp. 60, 61, 76.

14. Gragg, B. B., "Computation of Approximately Optimal Control", Stanford University Ph.D. Thesis, January 1964, SUDAER Report No. 179.

15. Fox, L., Numerical Solutions of Ordinary and Partial Differential Equations, Pergamon Press, 1962, p. 24.

16. Hales, Kenneth A., "Minimum-Fuel Control of a Sixth-Order Nonlinear Plant by an Extended Method of Steepest Descent", Stanford University Ph.D. Thesis, January 1966, SUDAER Report No. 257.

17. Haefner, K. B., "Attitude Control and Stabilization System for an Orbiting Vehicle", AFFDL-TR-64-165, May 1965.

18. Nichol, K. C., "Research and Investigation on Satellite Attitude Control, Parts I and II", AFFDL-TR-64-168, June 1965.

19. Wheeler, P. C., "Magnetic Attitude Control of Rigid Axially Symmetric Spinning Satellites in Circular Earth Orbits", Stanford University Ph.D. Thesis, April 1965, SUDAER Report No. 224.

20. Kane, T. R., and Barba, P. M., "Attitude Stability of a Spinning Satellite in an Elliptic Orbit", Journal of Applied Mechanics, Preprint, Paper No. 65-APMW-27.

21. Hyver, Gregory A., "The Optimization of a Relay Controlled System Subjected to Random Disturbances", Stanford University Ph.D. Thesis, October 1965.

22. Lange, B., "The Control and Use of Drag-Free Satellites", Stanford University Ph.D. Thesis, June 1964, SUDAER Report No. 194.

23. Fuller, A. T., "Relay Control Systems Optimized for Various Performance Criteria", Proceedings of IFAC Congress, Moscow, USSR, 1960. Published by Butterworths, London, England, 1962.

24. Kane, T. R., and Mingori, D. L., "Effect of a Rotor on the Attitude Stability of a Satellite in a Circular Orbit", AIAA Journal, Vol. 3, No. 5, May 1965, pp. 936-940.

25. Flügge-Lotz, I., and Craig, A., "The Choice of Time for Zeroing a Disturbance in a Minimum-Fuel Consumption Control Problem", ASME Journal of Basic Engineering, Vol. 87, Series D, No. 1, March 1965, pp. 29-38.